LONG TERM VOLTAGE STABILITY ANALYSIS FOR SMALL DISTURBANCES

A Dissertation

by

KUN MEN

Submitted to the Office of Graduate Studies of
Texas A&M University
in partial fulfillment of the requirements for the degree of

DOCTOR OF PHILOSOPHY

December 2007

Major Subject: Electrical Engineering

LONG TERM VOLTAGE STABILITY ANALYSIS FOR SMALL DISTURBANCES

A Dissertation

by

KUN MEN

Submitted to the Office of Graduate Studies of
Texas A&M University
in partial fulfillment of the requirements for the degree of

DOCTOR OF PHILOSOPHY

Approved by:

Chair of Committee,	Garng M. Huang
Committee Members,	Du Li
	Weiping Shi
	Chanan Singh
Head of Department,	Costas N. Georghiades

December 2007

Major Subject: Electrical Engineering

ABSTRACT

Long Term Voltage Stability Analysis for Small Disturbances.
(December 2007)
Kun Men, B.S., Xi'an Jiaotong University;
M.S., Tsinghua University
Chair of Advisory Committee: Dr. Garng Huang

This dissertation attempts to establish an analytical and comprehensive framework to deal with two critical challenges associated with voltage stability analysis:

1. To study the new competitive environment appropriately and give more incentive for reactive power supports, one has to evaluate the impacts of distributed market forces on voltage stability, which complicates the voltage stability analysis.
2. Accurately estimating voltage stability margin online is always the goal of the industry. Industry used to apply static analysis for its computation speed at the cost of losing accuracy. On the other hand, dynamic analysis can result in more accurate estimation, but generally has a huge computation cost. So a challenge is to estimate the voltage stability margin accurately and efficiently at a reasonable cost, especially for large system.

Considering the first challenge, this dissertation applied eigenvalue based bifurcation analysis to allocate the contribution of voltage stability. We investigate how parameters of the system influence the bifurcations. Three bifurcations (singularity induced bifurcation, saddle-node and Hopf bifurcation) and their relationship to several commonly used controllers are analyzed. Their parameters' impact on these bifurcations have been investigated, from which we found a way to allocate the contribution by analyzing the relative positions of the bifurcations.

For the second challenge, a new fast numerical scheme is developed to estimate voltage stability margin by intelligently adjusting the load increase ratio. A criterion, named EMD (Equilibrium Manifold Deviation) criterion, is proposed to gauge the accuracy of the

estimation. And based on this criterion, a new computation scheme is proposed. The validity of our new approach is proven based on the well-known Runge-Kutta-Fehlberg method, and can be extended to other explicit single-step methods easily. Numerical tests demonstrate that the new approach is very practical and has great potential for industrial applications.

This dissertation extends our new numerical scheme to stiff systems. When a system is ill-conditioned, the implicit method would be applied to achieve numerical stability. We further demonstrate the validity to combine the intelligent load adjustment technique with the implicit method to save the computation cost without loss of accuracy. This dissertation also delves into the auto detection of stiffness of the power system, and extends our new numerical scheme to general sytems.

DEDICATION

To My Family

ACKNOWLEDGMENTS

I would like to express my sincere gratitude to my graduate studies advisor, Dr. Garng Huang, and the members of my graduate studies committee, Dr. Chann Singh, Dr. Weiping Shi and Dr. Du Li. I also would like to thank Dr. Ali Abur for serving as my committee member until he left TAMU in 2005. In particular, Dr. Huang's advice, guidance and support throughout the course of my graduate studies are above and beyond appreciation. Thanks to his quick grasp of my intentions, his great engineering insights and his constant guidance, the research in this dissertation is truly original as well as useful. Moreover, his understanding and patience are indispensable to the completion of this work.

I would like to extend my thanks to Ms. Tammy Carda and Ms. Nancy Reichart for their help throughout my graduate study at Texas A&M University.

Acknowledgement is extended to US ABB Research Center (Raleigh, NC) for providing an internship opportunity during summer 2005, and to Dr. Xiaoming Feng and Dr. Le Tang for their wonderful supervision of my intern work.

I appreciate the encouragement from my colleagues and friends in the past years, in particular, Dr. Jiansheng Lei, Dr. Yan Ou, Dr. Xingbin Yu, Dr. Yishan Li, Dr. Bei Xu and Ms. Ping Yan and others.

Finally, I would like to thank my parents for their unfailing love and constant support in my all endeavors, as without their support and understanding this work would not have been possible. My special gratitude also goes to my dear wife, Jin Zhong, for her love, endurance and belief in me, and for her hard work all these years to support me and our family.

To all the people who have made this work possible, I once again say, Thank You!

TABLE OF CONTENTS

Page

CHAPTER Page

LIST OF FIGURES

Page

Page

LIST OF TABLES

Page

CHAPTER I

INTRODUCTION

1. Background

1.1 The emerging challenges faced by voltage stability analysis in deregulated power grid

Electric utility industry around the globe is in the process of deregulation and restructuring. Deregulation experiment was initiated by the U.K. and some Latin American countries in the 1980s, and rapidly spread to many other countries including the United States [1]. In the last two decades, power systems have been operated under much more stressed operating conditions than before. This is largely due to the environmental pressures on transmission expansions, increased electricity consumptions in some heavy load areas, and new system loading patterns for the deregulated electricity market, etc. Under these stressed conditions, a new type of dynamic unstable behaviors appeared in power systems, such as slow voltage drops, and even voltage collapse [1, 2].

Voltage collapse may cause severe system failures; for example, it is believed that the massive Tokyo blackout in July 1987 is caused by voltage collapse [3]. In a deregulated environment, in which the industry still lacks a market policy on reactive power compensation mechanism, electric utilities tend to reduce reactive power support equipments to save cost since money are only made in terms of real power transactions [4]. Accordingly, voltage stability analysis will become even more critical in the deregulation of the modern power systems if the trend continues.

Over last twenty years, many researchers have intensely studied voltage stability [1~9]. Many papers have focused on developing practical analysis techniques for voltage stability studies. For example, in paper [10], Dr. Huang and Dr. Tong Zhu have thorougly discussed the TCSC's enhancement on transient voltage stability, and in papers [11, 12], an efficient

---

This dissertation follows the style of *IEEE Trans. on Power Systems.*

method to find the static stability margin is proposed based on Arnoldi algorithm and curve fitting. Though research has been carried out in this area for decades, there are still some issues that need to be addressed and resolved. Some of these are as follows:

- Challenge 1, how to allocate the responsibility/contribution of voltage stability in deregulated environment?

The deregulated power system is based on transactions [13]; each part of the unbundled systems (generators, control systems and transmission parts, etc.) has its own contribution to voltage stability. It is of great economic and security importance to allocate these contributions so that the contributors can be appropriately awarded to encourage the needed infrastructure investments. Analyzing the influence of the parameters of the system on voltage stability will also help us design and optimize the system.

- Challenge 2, accurately estimating voltage stability margin online remains as a dream for industry.

So far, due to heavy computation burden, the major thrust in voltage stability analysis, especially for large systems, has been based on static power flow analysis. However, recent papers [5, 6, 7] have pointed out that the static estimation of voltage stability margin may be too optimistic. To accurately evaluate voltage stability margin, dynamic voltage stability analysis is required. Many dynamic analysis methods and analytic tools are proposed in literature [2, 3]; however, with these dyanamic methods, the accuracy of estimated stability margin cannot be rigorously guaranteed and the computation efficiency is far from satisfying for online calculation. Thus, we still need to find a more practical and comprehensive scheme to estimate the voltage stability margin with enough accuracy and computation efficiency.

This dissertation deals with the first challenge mentioned above in chapter II and III, where eigenvalue based bifurcation analysis will be applied. For the second challenge, we have developed a new numerical scheme in chapter IV and V to enhance the computation efficiency without sacrificing the accuracy.

1.2 Concepts of voltage stability

Before further discussion, we will first address a fundamental question: What is voltage stability?

There are many definitions of voltage stability. For example, IEEE and CIGRE Working Groups have given detail classification and definition of power system stability in [1]. In this dissertation, we would like to choose the definition given by T. V. Cutsem and C. Vournas in their book [2]:

"Voltage instability stems from the attempt of load dynamics to restore power consumption beyond the capability of the combined transmission and generation system. " This definition try to emphasize that load is the main driving force of a voltage collapse, and voltage stability is a stuctural stability problem with the load serving as an important system paramter to be disturbed. Also, the maximum loadability point is what we are interested in.

In Fig. 2-1 of book [3], C. W. Taylor demonstrated that voltage dynamics can span a range in time from a fraction of a second to tens of mintutes, which also implies a classification of voltage stability into transient and longer-term time frame. In [2], T. V. Cutsem and C. Vournas also gave classification of power system stability based upon two criteria: time scale and driving force of instability. A more comprehensive defination and classification of general power system stability was given in IEEE report [1]. From these definations and classifications, we can see that transient stability analysis does not mean angle stability exclusively, and voltage stability could also be involved . In this dissertation, we will focus on the long term voltage stability analysis with small disturbances.

For power systems, two kinds of stability issues are considered in long term time scale: frequency problems and voltage problems [2]. Generally frequency problem is due to generation-load imbalance irrespective of network aspects within each connected area, while voltage problem is due to electrical distance between generation and loads thus depends on the network structure [2]. Voltage stability is more like a system structure problem, thus a full network representation is required for its analysis [2]. And with the

definition given above, voltage instability could be considered as load driven. Actually in this dissertation, a key task is to detect the structurally unstable point of power system to estimate voltage stability margin analytically or numerically, with slowly increased load serving as small disturbances [14, 15].

Though it is easy to distinguish frequency problem from voltage problem conceptually, these two types of instability are often found entangled with each other in reality. To simplify our analysis, throughout the dissertation, we assume that we have ideal governors and there are no angle/frequency problems, which means that, the frequency problem is decoupled with voltage problems. However, it never means that the new numerical scheme developed in Chapter IV~V can only be used for long term voltage stability analysis; actually it can be easily extended to other long term dynamic analysis for small disturbances.

One term also widely used in association with voltage stability issues is voltage collapse. In this dissertation, the term “collapse” is used to signify a sudden catastrophic transition that is usually due to an instability occurring in a faster time-scale than the one considered [5]. Later in this dissertation, we will show that voltage instability may, or may not result in a sudden voltage collapse, for example, un-damped oscillation may also be the outcome of voltage instability.

As we mentioned before, voltage instability could be considered as load driven [2]. Please note that here we use the term ‘load driven’ instead ‘reactive load driven’. It is well known that voltage control hinges on reactive power. However, by not using the term ‘reactive load driven’, we do not want to overemphasize the role of reactive power in voltage stability, where both active power and reactive power share the leading role [2]. Please note that, only in normal operating conditions, it is approximately valid to decouple between active power and phase angles on one hand, and reactive power and voltage magnitudes on the other hand; and this decoupling is usually not valid for extreme loading conditions that is typical in voltage instability scenarios [16].

2. Topic 1: Eigenvalue based bifurcation analysis to allocate the responsibility / contribution of voltage stability

Dynamic analysis is time-consuming and more difficult than steady-state analysis. For this reason, people use steady-state analysis to estimate the stability margin [9], [17]. However, the dynamic stability margin is usually equal or smaller than the steady-state stability margin; the smaller of them is the valid stability margin, which is the margin that imposes practical loading restrictions. Accordingly, it is necessary to apply dynamic analysis to get the valid margin. Eigenvalue based bifurcation analysis will be used here for this purpose. Though it is time consuming, this analytic tool could give us some insights of the dynamic behavior of the system. We start our research from some simple systems. For such simple systems, the computation costs associated with bifurcation analysis are acceptable.

In deregulated power systems, we would like to know individual contributions to voltage stability, where the contribution can come from different parts of the power system—generator, control system and transmission part, etc. Here we focused on how to allocate the responsibility and contribution by bifurcation analysis. We investigate how parameters of the system influence the bifurcation points. Three bifurcations (the singularity induced bifurcation, saddle-node and Hopf bifurcation [18], and their relationship to several commonly used controllers [19, 20, 21] are analyzed. Their parameters' impact on the bifurcation points is investigated here, from which we found a way to allocate the contribution by analyzing the relative positions of the bifurcations.

In power system operations, there are many limits on the power system components [22]; here we focus on the size of the exciter, which has a significant impact on the voltage stability. Analyzing the impacts of exciter size will benefit system design and clarify the allocation of the responsibility of the voltage collapse in a deregulated environment.

3. Topic 2: Integration of intelligent load adjustment technique with explicit RK methods to estimate the stability margin for a large system accurately and efficiently

As discussed in Topic 1, eigenvalue based bifurcation analysis can be used to calculate dynamic voltage stability margin. Although bifurcation analysis is accurate and gives us insights about the dynamic behavior of the system, its heavy computation burden makes it very difficult to be applied to large systems due to the complexity of eigenvalue calculations [23, 24]. Thus, alternative efficient methods will be developed in this dissertation.

Numerical methods are widely used in the power system simulation. It is well known that power system dynamics are commonly expressed in a differential algebraic equation (DAE) form [25~28]. Numerical methods can be used to solve DAE systems. The procedure usually involves alternately solving the algebraic power flow equations representing the network and the differential equations representing the machines [26, 28]. We can use Gauss-Seidel (or Newton-Raphson) method to solve nonlinear algebraic equations (power flow equations) and use Euler's method (or Runge-Kutta method) to solve differential equations [29, 30]. The integration and algebraic solving are alternately applied.

Compared with transient analysis, voltage dynamic stability analysis has heavier computation burden since by definition the analysis is around equilibrium states with small disturbances [2, 14, 31]; thus, the analysis involves slow load increases to mimic real environment that is operated around steady state. To find the stability margin faster, we can accelerate the load increase since our interest is on the maximum load that the system can tolerate before system collapses and bifurcation occurs; and therefore there is no need to mimic the slow load increase as long as the computed state can stay around the steady state equilibrium point. Also, there is no need for eigenvalue analysis since bifurcation behaviors will be observed through integrated trajectory. Accordingly, how to select the appropriate load increase ratio becomes a key issue to speedup the computation. If the load increase

ratio is too small, it will take a long time to find the collapse point and thus a huge computation burden will be incurred. On the other hand, a too big load increase ratio will lead to inaccurate estimation of stability margin since the computed state may deviate far from the equilibrium state and results in a wrong estimate. Thus, a proper load increase ratio is of great importance for fast and reliable stability margin estimation.

Accordingly, a desirable stability margin estimation scheme should satisfy both accuracy and speed requirements. By definition of dynamic stability analysis, the computed state needs to stay around the equilibrium manifold for an accurate estimate of stability margin. This requirement implicitly constrain the speed of load increases and the integration step size so that it will stay around the equilibrium manfold. These constraints thus slow down the computation speed. In this dissertation, we will develop a scheme in which both requirements are considered and compromised.

- We introduce a criterion, Equilibrium manifold deviation (EMD), which can help us to gauge the accuracy requirement for estimation of dynamic stability margin [32], [33].
- A method is developed in this dissertation to accelerate the numerical solution without sacrificing accuracy. It is an acceleration technique based on EMD criterion to enhance the computation efficiency by adjusting the load increase ratio intelligently. This technique can be integrated with the step size adjustment method, and the integration of these two adjustments induces synergy on the computation efficiency.

The advantages of our new numerical scheme are rigorously proven for a single step explicit RK methods. It can be easily extended to all explicit RK methods, and to the whole family of RK methods.

4. Topic 3: Integration of intelligent load adjustment technique with implicit RK methods to estimate the stability margin for ill-conditioned systems

In Topic 2, the numerical scheme is based on explicit RK methods. However, for power system in extreme loading conditions, it may approach its structurally unstable point, such as a saddle node bifurcation, which may incur the stiffness problem when we numerically integrate the differential equations. It is well known that explicit methods are generally not efficient for stiff problems [34] and instead implicit methods should be applied.

This dissertation further extends our new numerical scheme to resolve stiffness problem of power systems. When system is ill-conditioned, implicit method is applied to achieve numerical stability. We further demonstrate that combining the intelligent load adjustment technique with implicit method can further save the computation cost without loss of accuracy.

Please note that in this Topic, ‘numerical stability’ is an issue, which is a totally different concept with ‘structure stability’. Essentially the ‘structure stability’ only depends on the physical network structure and the generation systems of the power grids, and it has nothing to do with whatever numerical simulation scheme we choose to detect the structurally unstable point. On the other hand, ‘numerical stability’ is an intrinsic property of adopted numerical methods. Basically, it is caused by accumulation of computation error and depends on the computing device and numerical method itself. For example, if we apply Euler and implicit Euler method to a stiff system respectively, different system structurally unstable point may be detected. But conceptually the structurally unstable point should not vary with the chosen numerical method. The difference of the estimation values only demonstrates different capability and feasible range of these numerical methods.

As emphasized, a key task of this dissertation is to detect the structurally unstable point of power system accurately and efficiently. It will be demonstrated that the EMD criterion proposed in Topic 2 is still valid to gauge the accuracy even with stiff systems. And for ill-conditioned systems, a big challenge is to enhance the computation efficiency and keep

solution numerically stable. Different implicit methods will be discussed in this Topic, and we will show that not all the implicit methods are capable to enhance the computation efficiency. Only those methods have A-stable [34] and L-stable [34] characters will be considered in this dissertation. And we will also attempt to integrate our intelligent load adjustment technique with proper implicit methods to further save the computation costs without sacrificing the accuracy.

It is well known that implicit methods generally have better numerical stability than explicit methods [29, 30, 34]. However, for a general implicit approach, it needs to solve the nonlinear equations iteratively at each single step and will result in extra computation costs. Thus, when system is lightly loaded or in normal operating conditions, explicit methods are naturally more attractive than implicit approach. On the other hand, when dealing with stiff problems, implicit method will be more efficient than explicit methods. Accordinly, a key question is that, during numerical simulations, how to detect stiffness automatically. If such a detection scheme is successfully developed, we can choose suitable methods at different system paramter ranges to enhance the overall computation efficiency and accuracy.

In 1977, Shampine & Hiebert proposed some ideas to deal with this problem [34], and there are other approaches in the literature [34], such as detect stiffness by directly estimating the dominant eigenvalue of the Jacobian matrix of the problem [30]. This dissertation attempts to adapt the ideas of Shampine & Hiebert for voltage stability analysis. However, though not a big burden, automatic stiffness detection does introducece extra computation costs. Based on our experience of power system, we deveop a simplified approach to further enhance the overall computation efficiency.

In this Topic, we also generalize our new numerical scheme evolved in Chapter IV for more general cases of long term dynamic analysis with small disturbances. A comprehensive numerical scheme is summarized in this Topic, which integrates the automatic stiffness detection, our new intelligent load adjustment skill, automatically step size control technique, EMD criterion, explicit and feasible implicit Runge Kutta methods.

At last, some MatLAB based codes are developed in this dissertation, which integrates our new research results and can be used for research and education purposes.

5. Objective and organization of the dissertation

The objective of this dissertation is to address the Challenge 1 and 2 faced by voltage stability analysis in deregulate environments. The detailed technique issues related to the two challenges are further discussed as Topic 1, 2 and 3 in Chapter II/III, IV and V respectively as follows:

In Chapter II, eigenvalue based bifurcation analysis will be applied to allocate contribution / responsibility of voltage stability in deregulated environment. Impacts of exciter size and different load model on voltage stability are discussed in Chapter III.

EMD criterion is proposed in Chapter IV, which can gauge the accuracy of numerical estimation of stability margin. Based on EMD criterion, a novel intelligent load adjustment technique is also proposed in this Chapter, which can be integrated with explicit RK method to enhance the computation efficiency.

Chapter V defines and resolves stiffness problem in voltage stability analysis. Here we discussed proper implicit methods to be applied for ill-conditioned power systems. We also extend our EMD criterion and intelligent load adjustment approach to implicit methods. Numerical tests verify the advantage of our new approach to solve stiffness problems.

In Chapter V, automatically stiffness detection will be discussed, and based on our numerical experience with power systems, we develop a simplified detection approach. Also, we try to extend our new numerical scheme evolved in Chapter IV to general long term dynamic analysis with small disturbances.

Finally, Chapter VI is a summary of the dissertation and reviews the contributions of this research. It also suggests the further directions of research based on this dissertation.

CHAPTER II

BIFURCATION ANALYSIS USED IN EVALUATING THE VOLTAGE STABILITY MARGIN

1. Introduction

1.1 Background and objectives

In deregulated power systems, each part of the unbundled systems (generator, control system and transmission part, etc.) has its own contribution to voltage stability [5]. It is of great economic and security importance to allocate these contributions for appropriate investment awards to encourage needed infrastructure investments. Three bifurcations (the singularity induced bifurcation, saddle-node and Hopf bifurcation [5, 18], and their relationship to several commonly used controllers [20, 21, 22] are analyzed. Their parameters' impact on the bifurcation points is investigated here, from which we find a way to allocate the contribution by analyzing the relative positions of the bifurcations.

Our research objective here is to give some insights about how to allocate contribution of voltage stability, thus to enhance competition and efficiency of energy market. Analyzing the influence of the system parameters on voltage stability will also help us design and optimize the system.

1.2 Static stability margin vs. dynamic stability margin

So far, industry used to apply static analysis to estimate voltage stability margin. The mostly common used methods are Continuous Power Flow (CPF) analysis and Quasi Steady State analysis (QSS) [2, 9, 35]. Essentially, the unstable point detected by these static methods is the nose of PV curve.

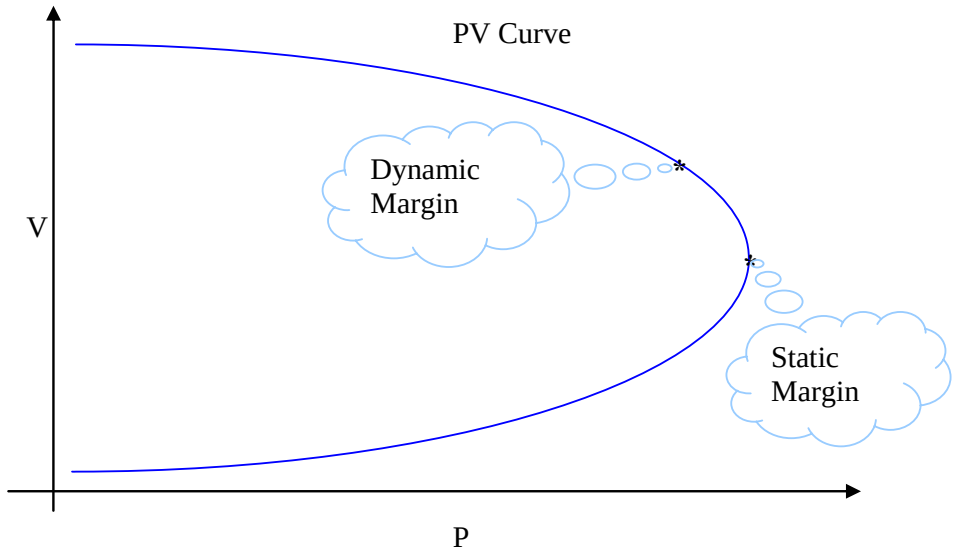

Figure II-1 Dynamic vs. static stability margin

However, as illustrated in Figure II-1, eigenvalue analysis shows that, before system reaches its static margin, there are other kinds of local bifurcation point may appear, such as Hopf Bifurcation (HB) and Singular Induced Bifurcation (SIB). In general, the static margin determined by SNB may be too optimistic [5, 7].

Therefore, throughout this dissertation, we will focus on the more meaningful dynamic margin and develop an efficient and accurate analysis scheme to detect the margin.

We begin this chapter by introducing the eigenvalue based bifurcation analysis.

2. Eigenvalue based bifurcation analysis for voltage stability

Before further discussion, we will first introduce mathematical model of power systems as follows:

2.1 Mathematical description of power systems

Parameter dependent DAE of the form (2.1) is widely used to model the dynamics of physical systems, such as dynamic voltage stability studies of power systems [4, 18]. In the parameter-state space of x, y and p, x is a vector of n state variables, y is a vector of m algebraic state variables, and p is a vector of q parameter variables.

$$\begin{cases} \dot{x} = f(x, y, p), & f : \Re^{n+m+q} \to \Re^n \\ 0 = g(x, y, p), & g : \Re^{n+m+q} \to \Re^m \end{cases} \qquad (2.1)$$
$$x \in X \subset \Re^n,\ y \in Y \subset \Re^m,\ p \in P \subset \Re^q$$

For power systems, the parameter p defines specific system configurations and operation conditions. x denotes the dynamic state variables and y denotes the instantaneous variables which satisfies algebraic constraints. The differential equation in (2.1) represents dynamics of generators, control systems and loads, and the algebraic equation represents the load flow equation.

2.2 Eigenvalue based bifurcation analysis and three kinds of bifurcation points

For a given value of p, equilibrium is a solution of equation (2.2)

$$\begin{cases} 0 = f(x, y, p) \\ 0 = g(x, y, p) \end{cases} \qquad (2.2)$$

The stability of equilibrium points can be determined by linearizing (2.1) around the equilibrium point:

$$\begin{bmatrix} \Delta\dot{x} \\ 0 \end{bmatrix} = J \begin{bmatrix} \Delta x \\ \Delta y \end{bmatrix} \qquad (2.3)$$

where J is the unreduced Jacobian of the differential-algebraic system:

$$J = \begin{bmatrix} f_x & f_y \\ g_x & g_y \end{bmatrix} \qquad (2.4)$$

According to implicit theory, if g_y is nonsingular, we can eliminate Δy from (2.3) as follows.

$$\Delta \dot{x} = [f_x - f_y g_y^{-1} g_x]\Delta x \qquad (2.5)$$

Hence, the reduced Jacobian matrix of the system (2.1) can be written as:

$$J_r = [f_x - f_y g_y^{-1} g_x] \qquad (2.6)$$

As defined in [36], the qualitative behavior of a system is determined by the pattern of its equilibrium points and periodic orbits, as well as by their stability propertities. If a system can maintain its qualitative behavior under infinitesimally small perturbations, the system is said to be structurally stable. In general, bifurcation is a change in the qualitative behavior as a parameter is varied. The parameter is called a bifurcation parameter, and the values at which changes occur are called bifurcation points [36].

Through the analysis of the eigenvalue of J_r, we can demonstrate the influence of the control system. We observed that three types of bifurcation usually occurred: Hopf Bifurcation (HB), Saddle Node Bifurcation (SNB) and Singularity Induced Bifurcation (SIB), correspondingly we denote these three types of bifurcation as A, B and C in this chapter. A brief introduction of these three bifurcations are give below [36]:

- HB, where there is an emergence of oscillatory instability. At this point, two complex conjugate eigenvalues of reduced Jacobian cross the imaginary axis.
- SNB, where two equilibrium (a Saddle and a Node) coalesce and then disappear, at this point the reduced Jacobian has a zero eigenvalue;
- SIB, at this point, g_y is singular, through the equation (2.6), we know that the inverse of g_y will become infinity, which is called “singularity induced infinity”, where it is not easy to compute and analyze the stability of the system.

In next section, we will show how different controllers and their parameters impact on the locations of A, B and C on the PV curve, and try to find some clues to allocate responsibility / contribution of voltage stability.

3. Allocation of responsibility / contribution of the system

In this section, a simple system, shown in Figure II-2, is used to demonstrate how to apply eigenvalue based bifurcation analysis in voltage stability analysis, and thus to allocate responsibility of voltage collapse.

3.1 Introduction of the test system

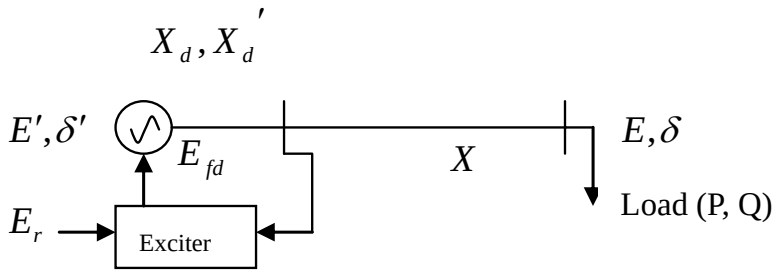

Figure II-2 A simple two bus system

As mentioned before, dynamics of power system can be described as DAE systems shown as equation (2.1). For the above system, we will first introduce its power flow equations as follows:

$$\begin{cases} P = \dfrac{E^{'}E}{x^{'}}\sin\delta^{'} \\ Q = \dfrac{-E^{2} + E^{'}E\cos\delta^{'}}{x^{'}} \end{cases} \qquad (2.7)$$

Here $x^{'} = X + X_d^{'}$, **a**nd detail description of this two bus test system can be found in [2].

Equation (2.7) can be simplified as:

$$0 = E'^2 E^2 - (x'P)^2 - (x'Q + E^2)^2 \tag{2.8}$$

Here equation (2.4) is the algebraic constraint function $g(x, y, p)$ in equation (2.1).

In this chapter, we will focus on three types of commonly used excitation controllers – P-controller, PI-controller and PID-controllers, and correspondingly the differential equations to describe system dynamics are given as follows:

P-controller:

$$\begin{cases} \dot{E}' = \dfrac{1}{T'_{d0}} \cdot \left[-\dfrac{x + x_d}{x'} E' + \dfrac{x_d - x_d'}{x'} \cdot \dfrac{(E^2 + x'Q)}{E'} + E_{fd} \right] \\ \dot{E}_{fd} = \dfrac{1}{T} \left\{ -(E_{fd} - E_{fd}^0) - K_p \left[\dfrac{1}{E} \sqrt{(xP)^2 + (xQ + E^2)^2} - E_r \right] \right\} \end{cases} \tag{2.9}$$

Here equation (2.5) is the differential equation $f(x, y, p)$ in equation (2.1).

PI-controller

$$\begin{cases} \dot{E}' = \dfrac{1}{T'_{d0}} \cdot \left[-\dfrac{x + x_d}{x'} E' + \dfrac{x_d - x_d'}{x'} \cdot \dfrac{(E^2 + x'Q)}{E'} + E_{fd} \right] \\ \dot{E}_{fd} = \dfrac{1}{T} \left\{ -(E_{fd} - E_{fd}^0) - E_{PI} / T_I - K_p \left[\dfrac{1}{E} \sqrt{(xP)^2 + (xQ + E^2)^2} - E_r \right] \right\} \\ \dot{E}_{PI} = \dfrac{1}{E} \sqrt{(xP)^2 + (xQ + E^2)^2} - E_r \end{cases} \tag{2.10}$$

Here equation (2.9) is the differential equation $f(x, y, p)$ in equation (2.1). Note that in this regulator, E_{fd}^0 is not constant, and it will be rescheduled to keep E_G as constant as load P changes. So the P-regulator used here is also called as rescheduled P-regulator.

PID-controller

For a PID controller, as decribed in [20, 22]

$$K_P + \frac{1}{T_I s} + K_D s \tag{2.11}$$

We know that $K_D s$ is not practical [20, 22], so if T_D is small enough, we can use equation (2.12) to replace (2.11):

$$K_P + \frac{1}{T_I s} + \frac{K_D s}{1 + T_D s} \tag{2.12}$$

Then the differential equations is listed as follows:

$$\begin{cases} \dot{E}' = \dfrac{1}{T_{d0}'} \cdot \left[-\dfrac{x + x_d}{x'} E' + \dfrac{x_d - x_d'}{x'} \cdot \dfrac{(E^2 + x'Q)}{E'} + E_{fd} \right] \\ \dot{E}_{fd} = \dfrac{1}{T} \left\{ -(E_{fd} - E_{fd}^0) - E_{PI} / T_I - E_D - (K_p + \dfrac{K_D}{T_D}) \left[\dfrac{1}{E} \sqrt{(xP)^2 + (xQ + E^2)^2} - E_r \right] \right\} \\ \dot{E}_{PI} = \dfrac{1}{E} \sqrt{(xP)^2 + (xQ + E^2)^2} - E_r \\ \dot{E}_D = -\dfrac{K_D}{T_D^2} \left(\dfrac{1}{E} \sqrt{(xP)^2 + (xQ + E^2)^2} - E_r \right) - \dfrac{E_D}{T_D} \end{cases} \tag{2.13}$$

3.2 Eigenvalue Analysis Results

Based on above test system, here we will show that the dynamic stability margin is smaller than the static margin. Please note that, it could be expected as a general case that the stability margin will shrink considering the time delay of generator dyanmic response to load increase, the physical limits of generators, the limit of excitor size and unpredictable load dynamic behavors, etc.

The regulator used in this example is a P-regulator with constant $E_{fd}^0 = 1.6$, and the other parameters is set as:

$$T_{d0}^{'} = 5, T = 1.5, x_d = 1.2, x = 0.1, x_d^{'} = 0.2, Q = 0.5P, E_r = 1.0$$

And throughout this section, we assume that the system load is constant load with a fixed power factor ($P = 2Q$), and we have infinite exciter size.

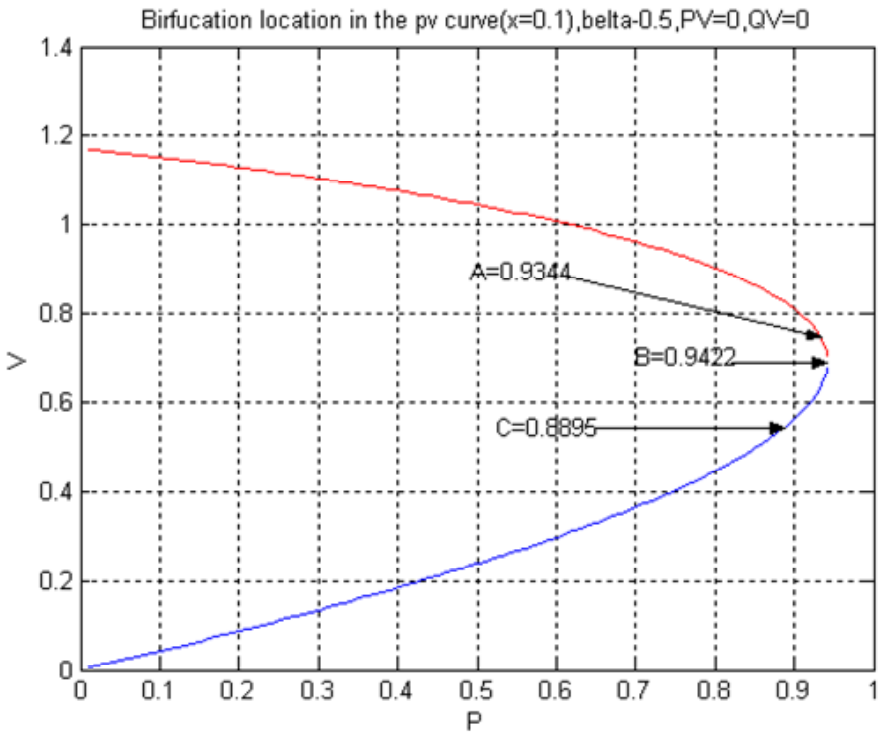

Figure II-3 Bifurcation locations on PV curve

In figure II-3, we found Hopf bifurcation point A in the upper part of the PV curve, which determines dynamic stability margin. We can see that P_A is smaller than the static margin P_B (here $P_B = P_{\max}$). Here $P_{A,B,C}$ denote active power load associated with bifurcation points A, B and C respectively.

When the system reaches Hopf bifurcation point, the system will no longer hold its stability in case there is a small disturbance, which will be demonstrated by time domain simulation with the test system.

Here we will start simulation at equilibrium point $P = 0.934$, and with a small disturbance of $\Delta P = 0.002$, we have time domain responses of voltages shown in Figure II-4.

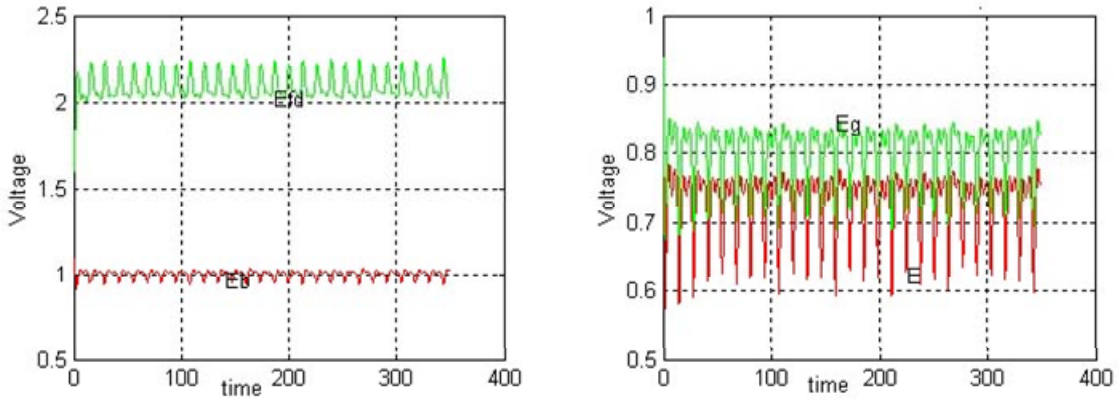

Figure II-4 Voltage responses in time domain

In above figure, we can see that when the system approaches Hopf point, the system has a severe oscillation and can not keep the stability with small disturbance, thus we know that the dynamic margin A is more meaningful than the static margin B point, so we need the bifurcation analysis to find it.

Now we will analyze the impacts of different controllers of the regulator on voltage stability of the test system. Based on it, we will give a method to allocate the responsibility of the voltage collapse.

3.2.1 P- regulator

Here we will show how K_P impact on the locations of bifurcation points:

When $K_P = 2.5, 5 \text{ or } 10$, the locations of the bifucation A, B and C and the eigenvalues of reduced Jacobian matrix J_r are shown in Figure II-5~II-7:

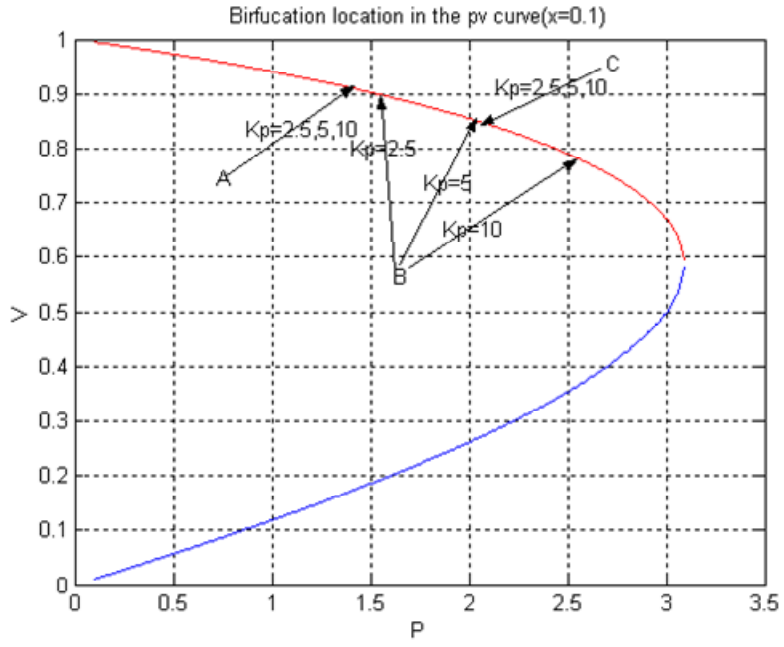

Figure II-5 The locations of the bifurcations when $K_P = 2.5, 5 \text{ or } 10$

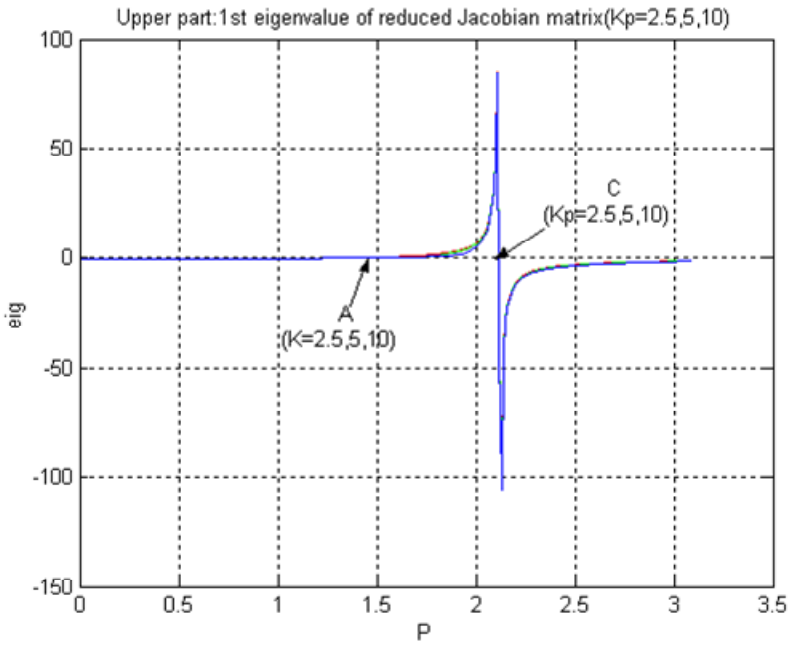

Figure II-6 The eigenvalue which is slightly influenced by K_P

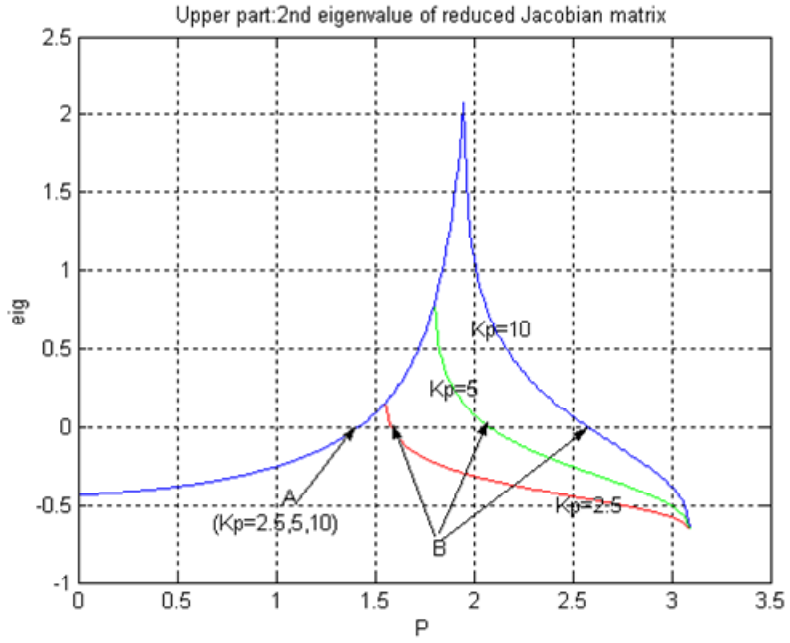

Figure II-7 The eigenvalue which is strongly affected by K_P

By our calculation, with constant load and the infinite exciter size, bifurcation point C is only determined by transmission system, it will not be influenced by the parameters of controller. However, point B will vary with the change of K_P. When $K_P \to \infty$, $P_B \to P_{\max}$; when $K_P > 5.25$, $P_B > P_C$; when $K_P = 1.895$, $P_B \approx P_A$; when $K_P < 1.895$, bifurcation point A will disappear; and when $K_P \to 0$, $P_B \to 0.735$.

In Figure II-6, note that K_P has little influence on one of the eigenvalues (denoted by EigT), while in Figure II-7, K_P has a substantial impact on the other eigenvalue (denoted by EigC).

When $K_P = 1.8$, FigII-10 shows the location of B and C in PV curve. Note that A disappeared. From Figures II-5 to II-10 we can see that the eigenvalue EigT is strongly related to the load flow, while the eigenvalue EigC is strongly influenced by the controller.

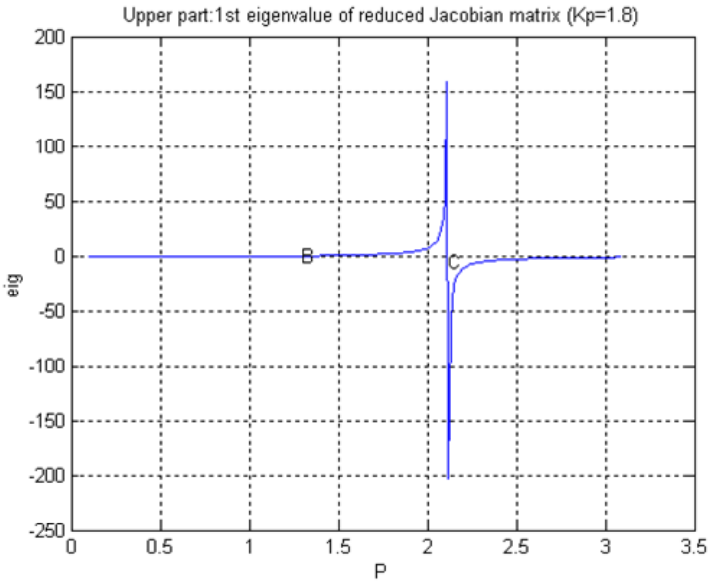

Figure II-8 The eigenvalue EigT ($K_P = 1.8$)

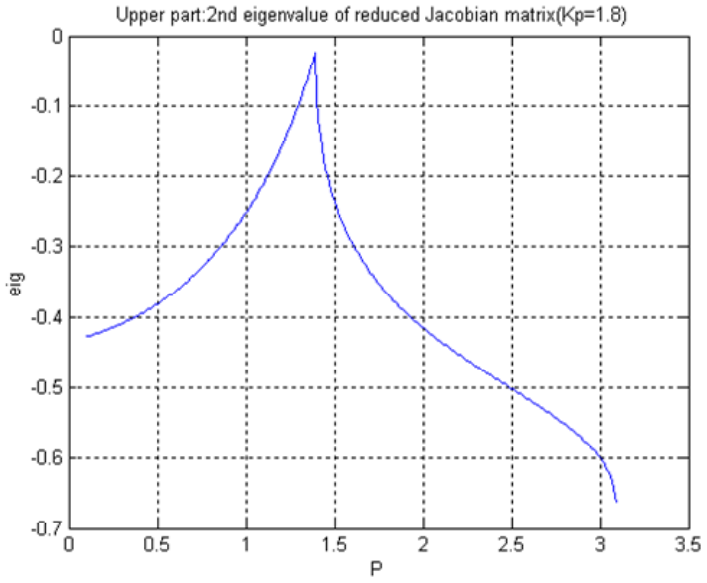

Figure II-9 The eigenvalue EigC ($K_P = 1.8$)

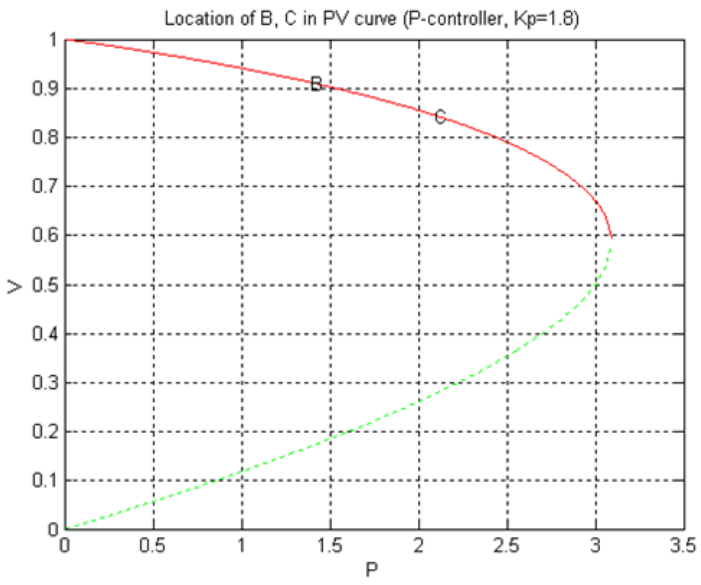

Figure II-10 The location of B and C when $K_P = 1.8$

We can conclude that there are three basic patterns:

- $P_A < P_B < P_C$. When $P \in (P_A, P_B)$, both Re($EigC$) and Re($EigT$) are positive; when $P \in (P_B, P_C)$, only Re($EigT$) is positive.
- $P_A < P_C < P_B$. When $P \in (P_A, P_C)$, both Re($EigC$) and Re($EigT$) are positive; when $P \in (P_C, P_B)$, only Re($EigC$) is positive.
- Bifurcation point A disappears and $P_B < P_C$. Only Re($EigT$) is positive when $P \in (P_B, P_C)$.

3.2.2 PI- regulator

Here the parameters of PI-regulator is given as $K_P = 2.5, T_I = 5.0$ or $T_I = 20$. Using equations (2.6), (2.8) and (2.10), we can calculate three eigenvalues of the reduced Jacobian matrix J_r. We found that one eigenvalue of J_r is always located in left side of imaginary axis, and the other two eigenvalues will across imaginary axis with load increase. One of

these two eigenvalues is strongly affected by parameters of PI-controller, K_P and T_I, especially by T_I, so similarly, we denote it as EigC, and the other eigenvalue is almost independent with controller, so we denote it as EigT. Three bifurcations, type A, B and C, are also found with PI-controllers.

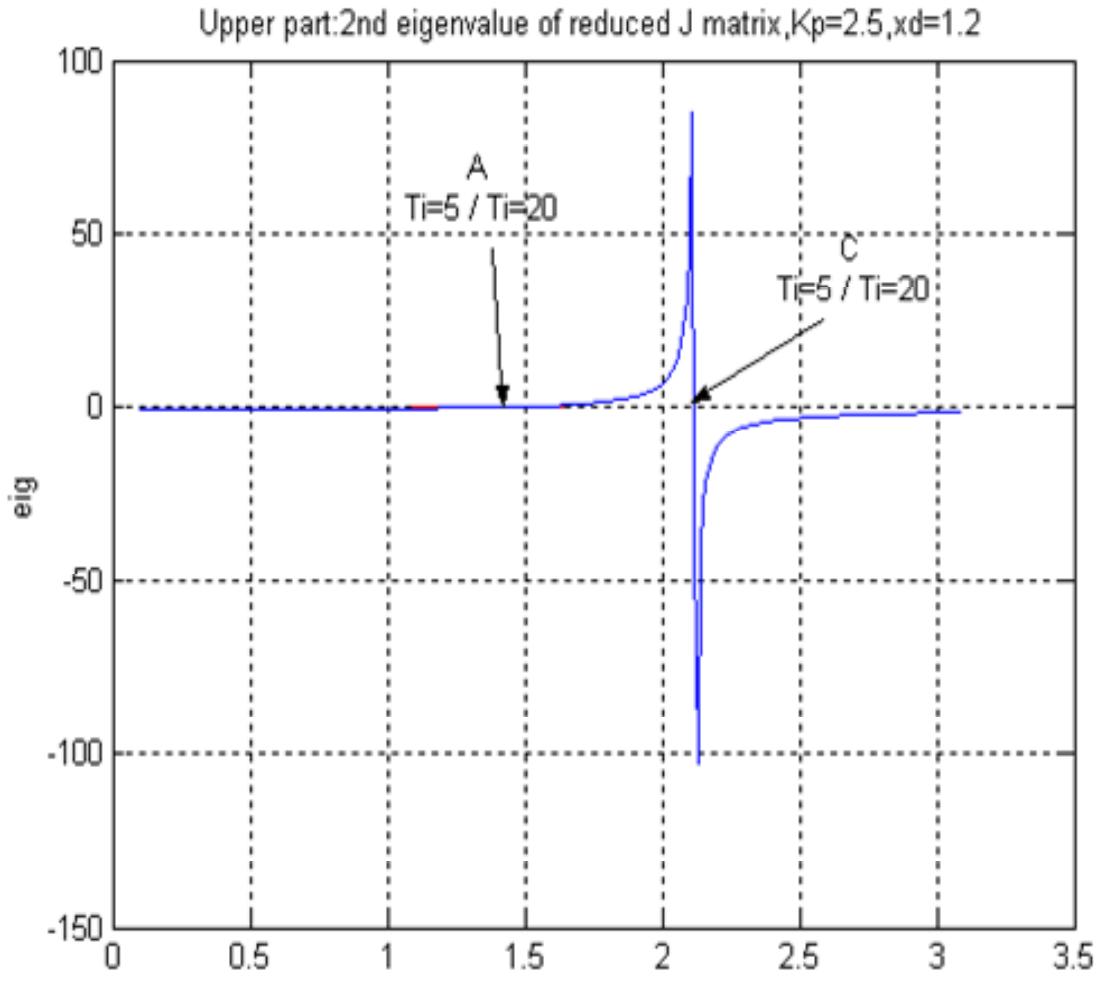

Figure II-11 The eigenvalue Eig T(PI-controller)

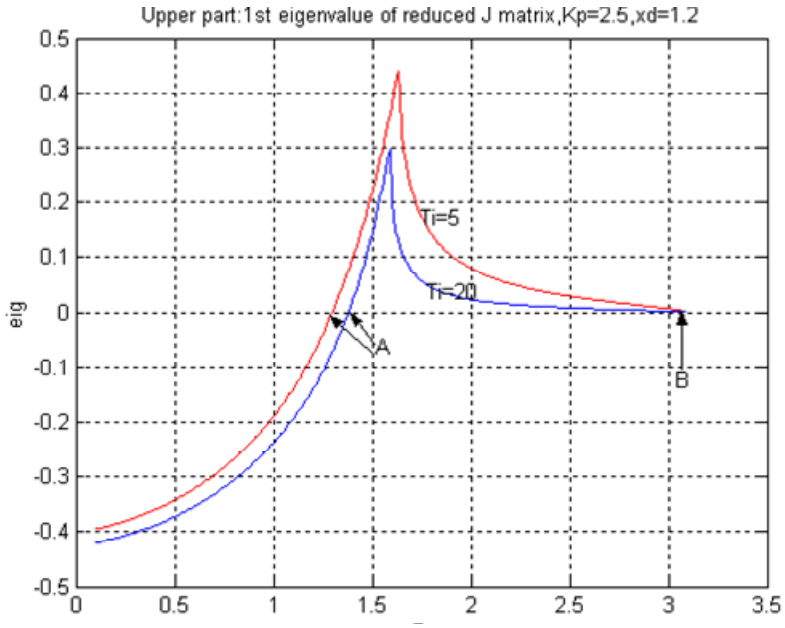

Figure II-12 The eigenvalue EigC (PI-controller)

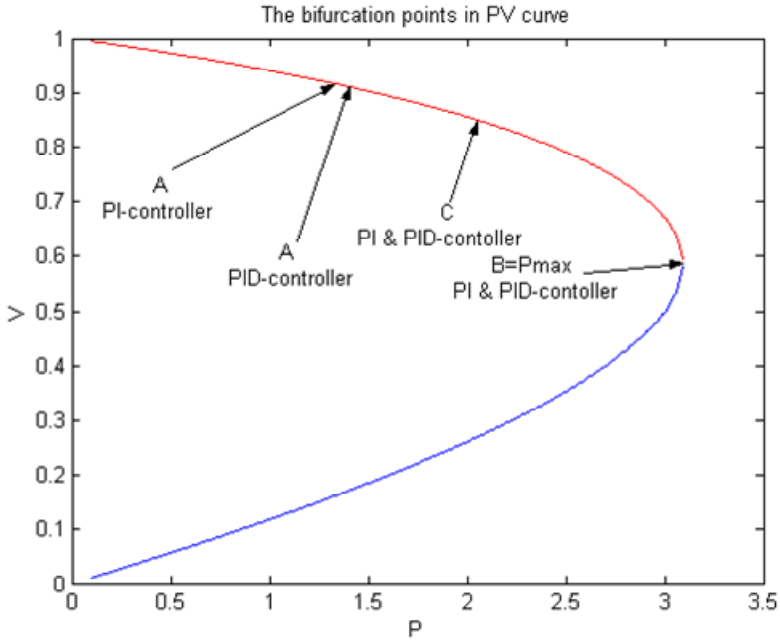

Figure II-13 The location of A, B and C in PV curve for a PI/PID controller

From Figure II-11~II-13, we can conclude that PI controller behaves very similar to the rescheduled P-controller as $K_P \to \infty$. When $P \in (0, P_A)$, all eigenvalues are negative; when $P \in (P_A, P_C)$, both Re($EigC$) and Re($EigT$) are positive; when $P \in (P_C, P_B)$, only Re($EigC$) is positive. Accordingly, it follows the second basic pattern as described in II.3.2.1.

3.2.3 PID-controllers in a regulator

Parameters of PID-controller are set as $K_P = 2.5, T_I = 5.0, K_D = 1.0, T_D = 0.01$ or $T_D = 0.005$, it behaves similar to a PI-controller as shown in Figure II-13. This also follows the second basic pattern as discussed in II.3.2.1.

Through above obeservations, given the constant load and infinite exciter size, we can conclude that the three basic ordering patterns of bifurcation points A, B and C as discussed in II.3.2.1 are generally true for all controllers which can keep $E_G \equiv E_r$. Our experience indicates that no other ordering of A, B and C is possible. Accordingly, we can draw the conclusion:

- $P_A < P_B < P_C$. When $P \in (P_A, P_B)$, both Re($EigC$) and Re($EigT$) are positive; when $P \in (P_B, P_C)$, only the Re($EigT$) is positive. From the parameter analysis, we can conclude that the voltage collapse is due to both controller and transmission when $P \in (P_A, P_B)$. The voltage collapse is only caused by transmission part when $P \in (P_B, P_C)$. In this case, $[P_A, P_C]$ is the unstable area, and bifurcation point A determines the dynamic stability boundary.
- $P_A < P_C < P_B$. When $P \in (P_A, P_C)$, both Re($EigC$) and Re($EigT$) are positive; when $P \in (P_C, P_B)$, only Re($EigC$) is positive. From the parameter analysis we can conclude that the voltage collapse is due to both controller and transmission when $P \in (P_A, P_C)$. The voltage collapse is caused by controller when $P \in (P_C, P_B)$. In this case, $[P_A, P_B]$ is the unstable area, and A determines the dynamic stability boundary.

- ❖ Bifurcation point A disappears and $P_B < P_C$. Only Re($EigT$) is positive when $P \in (P_B, P_C)$. Thus, the voltage collapse is only due to transmission when $P \in (P_B, P_C)$. In this case, $[P_B, P_C]$ is the unstable area, and bifurcation point B determines the dynamic stability boundary.

In conclusion, the tuning of the control parameters will influence the locations of bifurcation points and thus the dynamic stability margin of the system. And our observation may also benefit the design of power system.

Following the same argument, we can also unbundle the voltage collapse responsibility of the system by studying how the parameters of the three parts of the system (generator, controller and transmission part) affect the bifurcation patterns:

3.2.4 Impacts of other system parameters on voltage stability

The influence of the excitation system:

As discussed before, impacts of K_P in rescheduled P-controller are summarized as follows. K_P does not affect C, but have impacts on B and A. When $K_P \to \infty$, $B \to P_{\max}$; and when $K_P \to 0$, $B \to 0.735$; when $K_P = 1.895$, $P_A \approx P_B$; when $K_P < 1.895$, A disappear; when $K_P = 5.25$, $P_C \approx P_B$.

For PI and PID controllers, we did simulation with different parameters of the controller and the result summarized in table II-1: (Note: for PI and PID controller, A determines dynamic stability margin, and the unstable area is $[P_A, P_B]$)

From table II-1.A, we can see that K_P only has influence on A, which is different from P-controller. Here B and C remain the same. (With a constant power factor, it can be easily approved that B always appears at $P_{\max}$ when an I-controller is used in the regulator.) P_A will increase with bigger T_I and bigger K_D. T_D has little influence on A, but too large or too small T_D will decrease P_A. All parameters of PI and PID controllers have no impacts on B and C.

Table II-1.A Impacts of other parameters

X_d	K_P	T_I	K_D	T_D	A	B	C
1.2	2.5	1	0	0	P=0.98	P=3.09	P=2.115
		2			P=1.167		
		4			P=1.273		
		3			P=1.236		
			1	0.001	P=1.404		
				0.1	P=1.4105		
				0.01	P=1.415		
			3		P=1.416		
	2		0		P=1.1625		
	3				P=1.2839		
	0				P=0.5		
		8			P=0.648		
		15			P=0.685		
		100			P=0.726		

The location of bifurcation point C is independent of the controller as long as the voltage regulator has enough excitation capacity to keep terminal voltage at rated value.

Now we investigate the influence of the $T_{d0}^{'}$ on the stability margin: (In this case the regulator is rescheduled P-controller, $K_P = 2.5$)

Table II-2.B Impacts of $T_{d0}^{'}$

$T_{d0}^{'}$	Pmax	P_A	P_B	P_C
3	3.09	1.248	1.584	2.116
5	3.09	1.416	1.584	2.116
7	3.09	1.534	1.584	2.116

From table II-1.B we can see that $T_{d0}^{'}$ will influence the A point, but it have no influence on B and C. We verified the fact for all three controllers. P_A will increase with bigger $T_{d0}^{'}$, that means the dynamic stability margin will increase with bigger $T_{d0}^{'}$. However, the size of the exciter will limit the range of E_{fd} and thus the voltage regulation range [13].

The influence of generator reactance:

Now we investigate the influence of the x_d on the stability margin:

With rescheduled P-controller

Table II-3.A Impacts of x_d with P-controller

x_d	$P_{\max}$	P_A	P_B	P_C
1.2	3.09	1.416	1.584	2.116
0.3	3.09	2.016	2.719	2.116

With PI-controller

Table II-4.B Impacts of x_d with PI-controller

x_d	$P_{\max}$	P_A	P_B	P_C
1.2	3.09	1.297	3.09	2.116
0.3	3.09	2.005	3.09	2.116

With PID-controller

Table II-5.C Impacts of x_d with PID-controller

x_d	$P_{\max}$	P_A	P_B	P_C
1.2	3.09	1.415	3.09	2.116
0.3	3.09	2.0158	3.09	2.116

Through the table II-2.A, B and C, we can see that x_d has influence on A point; and if we use P-controller, it also influence the B point. It implies that the dynamic stability margin will increase with smaller x_d. However, C is independent of x_d.

The parameters of the transmission system:

Now we investigate how x impacts stability margin:

With rescheduled P-controller

Table II-6.A Impacts of x with P-controller

x	Pmax	A	B	C
0.1	3.09	1.416	1.584	2.116
0.12	2.58	1.360	1.509	1.966

With PI-controller

Table II-7.B Impacts of x with PI-controller

x	Pmax	A	B	C
0.1	3.09	1.297	3.09	2.116
0.12	2.58	1.2506	2.58	1.966

With PID-controller

Table II-8.C Impacts of x with PID-controller

x	Pmax	A	B	C
0.1	3.09	1.415	3.09	2.116
0.12	2.58	1.3589	2.58	1.966

Through analysis of table II-3.A, B and C, we see that x has influence on all of the three bifurcation points. The dynamic stability margin will increase with smaller x.

4. Conclusion

This chapter attempts to allocate the contribution of voltage stability to generator owners, transmission owners and excitation control owners, thus, an investment award system can be built to award investments on the corresponding power infrastructure. We showed that how the parameters of the three parts of the system (generator, controller and transmission) affect the bifurcation patterns, which can help us to design and optimize the system.

Please note that, all conclusions drawn in this chapter are based on a primitive system and several typical regulators. It is hard to rigorously verify these conclusions with large systems due to huge computation cost associated with eigenvalue analysis for large systems, and that is why a new comprehesive numerical analysis scheme will be proposed in chapter IV and V. However, as demonstrated in next chapter, our conlusions based on a typical two-bus system could be very useful for excitor design, especially when we try to optimize the excitor size to make the best use of a generator.

CHAPTER III

IMPACT ANALYSIS OF EXCITER SIZES ON VOLTAGE STABILITY

1. Introduction

So far, in deregulated environment, transactions are only paid by the real power amount and no incentive was given to install regular exciter sizes; the industry tends to reduce exciter size to save cost. In this chapter, we show that limits of the power system components, induced by the size of the exciter, limits of the stator (armature) current, the field current, and overheating limits of the stator core, etc., all have a influence on the voltage stability, especially exciter size. An algorithm to choose proper exciter size is developed in this chapter. The algorithm aims to maximize the loadability of system to fully utilize the generator.

2. The influence of physical limits on the voltage stability margin of the system

Various constraints on the system components, which will have a great influence on the voltage stability margin, will be analyzed here. Similarly as in Chapter II, three widely used regulators—adaptive P-regulator (E_{fd}^0 is rescheduled to keep $E_G \equiv E_r$), PI-regulator and PID-regulator, will be still considered in this chapter. We also consider a much weaker non-adaptive P-regulator that has a constant E_{fd}^0 .

2.1 Over excitation limit

When an exciter hits its upper limit, its output, E_{fd} , can no longer responds to the change of the voltage. E_{fd} will be saturated at $E_{fd\_\max}$. In this case, only two kinds of bifurcations are observed, SNB and SIB (still denoted by B and C points in PV curve respectively). This is also the case for the weaker P-regulator without rescheduling. On the other hand, for normal situations, where E_{fd} is within its limit and the voltage regulator is able to maintain $E_G \equiv E_r$, HB (still denoted by A point in PV curve) may also appear. As discussed in

Chapter II, in normal case, we may have three kinds of bifurcations (A, B, and C) located in PV curve.

We use the simple system shown in Figure III-1 to demonstrate our analysis. It is the same test system used in Chapter II, and the regulator used here is the rescheduled P-regulator. We also tested with other regulators, and found that the results are all included in the two basic patterns we got from the rescheduled P-regulator. Thus, without loss of generality, all the analysis in this chapter will be based on results associated with rescheduled P-regulator.

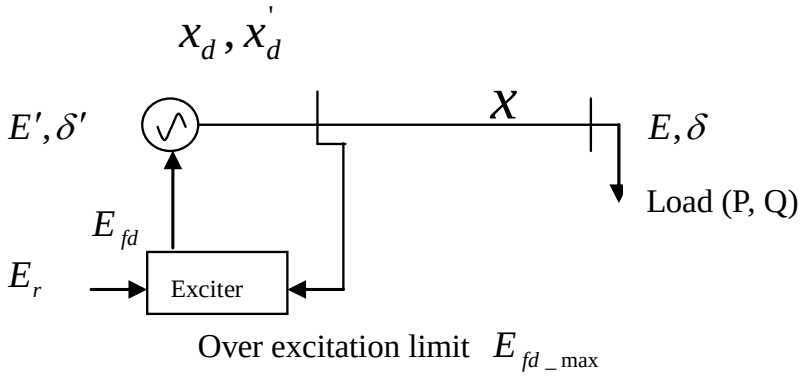

Figure III-1 Test system with over excitation limit

The parameters of above system are listed below. Note that all cases shown in this chapter will use the same system parameters unless specified otherwise.

$T_{d0}^{'} = 5, T = 1.5, x = 0.1, x_d^{'} = 0.2, Q = 0.5P, E_r = 1.0$

To demonstrate our analysis, two PV curves, with different length of nose, are drawn in Fig 2 and 3. The longer nosed curve represents an ideal case that has a big enough exciter size, in which the limit will never be reached. The shorter nosed curve denotes the case that the regulator is saturated, which has a constant input E_{fd} as the exciter hit its limit. The

system is first following the longer nosed curve since the regulator is working within its limit. Then when the exciter hits its limit, the system is moving along the shorter nosed curve. The switching point is D.

In Figure III-2 and III-3, we denote the saddle node point and the singularity point as B1 and C1 in the PV curve with shorter nose of the system that the E_{fd} is saturated. Let the intersection point of the two PV curves be D. Note that C1 always appears at the lower part of the PV curve, B1 appears at the maximum load point $P_{\max}$, and there is no Hopf bifurcation point when E_{fd} is saturated.

Please note that when we have big enough exciter size, the longer nose PV curve and the corresponding bifurcation points A, B and C will not change with the value of the exciter size since as long as the exciter is operated within its capacity, the system behavior will remain the same for different exciter sizes. With the same example shown in Figure III-2, we change the exciter size from 50 to 25 (both are big enough), and we found that the PV curve remains the same, and the corresponding A, B and C also remain on the same locations.

Comparing the PV curves and the locations of the bifurcation points for these two cases, we found two basic patterns, which are shown in Figure III-2 and III-3 respectively.

We describe the two possible patterns, depending on the location of D, as follows:

Pattern 1, D is located at the lower part of the shorter nose PV curve.

In this pattern, there are several possibilities for the dynamic stability margin: (For each point, say D, P_D is used to denote the real power load at point D.)

- $P_A < P_D$, then the dynamic stability margin is P_A (If A disappears and $P_B < P_D$, P_B is the dynamic stability margin)
- $P_A > P_D$ and $P_{C1} < P_D$, then the dynamic stability margin is P_D.
- $P_A > P_D$ and $P_{C1} >= P_D$, then the dynamic stability margin is P_{C1}.

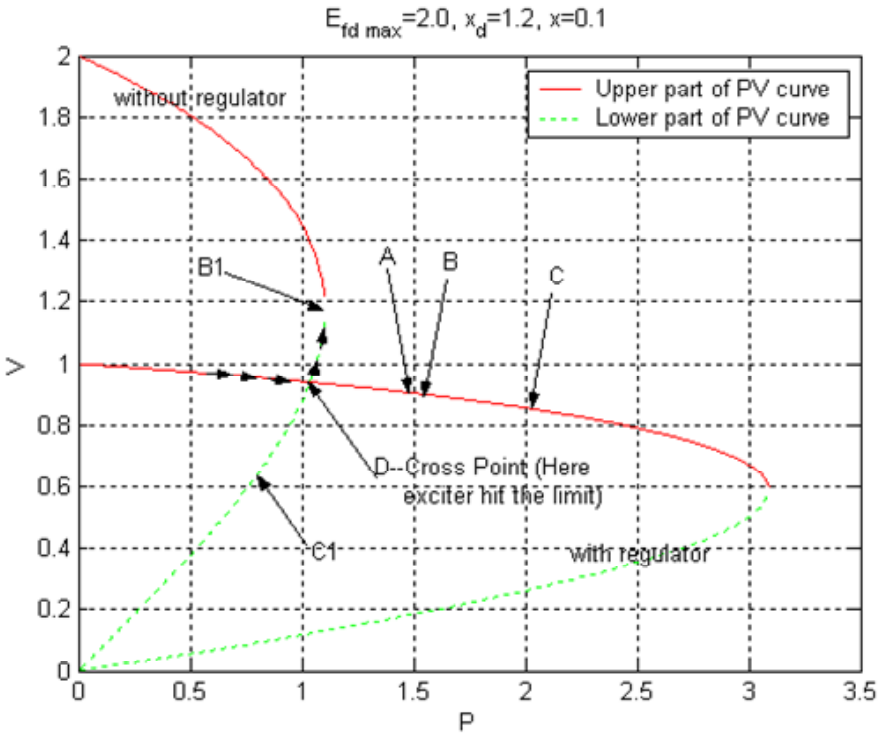

Figure III-2 The general pattern 1

For the steady stability margin, there are also several possibilities:

- $P_C < P_D$, then the steady-state margin is P_C.
- $P_C > P_D$ and $P_{C1} < P_D$, then the steady-state margin is P_{B1}.
- $P_C > P_D$ and $P_{C1} >= P_D$, then the steady-state margin is P_{C1}.

To our experience, $P_{C1} >= P_D$ seldom appears. For our example, it appears with a short transmission line.

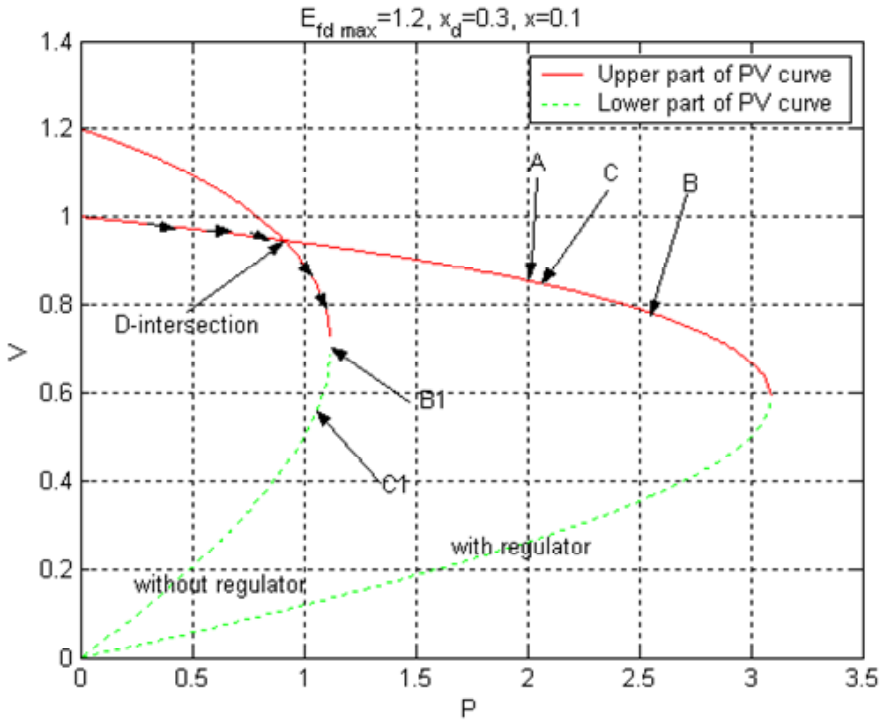

Figure III-3 The general pattern 2

Pattern 2, D is located at the upper part of the PV curve with shorter nose.

In this pattern, there are also several possibilities for the dynamic stability margin:

- $P_A < P_D$, then the dynamic stability margin is P_A (If A does not exist, then P_B is the dynamic stability margin)
- $P_A > P_D$, then the dynamic stability margin is P_{B1}

For the steady stability margin:

- $P_C < P_D$, then the steady-state margin is P_C
- $P_C > P_D$, then the steady-state margin is P_{B1}

The main system differences that cause different patterns as shown in Figure III-2 and Figure III-3, are that there is a bigger x_d and a bigger $E_{fd\_\max}$ in Figure III-2. Note that point D in Figure III-2 is nearly in the same location as the B1 in Figure III-2. It illustrates that a bigger x_d needs a larger exciter size to keep the same voltage stability margin for a given transmission line. We also found that longer transmission line needs larger exciter size to keep the same voltage stability margin for a given x_d.

The regulator used in Figure III-2 and Figure III-3 is a P-regulator with a rescheduled E_{fd}^0. For this type of P-regulator and PI, PID regulators, bifurcation points A, B and C are all located in the upper part of the PV curve and C point will stay at the same location for a given x [37]. For rescheduled P regulator, B point will go further down to $P_{\max}$ with $K_P \to \infty$, while A and B will go further up with smaller K_P. A will disappear and P_B may less than P_D with $K_P \to 0$. For PI or PID regulator, P_B will always equal to $P_{\max}$ and A will not disappear with $K_P \to 0$. The location of A will change slightly with K_P for a PID regulator. However, for a PI regulator, A will go further up with smaller K_P and P_A may become less than P_D [37].

Based on our analysis, we found that in the above two basic patterns, the situations $P_A < P_D$ or $P_B < P_D$ only appear when the regulator is not well tuned (e.g. K_P is too small), or the transmission line is too long. In this case, dynamic analysis is necessary, and P_A is the determining stability margin because that P_A is always less than P_C [37]. We know that A is mainly caused by the regulator for a given transmission line [37], and regulator is responsible for the voltage collapse in this case. We should notice that steady-state analysis is no longer good enough in this case, because that the real stability margin is determined by A point.

To our experience, in most cases we find that $P_A > P_D$, $P_C > P_D$ and $P_{C1} < P_D$, and thus P_D is usually the determining stability margin for basic pattern 1, while P_{B1} is the

determining stability margin for basic pattern 2. Both B1 and D can be found by the steady-state method, and steady state analysis is good enough here. For examples in Figure III-2, P_D is the stability margin; in Figure III-3, P_{B1} is the stability margin. For a given transmission line, P_D and P_{B1} is determined by the size of the exciter, and thus the exciter is mainly responsible for the voltage collapse in this case.

2.2 The influence of other limits on the system

Here we focus on the physical limits of the generator shown in Figure III-4 [22, 26] and the relationship of the above bifurcation points and these physical limits:

• Section E–F–G of the curve shows limits due to stator (armature) current. This section is a portion (arc) of a circle that has its center in the origin of – (MW-Mvar) coordinates of the generator.

• Section D–E of the curve is due to field current limit. This is a portion (arc) of a circle that has its center on the Y axis (Mvar) and shifted from the origin by a value proportional with the machine short-circuit ratio (SCR).

• Section H–G of the curve shows limit due to over-heating of the stator core end when the generator is under-excited in conditions of leading PF, when the generator is absorbing reactive power.

Accordingly, we observe three basic patterns based on the locations of A, B and C points relative to the boundary D-E-F-G-H determined by the physical limits:

i) Bifurcation points A, B and C are outside of the boundary D-E-F-G-H, and thus the boundary determines the real stability margin, and the maximum real power loadability point is F.

To our experience, when the transmission line is too long (x is very large) or the regulator is too weak (for example, K_P is very small, or we use P-regulator with constant E_{fd}^0), the power values associated with bifurcation points A, B and C may become less than the power at point F. Then A determines the dynamic stability margin (for cases that we do

not have A point, then B point will determine the dynamic stability margin), and C determines the steady-state stability margin (for the special case that P-regulator has a constant E_{fd}^{0}, B determines the steady-state stability margin). Thus, we have patterns ii and iii:

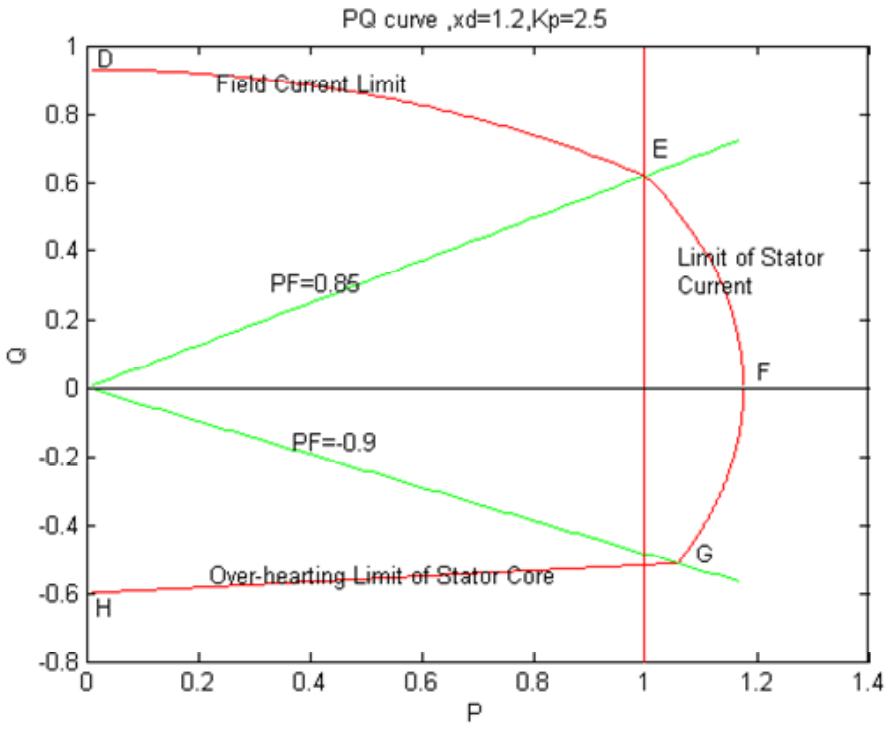

Figure III-4 The limits of the generator

ii) Bifurcation point A or B appear inside the boundary, but C is outside of the boundary, thus P_F is the steady-stage stability margin. The point A or B (when A disappears) will determine the dynamic stability margin.

iii) Bifurcation points A, B and C appear inside the boundary, and the point A or B will determine the dynamic stability margin; similarly, bifurcation point C or B will determine the steady-state stability margin.

Note: In case i), the steady-state analysis is good enough, but in case ii) and iii), dynamic analysis is needed.

In basic pattern i), the field current limit determines that how much reactive power the generator can supply-- $Q_{\max}$; The limit of stator current determines that how much real power the generator can supply-- $P_{\max}$; The Over-heating limit of the stator core determines that how much reactive power the generator can absorb-- $Q_{s-\max}$. But for pattern ii) and iii), it becomes much more complex. These maximum values are no longer be determined by the physical limits of the generator. Instead, they are determined by the regulator type, exciter size and the length of the transmission line.

Our experience shows that with the three widely used regulators, the basic pattern i) usually appears under the conditions that the regulator is not too weak, the size of exciter is not too small and the transmission line is not too long. For these cases, the steady-state and the dynamic stability margin is PF, and the limit of stator current determines the stability margin. But for the weak type of P-regulator (with constant E_{fd}^{0}), the basic pattern iii) usually appears, even when the transmission line is not very long. It also means that this type of P-regulator is weaker than those other three types of regulators as we discussed earlier. With this type of regulator, $Q_{\max}$ is no longer determined by the limit of the stator current, but by the regulator; while the maximum value of the reactive power that the generator can absorb is still usually determined by the over-heating limit of the stator.

3. An algorithm to choose the optimal exciter size

In this section, the test system in Figure II-2 is still used to demonstrate how to apply eigenvalue based bifurcation analysis in voltage stability analysis, and thus to allocate responsibility of voltage collapse.

3.1 The objective of the algorithm

The size of the exciter has a great influence on the voltage stability as shown in Figure III-2 and III-3, the longer nosed curve represents an ideal case that has a big enough exciter size. The shorter nosed curve has a constant input (E_{fd_size}) for the exciter as the exciter hit its limit. Our problem is formulated as follows: Given the system shown in Figure III-1 and the generator limits shown in Figure III-4, how to decide an appropriate exciter size that can fully utilize the capacity of the generator. This algorithm is developed to solve this problem.

Notation: In the algorithm, the exciter size is denoted by E_{fd_size}. We denote the lower limit of the desired bus voltage as $E_{low\_\lim}$, and we denote the corresponding load at the PV curve assuming the exciter can be unlimited regulated to keep $E_G \equiv E_r$ as $P_{low\_\lim}$. Point F shown in Figure III-2 is determined by the limit of the stator current, which denotes the critical point that the generator can be operated at. Point D shown in Figure III-2 and III-3 is the intersection of the two PV curves. At this point, the exciter hits its limit and the generator bus changes from a PV bus to a PQ bus. For each point, say D, we associate D with P_D (Q_D) and E_D as the real (reactive) loads and the voltage of the load bus at the point D.

3.2 Fundamental principle of the algorithm

Our algorithm is based on the principle that we should choose exciter size (E_{fd_size}) to make the best use of the generator. We should design in such a way that the generator bus still functions as a PV bus when the generator operates at the point F. Thus, we choose E_{fd_size} to make $P_D \geq P_F$. At the same time, we should guarantee that the E_D should be greater than the lower limit ($E_{low\_\lim}$), which requires that $P_D \leq P_{low\_\lim}$. Thus we should choose E_{fd_size} to satisfy $P_D = \min(P_F, P_{low\_\lim})$.

Accordingly, we decomposed our algorithm to the following two steps:

1st step: Determine D by *x*, F and $E_{low\_\lim}$.

From *x*, F and $E_{low\_\lim}$, we will determine the D point (P_D, Q_D and E_D). For an ideal exciter, which can regulate $E_G \equiv E_r$, we can calculate the PV curve by equation:

$$0 = E_G{}^2 E^2 - (xP)^2 - (xQ + E^2)^2 \qquad (3.1)$$

Substituting $E = E_{low\_\lim}$ into equation (3.1), we can calculate $P_{low\_\lim}$. Then we choose $P_D = \min(P_F, P_{low\_\lim})$, and we can obtain E_D by substituting P_D and Q_D back to equation (3.2).

2nd step: Determine E_{fd_size} by $x, x_d, x_d^{'}$ and D point.

Note that we can find $E_{fd\_\max}$ by making the PV curve without regulator pass through the D point. We can calculate the PV curve by equation (3.3) and (3.4).

$$0 = E'^2 E^2 - (x'P)^2 - (x'Q + E^2)^2 \qquad (3.2)$$

$$0 = \frac{1}{T_{d0}'} \cdot \left[-\frac{x + x_d}{x'} E' + \frac{x_d - x_d'}{x'} \cdot \frac{(E^2 + x'Q)}{E'} + E_{fd\_size} \right] \qquad (3.3)$$

Substitute P_D, Q_D and E_D into (3.2)

$$\Rightarrow E_D{}^{'} = \frac{\sqrt{(x'P_D)^2 + (x'Q_D + E_D{}^2)^2}}{E_D} \qquad (3.4)$$

Substitute (3.4) and P_D, Q_D and E_D into (3.3), we can get:

$$E_{fd\_size} = \frac{x + x_d}{x'} \frac{\sqrt{(x'P_D)^2 + (x'Q_D + E_D^2)^2}}{E_D} - \frac{x_d - x'_d}{x'} \frac{(E_D^2 + x'Q_D)E_D}{\sqrt{(x'P_D)^2 + (x'Q_D + E_D^2)^2}} \qquad (3.5)$$

Note that $x' = x + x_d'$

3.3 Verifying this algorithm with large systems

So far, this algorithm is developed for the simple system shown in Figure III-1. However, we can use P_G, Q_G instead of P_D, Q_D and *x* to estimate the exciter size. Thus the algorithm will be possible to be extended to large systems.

For a large system, we can specify the sum of the active load as $\sum_{i=1}^{N} P_{Fi}$. Here, N is the number of the generators in the system. We calculate the power flow at the most heavily loaded situation, and then we know the P_G and Q_G for each generator at the most stressed situation.

Then, we use another simplified power flow equation:

$$E'^2 E_G^2 - (x_d' P_G)^2 - (x_d' Q_G + E_G^2)^2 \qquad (3.6)$$

and the exciter equation :

$$0 = \frac{1}{T_{d0}'}\left[-\frac{x_d}{x_d'} E' + \frac{x_d - x_d'}{x_d'} \frac{(E_G^2 + x_d' Q_G)}{E'} + E_{fd\_size} \right] \qquad (3.7)$$

Knowing E_G and $P_G + jQ_G$, by (3.6) ~(3.7) we can get:

$$E_D' = \frac{\sqrt{(x_d' P_G)^2 + (x_d' Q_G + E_G^2)^2}}{E_G} \qquad (3.8)$$

And

$$E_{fd\_size} = \frac{x_d}{x_d'} E_D' - \frac{x_d - x_d'}{x_d'} \frac{(E_G^2 + x_d' Q_G)}{E_D'} \qquad (3.9)$$

From the equation (3.8) and (3.9), we can estimate the exciter size by P_G and Q_G instead of P_D, Q_D and *x*.

3.4 Demonstrating example

Based on above analysis, we can decouple a big system and use our algorithm to design the exciter size for each generator. Here the load flow result has decoupled one of the generators from the remaining system, and the problem becomes:

Given $E_r = 1,\ P_F = 1.2,\ x = 0.1,\ x_d = 1.2,\ x_d^{'} = 0.2$, and $E_{low\_\lim} = 0.9$, how to choose E_{fd_size}? (The power factor of load is constant, $P = 2Q$)

1st step:

Substitute $E_{low\_\lim} = 0.9$ into equation (3.1), then we can get $P_{low\_\lim} = 1.5359$, $P_D = \min(P_F, P_{low\_\lim}) = 1.2$ and $Q_D = 0.6$. Substituting P_D, Q_D into equation (3.1), we can obtain $E_D = 0.9268$

2nd step:

By equation (3.5) and known P_D, Q_D and E_D, we can obtain E_{fd_size} = 2.22. From load flow analysis, we got P_G =1.2, Q_G =0.80953. By equation (3.8) we got $E_D^{'}$ = 1.18643, then by equation (3.9) we can get E_{fd_size} = 2.22. The result is the same as we obtained from equation (3.5). This confirms that we can estimate the exciter size by P_G, Q_G, instead of P_D, Q_D and *x*.

Now we use E_{fd_size} = 2.22 as the exciter size to simulate the system, the result is shown in figure III-5.

From the Figure III-5, we can see that P_D =1.2 and $E_D = 0.9268 > 0.9$ are exact the same as the result we obtained by our algorithm. It shows that our algorithm is an easy and credible way to determine the exciter size.

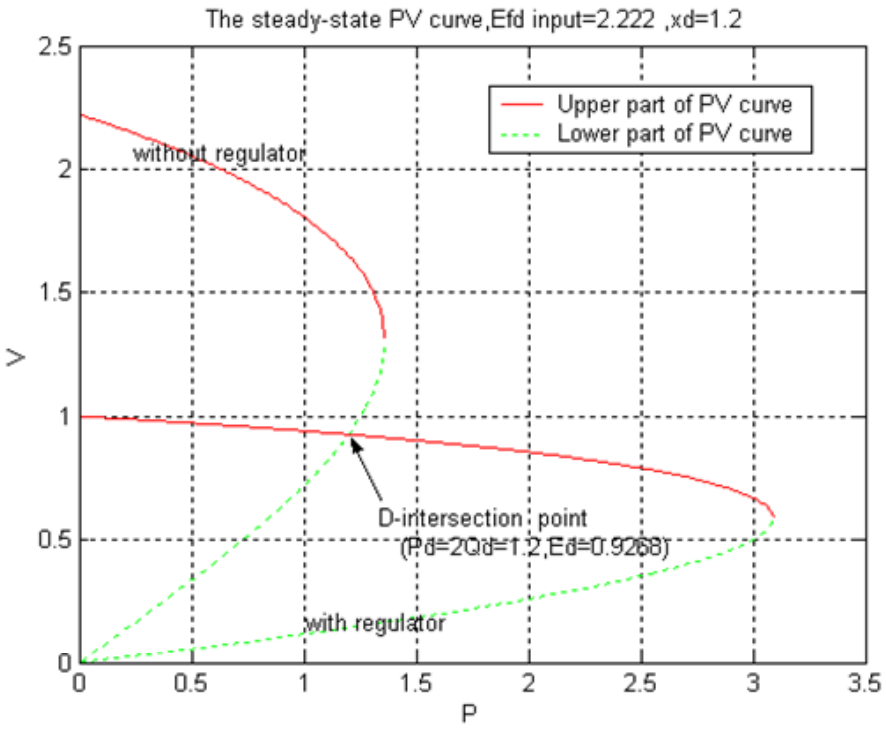

Figure III-5 The result of our example

4. Conclusion

In this chapter, we analyzed the influence of physical limits and controller types on the voltage stability margin of the power system, which will help us to design the system and allocate the responsibility of the voltage collapse. Based on these work, we developed an algorithm to choose the right exciter size to fully utilize the capacity of the generator.

A simple two-bus system is used to verify our approach, which shows our analysis is reasonable and credible. We also extend the algorithm to large systems.

CHAPTER IV

OPTIMAL LOAD ADJUSTMENT FOR FAST DYNAMIC VOLTAGE STABILITY MARGIN ESTIMATION USING EXPLICIT RK METHODS

1. Introduction

1.1 Background and objectives

Traditionally, static methods, Continuous Power Flow (CPF) [9] and the Quasi-Steady-State (QSS) approximation [2] of long-term dynamics, are used for estimating the loadability margin. However, both of them may not be obvious to account for discrete-type devices whose final state depends on the system time evolution [2]. Moreover, there are some situations where the existence of equilibrium does not guarantee a stable system behavior [2]. For example, Chapter II and paper [18] demonstrated an example showing a system encounter a Hopf bifurcation point before it reaches a saddle node.

Dynamic analysis methods, such as eigenvalue based bifurcation analysis and time domain simulation, have higher modeling accuracy than static methods. With dynamic analysis, it is possible to study other instability mechanism than the loss of equilibrium captured by static methods. As demonstrated in Chapter II and III, by solving for equilibrium manifold as load changes and calculating corresponding eigenvalues of reduced Jacobian matrix, one can accurately locate dynamic voltage stability margin. Although eigenvalue based bifurcation analysis is accurate and gives us insights about the dynamic behavior of the system, eigenvalue calculation is very complex and time consuming, and more importantly, the computation cost will further increase drastically with increase of system size. Its heavy computation burden makes it very difficult for large system applications. Some industrial grade software, i.e., Eurostag, can perform eigenvalue analysis along its numerically simulated trajectories. However, our experience indicates that the obtained loadability margin may not be accurate since the simulated trajectories cannot be guaranteed to be around the equilibrium manifold and thus the small disturbance

analysis has become meaningless and gives wrong results. For example, with eurostag, if we want to find the dynamic voltage stability margin, we need to arbitrarily set a load increase speed. Simulation trajectories vary with different load increase speeds, and the accuracy of estimated dynamic margin can only be guaranteed by a very inefficient way -- Run simulation with several different load increase ratio till the trajectories no longer exhibit relative big changes with different load increase speeds, then people can claim that they have found the structural unstable, which should be independent with the load increase speed by defination of long term dynamic analysis with small disturbance [2]. Therefore, alternative efficient methods need to be developed.

As discussed, a desirable stability margin estimation scheme should satisfy both accuracy and speed requirements. Finding a numerical approach to satisfy these two requirements is our research objective here. In this chapter, a novel numerical approach is proposed based on explicit Runge-Kutta (RK) methods. With this new method, the computation efficiency and accuracy of stability margin estimate are both significantly improved.

1.2 Introduction of the numerical method used for voltage stability analysis

Before further discussion, we will first give a brief review of commonly used numerical scheme for voltage stability analysis.

As discussed earlier, power system dynamics can be described in a DAE form as follows:

$$\begin{cases} \dot{x} = f(x, y, p), & f : \Re^{n+m+q} \to \Re^{n} \\ 0 = g(x, y, p), & g : \Re^{n+m+q} \to \Re^{m} \end{cases} \qquad (4.1)$$
$$x \in X \subset \Re^{n},\ y \in Y \subset \Re^{m},\ p \in P \subset \Re^{k}$$

where the parameter p defines specific system configurations and operation conditions. x denotes the dynamic state variables and y denotes the instantaneous variables which satisfies algebraic constraints.

As defined in [36], the structurally stable region in the parameter space p has the property that the system operated at a locally structural stable equilibrium point can tolerate slow parametric changes within the region without losing local stability around the equilibrium. As system parameters vary in this region, the dynamics of the system changes continuously; in other words, topologically the structure remains unchanged under small disturbance provided the system is structurally stable at the given parameter value. Structurally unstable points then pinpoint the parameter boundary values where the structure or the type of the system undergoes changes with small perturbations [2, 14]. Accordingly, these local bifurcation points characterize the structural stability region. To find the dynamic stability margin of power system, we will locate the first-appeared bifurcation point as p changes. Eigenvalue based bifurcation analysis provides a tool to study the parameter space phenomena; however, the analysis carries a huge computation burden. Thus, numerical algorithm will be developed here to speed up the computation to locate the bifurcation point.

For power system expressed as (4.1), the differential equations are the dynamic equations, and the algebraic constraints denote the power flow equations. p denotes loads, generation, voltage setting points, etc. In this paper, we will focus on system dynamics with changing loads, and p will denote the loads of the system.

In terms of the structural stability concept one needs to slowly increase the loads p until the structurally unstable loading is found, where p starts from an equilibrium point $\{x_0, y_0, p_0\}$ along system (4.2):

$$\begin{cases} \dot{x} = f(x, y, p) \\ 0 = g(x, y, p) \\ \dot{p} = k \times c \\ x(t_0) = x_0, y(t_0) = y_0, p(t_0) = p_0 \end{cases} \tag{4.2}$$

Here $k \in \Re^1, c \in C \subset \Re^k$, $k \times c$ denotes the load increase speed, where c is a constant vector that denotes the load increase ratio among all loads and is defined by a scheduled

system operating strategy. If all loads in the network increase in the same ratio, *c* will be a unit vector (c=[1,1, …, 1]) . Without losing generality, we assume all loads will increase in the same ratio to simplify our presentation.

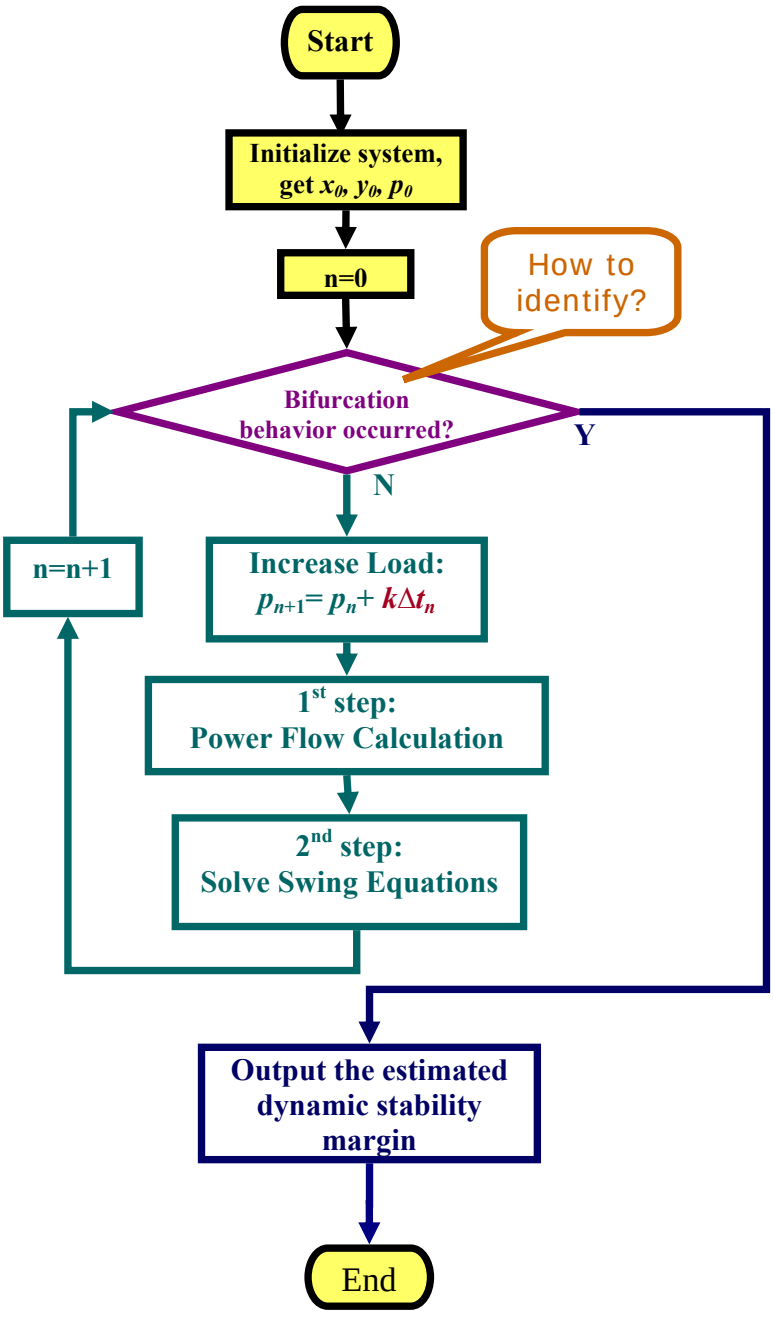

Figure IV-1 A preliminary scheme to estimate stability margin of power systems

Note that in this chapter, the numerical computation carried out by (4.2) aims to find the structurally unstable point, which is different from simulating a system in an assumed load changes. So the load increase ratio is not necessarily a constant as long as we can locate bifurcation point accurately.

A numerical solution for DAE systems combined with a bifurcation detection criterion is developed for stability margin estimation as shown in Figure IV-1. In this scheme, with intelligently increasing load, the algebraic solving and integration are alternately applied until a bifurcation behavior is detected, where the load value is then the estimated margin. A criterion to identify a bifurcation behavior will be addressed later.

Before further discussion, we first give a quick review on the adopted integration method. In the first step of Figure IV-1, we use x_n and increasing load p_{n+1} as known variables to solve power flow variable y_{n+1}. While in the second step, p_{n+1}, y_{n+1} will be taken as known variables to obtain x_{n+1}. Without loss of generality, we assume RKF [38] method will be applied in the second step as equation (4.3).

$$\begin{cases} x_{n+1} = x_n + \Delta t_n H \\ H = \sum_{i=1}^{6} \alpha_i K_i \end{cases} \tag{4.3}$$

where

$$\begin{cases} k_1 = f(t_n, y_n) \\ k_2 = f(t_n + \frac{1}{4}\Delta t_n, y_n + \frac{1}{4}k_1) \\ k_3 = f(t_n + \frac{3}{8}\Delta t_n, y_n + \frac{3}{32}k_1 + \frac{9}{32}k_2) \\ k_4 = (t_n + \frac{12}{13}\Delta t_n, y_n + \frac{1932}{2197}k_1 - \frac{7200}{2197}k_2 + \frac{7296}{2197}k_3) \\ k_5 = f(t_n + \Delta t_n, y_n + \frac{439}{216}k_1 - 8k_2 + \frac{3680}{513}k_3 - \frac{845}{4140}k_4) \\ k_6 = f(t_n + \frac{1}{2}\Delta t_n, y_n - \frac{8}{27}k_1 + 2k_2 - \frac{3544}{2565}k_3 + \frac{1859}{4140}k_4 - \frac{11}{40}k_5) \end{cases}$$

And $\alpha_{1,2,\ldots 6}$ are constants independent of integrand f, which are derived by comparing the Taylor expansion of K_i terms in (4.3) with Taylor expansion of the exact solution $x(t_{n+1})$. In [38], we can find the value of $\alpha_{1,2,\ldots 6}$ shown as below:

$$\alpha_1 = \frac{16}{135}, \alpha_2 = 0, \alpha_3 = \frac{6656}{12825}, \alpha_4 = \frac{28561}{56430}, \alpha_5 = -\frac{9}{50}, \alpha_6 = \frac{2}{55}$$

At each step, we will try to adjust the step size Δt by a two-step process shown as follows:

Firstly, we will Calculate θ by

$$\begin{cases} \theta = 0.84 \left| \dfrac{\xi \Delta t_n}{d^*_{n+1}} \right|^{1/4} \\ d^*_{n+1} = \Delta t_n \left(\dfrac{1}{360} K_1 - \dfrac{128}{4275} K_3 - \dfrac{2197}{75240} K_4 + \dfrac{1}{50} K_5 + \dfrac{2}{55} K_6 \right) \end{cases} \tag{4.4}$$

Here ξ is a small constant used to control the 'one-step error' of numerical calculation [29].

Secondly, if $\theta < 1$, we will adjust Δt by (4.5); otherwise Δt will keep unchanged.

$$\Delta t_{n+1} = \theta \Delta t_n \tag{4.5}$$

It is well known that when system is light-loaded or operating in normal conditions, the solution of the DAE system (4.2) is rather smooth, so bigger Δt can be selected; while increasing load makes system more stressed, a smaller Δt is needed. Thus we can choose a big initial value for Δt [29, 38]. With an increased load, Δt will be adjusted by (4.4) and (4.5). Numerical tests have shown that with automatically adjustment of Δt, RKF method has much higher computation efficiency than typical 4th-order RK method [29, 30].

1.3 Challenges faced by numerical simulation

For the numerical scheme shown in Figure IV-1, a key question is how to detect bifurcation behavior. Till now, there still lacks a sound criterion for it. People used to claim a bifurcation behavior is detected as long as numerical simulation results exhibit an oscillation or a sudden catastrophic transition as discussed in [2], thus the integration trajectory will exhibit a big deviation from the equilibrium manifold (EM). However, given the simulation is numerically stable, there are still two possible reasons for a big deviation from EM in simulation results. The first possibility is that the system indeed encounters its structurally unstable point, and in this case, it is correct to claim the detection of bifurcation behavior. The second possibility is that, the load increases too fast, thus the disturbance for the system will be too big to be attracted back to stable area. Accrodingly, claim of bifurcation behavior of this case is clearly wrong. Thus, the key question arises--how to determine if a disturbance is small enough? How to choose proper speed of increasing load? Further discussion about this dilemma will be demonstrated later in details.

Another challenge faced by industry is on line calculation of voltage stability margin. Computation efficiency is of great importance for online monitoring of security. The automatically step size control technique can be utilized to save computation cost, however, online estimation of maximum loadability is still difficult, especially for huge systems, for which the computation burden could be a nightmare for online monitoring. Thus, we need to find a way to further enhance numerical computation efficiency.

In short, two requirements should be satisfied by a sound numerical scheme: Accuracy and Efficiency.

2. EMD criterion and load adjustment technique

As discussed former, we locate the dynamic stability margin by detecting the bifurcation behavior. When a system goes near to its bifurcation point, the system behavior will change drastically. As shown in [5, 18], the Hopf bifurcation point determines the stability margin for power system applications. It is well known that when a system is approaching its Hopf

bifurcation point, oscillation will appear. So oscillation in numerical solution can be taken as a signal of reaching dynamic voltage stability margin. For the cases that the stability margin is determined by other types of bifurcation points, numerical solution will suddenly exhibit a big deviation from the equilibrium point. All these bifurcation behaviors make it possible to estimate dynamic stability margin by numerical solution.

However, it is observed that with too fast load increase ratio (k is too big), the numerical solution will also exhibit a big deviation from equilibrium manifold since its dynamic is unable to settle down to the equilibrium for fast load changes. It can lead to a misjudgment as a bifurcation behavior and an inaccurate estimate of stability margin as a consequence. Therefore, for accurate estimation of stability margin, k should be selected to make the numerical solution stay around the equilibrium manifold until bifurcation occurs. Thus, a critical step is to judge whether the numerical solution is able to stay around the equilibrium manifold. Accordingly, a criterion, named as EMD criterion, was proposed in here to gauge the deviation.

2.1 The EMD criterion

The equilibrium manifold is defined by the equilibrium point path as the load increases.

$$\begin{cases} 0 = f(x, y, p) \\ 0 = g(x, y, p) \end{cases} \tag{4.6}$$

By (4.6), staying around equilibrium manifold means that after each step of the numerical computation, we should have:

$$\begin{cases} 0 \approx f(x_{n+1}, y_{n+1}, p_{n+1}) \\ 0 \approx g(x_{n+1}, y_{n+1}, p_{n+1}) \end{cases} \tag{4.7}$$

Let $e = (e_1, e_2, ...e_{n+m})$

$$\text{where } \begin{cases} e_1 = f_1(x_{n+1}, y_{n+1}, p_{n+1}) \\ : \\ e_n = f_n(x_{n+1}, y_{n+1}, p_{n+1}) \\ e_{n+1} = g_1(x_{n+1}, y_{n+1}, p_{n+1}) \\ : \\ e_{n+m} = g_{n+m}(x_{n+1}, y_{n+1}, p_{n+1}) \end{cases} \tag{4.8}$$

Thus we can define an equilibrium manifold deviation (EMD) error as the Euclidean norm of e:

$$Err = \|e\| \tag{4.9}$$

After each step, *Err* can be used as an error signal to gauge the deviation. A fundamental requirement of *k* is that, to keep the numerical trajectory stay around the equilibrium manifold, we should choose a number k that is small enough to satisfy $Err < \varepsilon$ (ε is a small constant).

Note that during the numerical computation, *k* can be varying as long as we can satisfy the fundamental requirement. So we can adjust *k* to maintain *Err* in a certain range. However, numerical tests show that when a system is approaching its structurally unstable point, no matter how we adjust *k*, *Err* will no longer be controllable. Accordingly, when no adjustments can work, we claim a bifurcation behavior is detected.

Now we will face several questions:

- How to adjust k to control Err ?
- Can we adjust Δt to control Err ?

To answer these questions, we need to know the impacts of *k* and Δt on *Err* , which will be discussed below.

2.2 Impact analysis of k and Δt on Err

From (4.8), we know that

$$e_i = h_i(x_{n+1}, y_{n+1}, p_{n+1}) \tag{4.10}$$

Here $i \in \{1,2,...n+m\}, h \in \{f_{1,2,...,n}, g_{1,2,...,m}\}$, f and g are shown in (4.6)

Assume that (x_n, y_n, p_n) is an equilibrium point of system, we define a local truncation EMD error shown in figure IV-2, which is similar as a local numerical trunction error has been defined in [32, 33]:

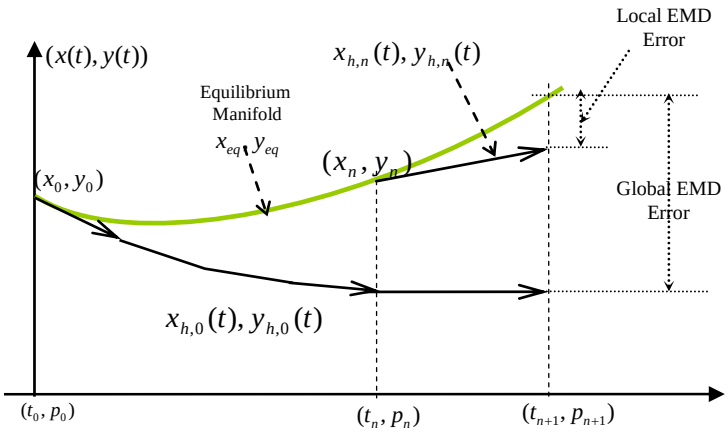

Figure IV-2 Local truncation EMD error

In figure IV-2, $[x_{h,0}(t), x_{h,0}(t)]$ is the numerical trajectory start from equilibrium point (x_0, y_0), and $[x_{h,n}(t), x_{h,n}(t)]$ is the numerical trajectory start from equilibrium point (x_n, y_n). The local EMD error is defined as (4.11). Later we will prove that, if we can control $\frac{\overline{err}}{\Delta t_n}$ (the local EMD error per unit time), then we can also control the global EMD error Err.

$$\begin{cases} \hat{e}_i = h_i(x_{n+1}, y_{n+1}, p_{n+1}) \\ \quad = h_i(x_n + \Delta x_n, y_n + \Delta y_n, p_n + \Delta p_n) \\ \quad \approx h_i(x_n, y_n, p_n) + h_{i,x}\Delta x_n + h_{i,y}\Delta y_n + h_{i,p}\Delta p_n \\ \quad = h_{i,x}\Delta x_n + h_{i,y}\Delta y_n + h_{i,p}\Delta p_n \\ \overline{err} = \|\hat{e}\| \end{cases} \qquad (4.11)$$

$h_{i,x}$, $h_{i,y}$ and $h_{i,p}$ denote the partial derivative of h_i respect to *x*, *y* and *p* respectively. $\overline{err}$ is defined as local truncation EMD error since it is an induced error from the single step. On the other hand, *Err* is called as global EMD error, which is an accumulated error from all former steps.

Here $\Delta p_n = k\Delta t_n$, and Δy_n is obtained by power flow calculation as shown in the first step of Figure IV-1. Neglecting high order terms, we have:

$$\begin{aligned} 0 &= g(x_n, y_{n+1}, p_{n+1}) \\ &= g(x_n, y_n, p_n) + g_y \Delta y_n + g_p k\Delta t_n \\ &= g_y \Delta y_n + g_p k\Delta t_n \end{aligned}$$

And we got

$$\Delta y_n = -\frac{g_p}{g_y}\bigg|_{(x_n, y_n, p_n)} k\Delta t_n = \Phi(x_n, y_n, p_n) k\Delta t_n \qquad (4.12)$$

For any explicit single-step method to solve differential problem, we have [29, 38]:

$$\Delta x_n = H(x_n, y_n, p_n)\Delta t_n \qquad (4.13)$$

Here $H(x_n, y_n, p_n)$ is determined by the numerical method applied to solve differential equations [32, 33]. For example, if RKF45 method is applied, by equation (4.3), we will have:

$$\Delta x_n = \Delta t_n \sum_{i=1}^{6} \alpha_i K_i$$

α_i and K_i can be found in (4.3).

$$\begin{aligned} K_1 &= f(x_n, y_{n+1}, p_{n+1}) \\ &= f(x_n, y_n, p_n) + f_y \Delta y_n + f_p \Delta p_n \\ &= f_y \Delta y_n + f_p k\Delta t_n \end{aligned} \qquad (4.14)$$

Substituting (4.12) into (4.14), we have

$$\begin{aligned} K_1 &= f_y \Phi(x_n, y_n, p_n) k\Delta t_n + f_p k\Delta t_n \\ &= \overline{C}_{11}(x_n, y_n, p_n) k\Delta t_n \end{aligned} \tag{4.15}$$

Here $\overline{C}_{11} = f_y \Phi(x_n, y_n, p_n) + f_p$.

Similarly we have (4.16). The detailed forms of $\overline{C}_{ij}$ in (4.16) can be easily calculated following similar procedures for $\overline{C}_{11}$, and they are all in terms of derivatives of function *f* and *g*.

$$\begin{cases} K_1 = \overline{C}_{11}(x_{n,} y_n, p_n) k\Delta t_n \\ K_2 = f(x_n + \dfrac{\Delta t_n}{4} K_1, y_{n+1}, p_{n+1}) \\ = f_x \dfrac{\Delta t_n}{4} \overline{C}_{11}(x_n, y_n, p_n) k\Delta t_n + f_y \Phi(x_n, y_n, p_n) k\Delta t_n \\ \quad + f_p k\Delta t_n \\ = \overline{C}_{21}(x_{n,} y_n, p_n) k\Delta t_n + \overline{C}_{22}(x_{n,} y_n, p_n) k\Delta t_n^2 \\ : \\ : \\ K_6 = \overline{C}_{61}(x_{n,} y_n, p_n) k\Delta t_n + \overline{C}_{62}(x_{n,} y_n, p_n) k\Delta t_n^2 \\ \quad + \overline{C}_{63}(x_{n,} y_n, p_n) k\Delta t_n^3 + \overline{C}_{64}(x_{n,} y_n, p_n) k\Delta t_n^4 \\ \quad + \overline{C}_{65}(x_{n,} y_n, p_n) k\Delta t_n^5 + \overline{C}_{66}(x_{n,} y_n, p_n) k\Delta t_n^6 \end{cases} \tag{4.16}$$

By (4.13) - (4.16), we have

$$\Delta x_n = k\Delta t_n \sum_{j=1}^{6} \overline{C}_j(x_n, y_n, p_n) \Delta t_n^j \tag{4.17}$$

Here $\overline{C}_j = \sum_{i=j}^{6} \alpha_i \overline{C}_{ij}$, $j = 1,2,...,6$

Substituting $\Delta x_n, \Delta y_n, \Delta p_n$ into (4.11), we have

$$\hat{e}_i \approx h_{i,x} k\Delta t_n \sum_{j=1}^{6} \overline{C}_j \Delta t_n^j + h_{i,y} \Phi k\Delta t_n + h_{i,p} k\Delta t_n$$
$$= \left(h_{i,x} \sum_{j=1}^{6} \overline{C}_j \Delta t_n^j + h_{i,y} \Phi + h_{i,p} \right) k\Delta t_n$$
$$= \left(o(\Delta t_n) + C_i \right) k\Delta t_n$$

Where

$C_i = h_{i,y} \Phi + h_{i,p}$.

So we have:

$$\overline{err} = \left\| \left(o(\Delta t_n) + C(x_n, y_n, p_n) \right) k\Delta t_n \right\| \qquad (4.18a)$$

Where

$$C(x_n, y_n, p_n) = \sqrt{\sum_{i=1}^{n+m} C_i^2} .$$

Note that (4.18a) is expressed in terms of the derivatives of function *h*.

This concludes the following lemma:

Lemma 1:

Applying explicit single-step method to solve the system equation described as (4.2), we have the local EMD error $\overline{err}$ as shown in (4.18a) with positive scalars *k* and Δt_n pulled out.

$$\overline{err} = \left\| \left(o(\Delta t_n) + C(x_n, y_n, p_n) \right) \right\| k\Delta t_n \qquad (4.18)$$

For other explicit single-step methods, the proof follows similar steps as with RKF45 method.

Our next task is to estimate global EMD error *Err* by $\overline{err}$. Enlightened by the Theorem 3.4 in Chapter II of [38], we have a similar theorem:

Theorem 1:

Suppose a system described as (4.2) satisfies three conditions:

i) f and g of (4.1) are continuous and satisfies the *Lipschitz* condition corresponding to x and y respectively.

ii) The increment function H in (4.3) and the function Φ in (4.12) are bounded:

$$\begin{cases} \left|\frac{\partial H}{\partial x}\right| \le L \\ k\left|\frac{\partial \Phi}{\partial y}\right| \le L \end{cases}$$

Here L is a constant.

iii) Before the system reach its bifurcation point, f and g in (4.2) satisfy

$$\begin{cases} \left\|\tilde{C}_x\right\| = \left\|\frac{f_y g_p - f_p g_y}{f_x g_y - f_y g_x}\right\| \le \lambda \\ \left\|\tilde{C}_y\right\| = \left\|\frac{f_p g_x - f_x g_p}{f_x g_y - f_y g_x}\right\| \le \lambda \end{cases}$$

Here λ is a constant.

Then we can conclude:

Before the system reach its bifurcation point, if we can control the local EMD error per unit time as:

$$\frac{\overline{err}}{\Delta t_n} = k\left\|o(\Delta t_n) + C(x_n, y_n, p_n)\right\| \le \varepsilon \qquad (4.19)$$

Then we will have:

$$Err \le \varepsilon \tilde{K} \qquad (4.20)$$

where, $\tilde{K} = \frac{\lambda \tilde{C}(x_n, y_n, p_n)}{CL}\left(e^{L(t_{n+1}-t_0)} - 1\right)$

Detailed forms of $\widetilde{C}(x_n, y_n, p_n)$ are given in the proof, which are also in terms of derivatives of function *h*.

The proof of this theorem is inspired by the proof of Theorem 7.3 in Chapter I of [38]. Before further discussions, we introduce and prove a Lemma as follows:

Lemma 2:

Suppose a system described as (4.2) satisfies the condition i), ii) and iii) of Theorem 1, then we have:

$$\left|x_{eq}(t) - x_h(t)\right| \le \frac{k\lambda}{L}\left(e^{L(t-t_0)} - 1\right) \qquad (4.21)$$

$$\left|y_{eq}(t) - y_h(t)\right| \le \frac{k\lambda}{L}\left(e^{L(t-t_0)} - 1\right) \qquad (4.22)$$

Here $\left[x_h(t), y_h(t)\right]$denotes the numerical solution of the system start from an equilibrium point(x_0, y_0, p_0, t_0), and $[x_{eq}(t), y_{eq}(t)]$ denotes the equilibrium manifold of the system.

Proof of Lemma 2:

Here we will draw a figure to demonstrate our proof, which follows a similar logic as the 'Lady Windermer's Fan (O.Wilde 1892)' in chapter I.7 of [38]. In Figure IV-3, $[x_{h(1)}(t), y_{h(1)}(t)]$, $[x_{h(2)}(t), y_{h(2)}(t)]$ … $[x_{h(n-1)}(t), y_{h(n-1)}(t)]$ denote the numerical solution of the system start from equilibrium point at $t = t_1, t_2, ..., t_{n-1}$ respectively.

By condition i) and ii), f satisfies the *Lipschitz* condition and $\left|\frac{\partial H}{\partial x}\right| \le L$, then by Lemma 7.2 in chapter I of [38], we will have:

$$\left|x_{h(1)}(t) - x_h(t)\right| \le e^{L(t-t_1)}\left|x_{h(1)}(t_1) - x_h(t_1)\right| \qquad (4.23)$$

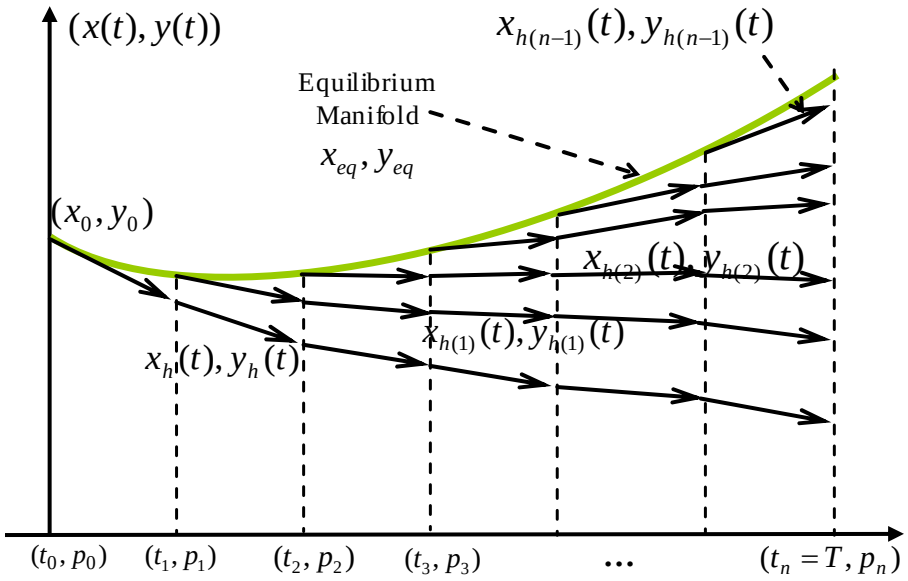

Figure IV-3 Illustration of our proof

for $t_1 < t < T = t_n$

From (4.17), we know that

$$x_h(t_1) = x_0 + \Delta x_0 = x_0 + k\Delta t_0 \sum_{j=1}^{6} \overline{C}_j \Delta t_0^j \qquad (4.24)$$

and by definition of $x_{h(1)}(t_1)$, we know:

$$x_{h(1)}(t_1) = x_{eq}(t_1) \qquad (4.25)$$

Let

$$\begin{cases} \Delta\tilde{x}_0 = x_{eq}(t_1) - x_0 \\ \Delta\tilde{y}_0 = y_{eq}(t_1) - y_0 \end{cases}$$

From

$$\begin{cases} 0 = f(x_{eq}(t_1), y_{eq}(t_1), p(t_1)) = f(x_0 + \Delta\tilde{x}_0, y_0 + \Delta\tilde{y}_0, p_0 + k\Delta t_0) \\ 0 = g(x_{eq}(t_1), y_{eq}(t_1), p(t_1)) = g(x_0 + \Delta\tilde{x}_0, y_0 + \Delta\tilde{y}_0, p_0 + k\Delta t_0) \end{cases}$$

we can get

$$\begin{bmatrix} f_x & f_y \\ g_x & g_y \end{bmatrix} \begin{bmatrix} \Delta\tilde{x}_0 \\ \Delta\tilde{y}_0 \end{bmatrix} \approx -\begin{bmatrix} f_p \\ g_p \end{bmatrix} k\Delta t_0$$

We have:

$$\begin{cases} \Delta\tilde{x}_0 = \left. \dfrac{f_y g_p - f_p g_y}{f_x g_y - f_y g_x} \right|_{(x_0, y_0, p_0)} k\Delta t_0 = \tilde{C}_x k\Delta t_0 \\ \Delta\tilde{y}_0 = \left. \dfrac{f_p g_x - f_x g_p}{f_x g_y - f_y g_x} \right|_{(x_0, y_0, p_0)} k\Delta t_0 = \tilde{C}_y k\Delta t_0 \end{cases} \tag{4.26}$$

Then by (4.24), (4.25) and (4.26), we can get:

$$\begin{aligned} & x_{h(1)}(t_1) - x_h(t_1) \\ &= \Delta\tilde{x}_0 - \Delta x_0 \\ &= k\Delta t_0 \left(\tilde{C}_x(x_0, y_0, p_0) - \sum_{j=1}^{6} \overline{C}_j \Delta t_0^j \right) \\ &= k\Delta t_0 \tilde{C}_x + o(\Delta t_0^2) \end{aligned}$$

By condition iii), we know $\left|\tilde{C}_x\right| \le \lambda$, and then we have:

$$\left| x_{h(1)}(t_1) - x_h(t_1) \right| \le k\Delta t_0 \lambda = k\lambda(t_1 - t_0) \tag{4.27}$$

Substitute (4.27) into (4.23), we have:

$$\left| x_{h(1)}(t) - x_h(t) \right| \le e^{L(t-t_1)}(t_1 - t_0) k\lambda \tag{4.28}$$

Similarly we have:

$$\left| x_{h(2)}(t) - x_{h(1)}(t) \right| \le e^{L(t-t_2)}(t_2 - t_1) k\lambda \tag{4.29}$$

for $t_2 < t < T$

The entire situation is sketched in Figure IV-3, and we obtain for $t_n < t \le t_{n+1}$:

$$\begin{aligned}
&\left|x_{eq}(t) - x_h(t)\right| \\
&\quad \le \left|x_{h(1)}(t) - x_h(t)\right| + \left|x_{h(2)}(t) - x_{h(1)}(t)\right| + \ldots + \left|x_{eq}(t) - x_{h(n)}(t)\right| \\
&\quad \le k\lambda\left(e^{L(t-t_1)}(t_1 - t_0) + \ldots + e^{L(t-t_n)}(t_n - t_{n-1})\right) + k\lambda(t - t_n) \\
&\quad \le k\lambda\int_{t_0}^{t} e^{L(t-s)}ds
\end{aligned} \tag{4.30}$$

Thus for $t_n < t \le t_{n+1}$, we have:

$$\left|y_{eq}(t) - y_h(t)\right| \le k\lambda\int_{t_0}^{t} e^{L(t-s)}ds = \frac{k\lambda}{L}\left(e^{L(t-t_0)} - 1\right) \tag{4.31}$$

From (4.30) and (4.31), we can get (4.21) and (4.22), so Lemma 2 is proved. Now we are ready for the proof of Theorem 1—If the system satisfy the three conditions listed before, then we can conclude that, before the system reach its bifurcation point, if we can control the local EMD error per unit time as:

$$\frac{\overline{err}}{\Delta t_n} = k\left\|o(\Delta t_n) + C(x_n, y_n, p_n)\right\| \le \varepsilon$$

Then we will have:

$$Err \le \varepsilon\tilde{\tilde{K}}$$

where, $\tilde{\tilde{K}} = \dfrac{\lambda\tilde{C}(x_n, y_n, p_n)}{CL}\left(e^{L(t_{n+1}-t_0)} - 1\right)$

Proof of Theorem 1:

We know that:

$$\begin{aligned}
e_i &= h_i(x_{n+1}, y_{n+1}, p_{n+1}) \\
&= h_i(x_h(t_{n+1}), y_h(t_{n+1}), p_{n+1}) \\
&\approx h_i(x_{eq}(t_{n+1}), y_{eq}(t_{n+1}), p_{n+1}) + h_{i,x}(x_h(t_{n+1}) - x_{eq}(t_{n+1})) \\
&\quad + h_{i,y}(y_h(t_{n+1}) - y_{eq}(t_{n+1})) \\
&= h_{i,x}(x_h(t_{n+1}) - x_{eq}(t_{n+1})) + h_{i,y}(y_h(t_{n+1}) - y_{eq}(t_{n+1}))
\end{aligned}$$

By (4.21), (4.22), we will have:

$$\begin{aligned}|e_i| &\le |h_{i,x}|\|x_h(t_{n+1}) - x_{eq}(t_{n+1})| + |h_{i,y}|\|y_h(t_{n+1}) - y_{eq}(t_{n+1})| \\ &\le (|h_{i,x}| + |h_{i,y}|)\frac{k\lambda}{L}\left(e^{L(t_{n+1}-t_0)} - 1\right) \\ &= \tilde{C}_i(x_n, y_n, p_n)\frac{k\lambda}{L}\left(e^{L(t_{n+1}-t_0)} - 1\right)\end{aligned}$$

Where $\tilde{C}_i = |h_{i,x}| + |h_{i,y}|$

So we have:

$$Err = \|e\| \le \tilde{C}\frac{k\lambda}{L}\left(e^{L(t_{n+1}-t_0)} - 1\right) \qquad (4.32)$$

Here $\tilde{C} = \sqrt{\sum_{i=1}^{n+m}\tilde{C}_i^2}$

If we have

$$\frac{\overline{err}}{\Delta t_n} = k[o(\Delta t_n) + C(x_n, y_n, p_n)] \le \varepsilon,$$

then we will have:

$$k \le \frac{\varepsilon}{C(x_n, y_n, p_n)} \qquad (4.33)$$

Then by (4.32) and (4.33), we have:

$$Err \le \varepsilon\frac{\lambda\tilde{C}}{LC}\left(e^{L(t_{n+1}-t_0)} - 1\right) \qquad (4.34)$$

Thus the Theorem 1 has been proven.

From (4.32) and (4.19), we can conclude that Err is mainly determined by k, and the impact of Δt is not dominant and usually can be neglected. This conclusion is also verified by our numerical tests.

Thus, to control *Err*, we only need to adjust *k*.

3. The new numerical scheme

3.1 With fixed Δt, computation speed can be accelerated by adjustment of k

We know that within the feasible operating region of a system, each stable equilibrium point has its own attraction area. As shown in Figure IV-4, when the small disturbance is remained in the attraction area, the numerical solution will be attracted to equilibrium manifold and *Err* will decrease. On the other hand, when the parametric perturbation is big enough to exceed the attraction area, the numerical solution will also deviate from the EM and *Err* will increase. It is well known that for power system, the attraction area of EM will shrink as load increase. Thus, bigger k can be selected when system is lightly loaded; while under stressed operating condition, smaller k is needed. We know that the computation speed is roughly determined by $1/(k\Delta t)$. Bigger k and Δt imply less numerical computation time. So enlightened by RKF method, we can set a big initial value of k; and at each step, we can choose the possible biggest k which can guarantee $Err \le \varepsilon$. Therefore, the computation burden can be reduced without loss of accuracy.

After a step, if we find that *Err* is bigger than expected, we need to adjust k to control *Err*. By theorem 1, we know that *Err* can be controlled if we can control $\frac{\overline{err}}{\Delta t_n}$. Thus, k can be adjusted by (4.19):

$$k\left\|C(x_n, y_n, p_n\right\| \le \varepsilon \Leftrightarrow k \le \frac{\varepsilon}{\left\|C(x_n, y_n, p_n)\right\|},$$

So we can choose new k as:

$$k = \hat{\lambda}\frac{\varepsilon}{\left\|C(x_n, y_n, p_n)\right\|}, \qquad (4.35)$$

here $\hat{\lambda}$ is a constant and satisfies $0 < \hat{\lambda} \le 1$.

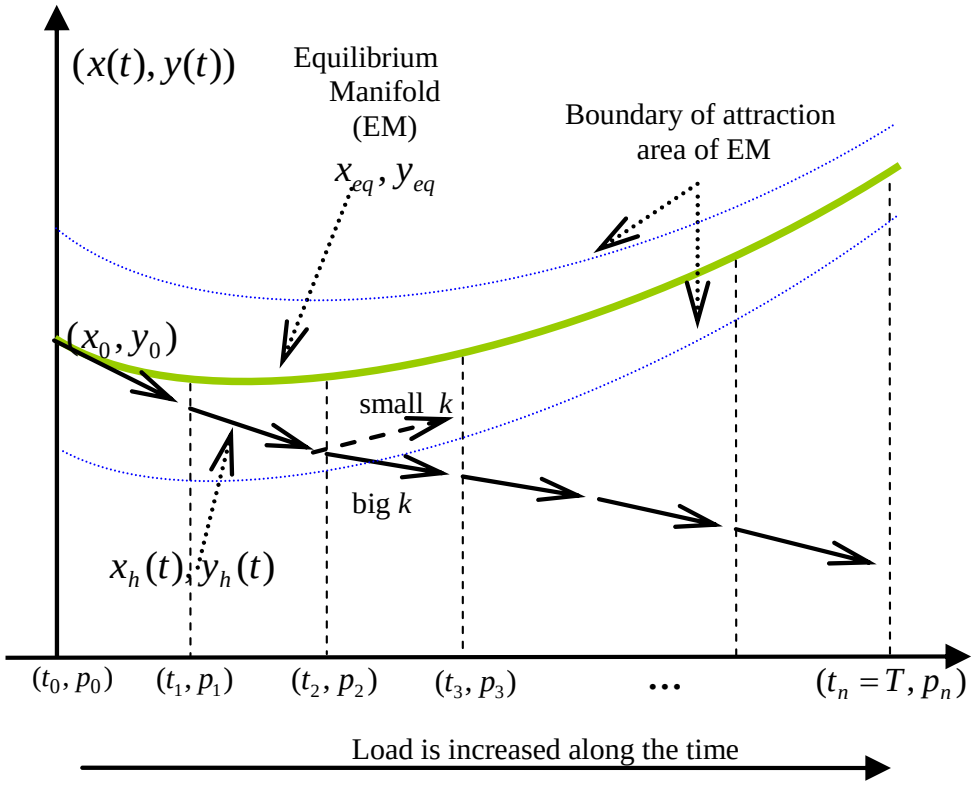

Figure IV-4 Impacts of adjustment of *k*

$\hat{\lambda}$ can be selected as 1, however, to compensate the approximation in deriving (4.19), we may choose $\hat{\lambda}$ as 0.8 or 0.9.

It is easy to calculate *Err* by (4.8) and (4.9), however, derivation and calculation of $\|C(x_n, y_n, p_n)\|$ can also induce some computation burden. From (4.20), we can see that bigger *k* will lead bigger *Err*, so if $Err > \varepsilon$, we need to choose a smaller *k* to decrease *Err*. Now the question is how to adjust *k* in a computation efficient way?

In practice, a simple and straightforward way could be applied to adjust *k*:

If $Err > \varepsilon$, then we can choose

$$k = \beta k \tag{4.36}$$

where β is a constant and satisfies $0 < \beta < 1$. According to our experience, it can be selected as 0.6~ 0.8. We know that when the system encounters the bifurcation point, the attraction area will shrink to zero. In such a situation, no matter how we decrease *k*, *Err* will no longer be controllable. However, how to make reliable judgment is not trivial in numerical computation. Again, a straightforward but primitive way is to set a minimum value of *k* to detect the bifurcation behavior. When we find that *k* hits its lower limit $k_{\min}$ and *Err* is still uncontrollable, we can conclude that a bifurcation behavior is detected. This primitive adjustment performs very well to enhance computation speed in most cases, which can be verified in numerical tests shown later.

However, with this primitive adjustment approach, there is no guarantee that the adjustment will be accepted. So, repeated trials and thus extra computation burden will be induced. On the other hand, for cases that need only small adjustment, the proposed adjustment by (4.36) may be inappropriately big. Thus, unnecessary computation burden will be imposed.

Another drawback of this primitive approach is that, apparently, the estimate will be impacted by $k_{\min}$. However, $k_{\min}$ is selected based on experience on the system, and it is mathematically difficult to set a reasonable value without trial and error. If $k_{\min}$ is improperly big, the accuracy of estimated margin will suffer.

In short, an optimal load adjustment should satisfy two requirements shown as follows:

- An optimal scheme , after an adjustment of *k*, should guarantee that $Err < Tolerance$, which means that *k* will not immediately get rejected again. In addition, *k* should not be over adjusted, which means the biggest allowed *k* should be used to accelerate computation without sacrificing accuracy.
- The accuracy of an optimal scheme should not depend on selected algorthm parameters; and accurate detection of bifurcation point should be guaranteed

mathematically. Accordingly, selected minimum value of *k* should no longer play a role on the estimate.

Bearing these two requirements in mind, we develop a new approach here by investigating how *k* impact on $\overline{err}$ and *Err*:

$$\overline{err} = \left\| \left(o(\Delta t_n) + C(x_n, y_n, p_n) \right) \right\| k \Delta t_n \tag{4.37}$$

Detail form of $C(x_n, y_n, p_n)$ has already been discussed before and can also be found in [29, 38], which is in form of partial derivatives of f, g respect to x, y, p.

Based on theorem 1 introduced former, we know that if we can control the local EMD error per unit time as:

$$\frac{\overline{err}}{\Delta t_n} \le \varepsilon \tag{4.38}$$

Then we can control the global EMD error *Err* as:

$$Err \le \varepsilon \widetilde{K} \tag{4.39}$$

where,

$$\widetilde{K} = \frac{\lambda \widetilde{C}(x_n, y_n, p_n)}{C(x_n, y_n, p_n) L} \left(e^{L(t_n - t_0)} - 1 \right) \tag{4.40}$$

Here $\widetilde{C}(x_n, y_n, p_n)$ is also in a form of partial derivatives of f, g with respects to x, y, p. L and λ are constants as shown in section 2.2 of this chapter. Moreover, before we start $(n+1)^{th}$ iteration, x_n, y_n, p_n are all calculated, so $C(x_n, y_n, p_n)$ and $\widetilde{C}(x_n, y_n, p_n)$ are known at $(n+1)^{th}$ step. Thus, $\widetilde{K}$ can also be taken as known.

Suppose after $n+1$ step calculation, we found $Err_{n+1} \ge T$, here T is the tolerance of global EMD error. Then we need select a new *k* to redo the $n+1$ step calculation. Neglecting the high order term in (4.37) and substituting it into (4.38), we have:

$$\frac{\overline{err}}{\Delta t_n} \approx k\left\|C(x_n, y_n, p_n)\right\| \le \varepsilon \qquad (4.41)$$

As $\tilde{K}$ in (4.39) is a constant, we know that if we want to control the global EMD error as $Err < T$, we should decrease ε_{n+1} as

$$\varepsilon_{n+1}^{new} = \varepsilon_{n+1}^{old} \frac{T}{Err_{n+1}} \qquad (4.42)$$

Also, as $C(x_n, y_n, p_n)$ in (4.41) is known at n+1 step, and there is almost a linear relation between $\frac{\overline{err}}{\Delta t_n}$ and *k*, we can adjust the load increase ratio as:

$$k^{new} = k^{old} \frac{T}{Err_{n+1}} \qquad (4.43)$$

To be safe, considering those neglected high order term and calculation error, we can adjust *k* by:

$$k^{new} = \alpha k^{old} \frac{T}{Err_{n+1}} \qquad (4.44)$$

Here $0 < \alpha < 1$ is a constant, and can be selected as 0.9.

Due to these linear relations shown in (4.39) and (4.41), we can guarantee that our adjustment of *k* as (4.44) will not be rejected for the step. With this new approach, we no longer need to set a minimum value *k* to detect the bifurcation point. As we have demonstrated, after adjustment of *k*, we can guarantee that *Err* will be within the tolerance. Thus, if we found that after the adjustment, *Err* is still uncontrollable, we can conclude that we have reached the structurally unstable point. To be safe, we can continue to adjust three times by (4.44), if we still cannot control *Err*, then we can claim that the small disturbance loadability margin is located.

Later on, we will use numerical experiments to demonstrate and compare the primitive adjustment approach and optimal adjustment approach. We will find that both methods can

greatly enhance the computation efficiency, and our optimal approach could perform better in guaranteeing accuracy and saving computation costs.

3.2 A new scheme to accelerate numerical computation speed by adjusting k and Δt simultaneously

As discussed before, automatically adjustment of k or Δt has its own contribution to improvement of computation efficiency. We would like to explore the synergy of simultaneous adjustments of these two variables.

Keeping the requirement of accuracy in mind, we propose a scheme to integrate both techniques as shown in Figure IV-5.

In this scheme, we will first check the accuracy after each step. If $Err > \varepsilon$ (ε is the tolerance of global EMD error), we will adjust k and repeat the n^{th} step calculation with adjusted k.

If $Err < \varepsilon$ and $\theta < 1$ (θ is defined as in equation 4.45), we will adjust Δt and repeat the n^{th} step calculation with adjusted Δt. If $Err < \varepsilon$ and $\theta > 1$, we will continue the n+1$^{\text{th}}$ step calculation.

Now we will investigate the interaction between these two adjustments. Without losing generality, here we assume that we will adjust Δt by RKF method.

3.2.1 The influence of adjustment of k on the adjustment of Δt

In RKF method, we adjust Δt as following [29, 38]:

$$\theta = 0.84 \left| \frac{\xi \Delta t_n}{d^*_{n+1}} \right|^{1/4} \qquad (4.45)$$

if $\theta < 1$, we will adjust step size as $\Delta t_{n+1} = \theta \Delta t_n$, otherwise $\Delta t_{n+1} = \Delta t_n$ [29, 38].

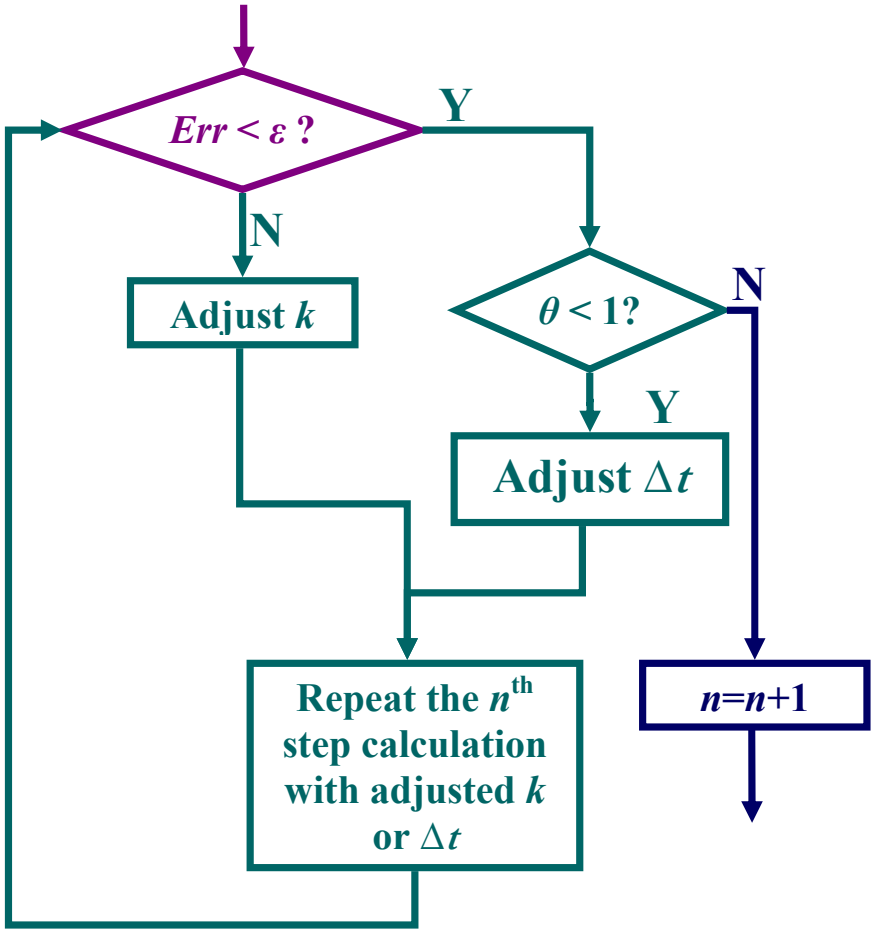

Figure IV-5 Combination of the two techniques

Here d_{n+1}^{*} can be calculated by (4.4). Substituting equation (4.16) into (4.5), similarly as the derivation of (4.17), we have:

$$d_{n+1}^{*} = k\Delta t_n \sum_{i=1}^{6} \tilde{C}_i(x_n, y_n, p_n)\Delta t_n^i \qquad (4.46)$$

Substituting (4.46) into (4.4), we have:

$$\theta = 0.84\left|\frac{\xi}{k\sum_{i=1}^{6}\tilde{C}_i(x_n, y_n, p_n)\Delta t_n^i}\right|^{1/4} \qquad (4.47)$$

After adjusting k to a smaller value, by (4.39), we can see that such an adjustment of k will increase θ, therefore the chances to adjust Δt will be reduced.

3.2.2 The influence of adjustment of Δt on the adjustment of *k*

Procedures of (4.4) and (4.5) will lead to a smaller Δt. Equation (4.19) indicates that the local EMD error per unit time depends only on $o(\Delta t)$. Accordingly, we can neglect Δt's impact on the adjustment of *k*.

From above discussion, we can see that the integration of these two techniques induces synergy on the computation efficiency.

4. Numerical tests

In this section, we demonstrate the validity of our new approach by a few numerical tests. In subsection 4.1 and 4.2, we will demonstrate that our new approach can guarantee the accuracy and enhance the computation efficiency. Here a 2-bus system will be used to demonstrate how our approach works. In subsection 4.3, we will compare the primitive load adjustment approach with the optimal approach. In subsection 4.4, the IEEE 162-bus system will be used to demonstrate that the applicability of our approach to big systems.

4.1 Our EMD criterion accurately estimates the stability margins

The simple 2-bus system is also the test system used in Chaper II, which is shown as Figure IV-6:

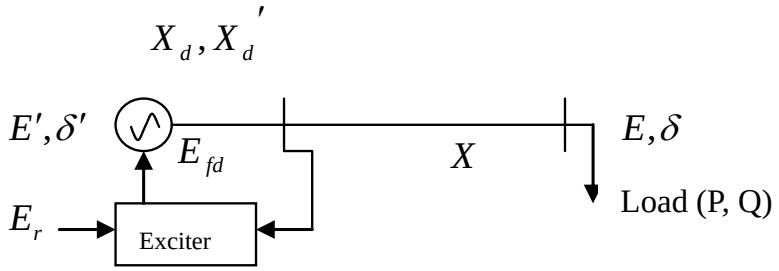

Figure IV-6 Simple two bus system

Here we assume the load is constant power load with a fixed power factor ($P = 2Q$). Also, we assume the regulator is the non-rescheduled P-regulator. All the parameters are the same as used in [18].

Eigenvalue based bifurcation analysis shows that a Hopf bifurcation point will appear at $P = 0.9344$, which will be benchmarked against other approaches.

Here we compare four cases to demonstrate how our EMD criterion worked:

1) RKF method, with $k = 10^{-1}\, p.u./s$
2) RKF method, with $k = 10^{-3}\, p.u./s$
3) RKF method, with $k = 10^{-4}\, p.u./s$
4) RKF method, with adjustment of k. Here k is adjusted by (4.36), and $\beta = 0.8$. Initial value of k is $2 \times 10^{-3}\, p.u./s$, and $k_{\min} = 0.5 \times 10^{-4}$.

Numerical solutions are demonstrated in Figure IV-7. In this figure, we can observe that bigger deviation of numerical solutions from the equilibrium manifold for bigger k. When $k = 10^{-1}$, the solution deviate from its equilibrium manifold and no bifurcation oscillation is observed. Note that when k is too big, the load perturbation is no longer small and a transient will occur. Thus, the obtained PV curve is questionable and invalid for

dynamic voltage stability analysis. On the other hand, when $k = 10^{-4}$ or intelligently adjusted, the numerical solution stays around the equilibrium manifold and an bifurcation behavior, oscillation, is observed accurately.

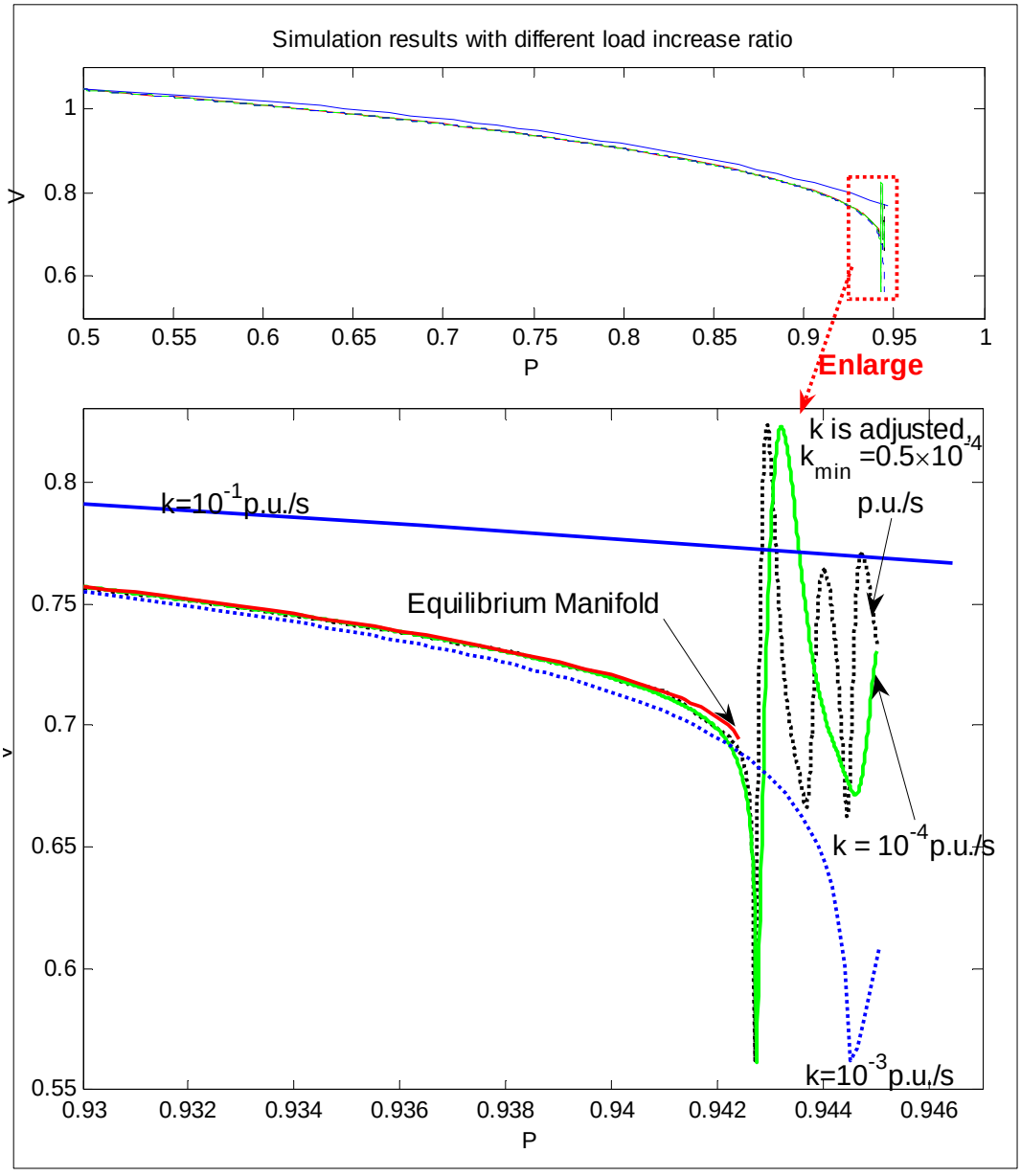

Figure IV-7 Comparison of numerical solutions

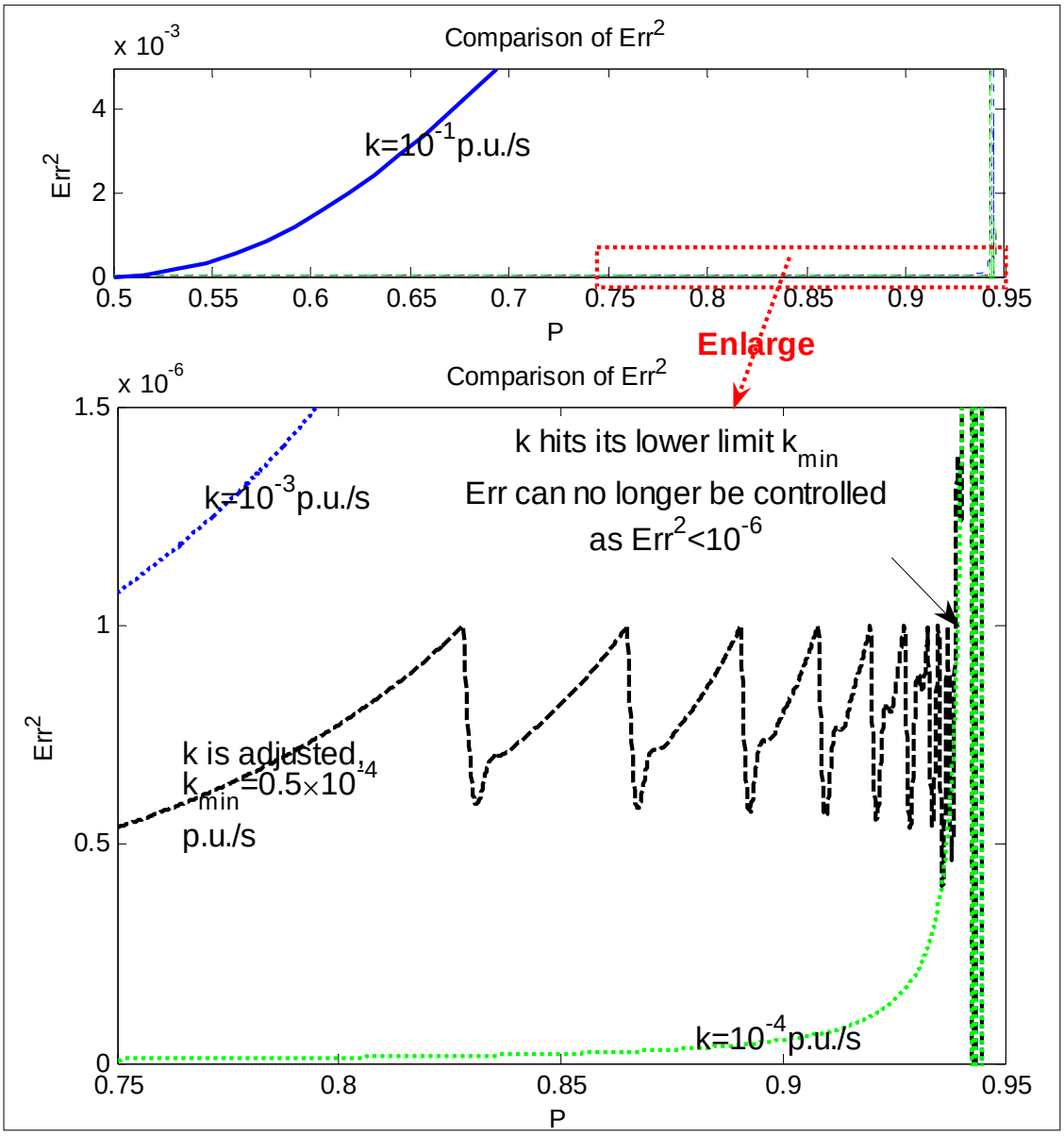

Figure IV-8 Comparison of global EMD error

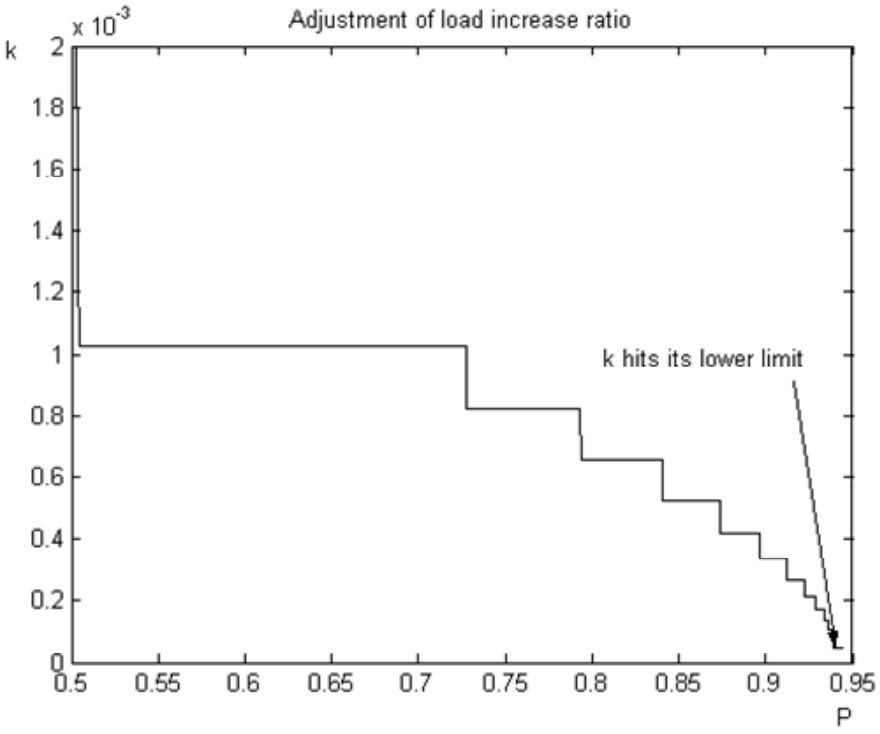

Figure IV-9 Adjustment of *k*

Comparing the results for case 3) and 4) in Figure IV-7, we can see that the trajectories are similar when *k* is small enough or intelligently adjusted. The difference of *Err* of four cases is shown in Figure IV-8. In the enlarged part of this figure, we can see that when system is approaching its Hopf bifurcation point, *Err* will increase drastically and no longer be controllable. Figure IV-8 and IV-9 demonstrate that our new scheme automatically adjusts *k* to control *Err* ($Err^2 < 10^{-6}$). Figure IV-9 indicates that *k* will be adjusted more frequently under stressed situation than in lightly loaded situation.

For case 4), when $P = 0.9385$, k hits its lower limit and Err is no longer controllable. $P = 0.9385$ is the estimated stability margin, which is close enough to the result obtained from eigenvalue analysis. For case 3), we found that when $P = 0.9394$, we no longer have $Err^2 < 10^{-6}$; we can see $P = 0.9394$ is also a good enough estimated margin.

However, for case 1) and 2), we have $Err^2 > 10^{-6}$ when $P = 0.503$ and $P = 0.739$ respectively, which apparently are wrong estimates as confirmed by eigenvalue analysis.

With these numerical tests, we can see that without our new EMD error criterion it is difficult to guarantee the estimation accuracy unless *k* is chosen extremely small. And our EMD reliably pinpoints the bifurcation point.

4.2 Our approach enhances computation efficiency

Here we compare the computation cost of several methods used to estimate the stability margin. All numerical solutions start from an equilibrium point at P=0.5, and will end at P=0.945.

1) Typical RK method —*k* and Δt are both fixed:
   $\Delta t = 0.01, k = 10^{-4}\ p.u./s$
2) Typical RK method with adjustment of *k* by (4.36)—only *k* will be adjusted:
   $\Delta t = 0.01$, initial value of $k = 10^{-3}\ p.u./s$, $k_{\min} = 0.5 \times 10^{-4}\ p.u./s$, $\varepsilon = 10^{-3}$ and $\beta = 0.8$.
3) Typical RKF method—only Δt will be adjusted:
   $k = 10^{-4}\ p.u./s$, initial value of $\Delta t = 0.5$, $\Delta t_{\min} = 10^{-4}$ and $\xi = 10^{-7}$
4) Our new approach using RKF method with adjustment of *k* by (4.36) —*k* and Δt are both adjusted:
   Initial value of $k = 0.001$, $k_{\min} = 0.5 \times 10^{-4}\ p.u./s$ and $\varepsilon = 10^{-3}$; initial value of $\Delta t = 0.5$, $\Delta t_{\min} = 10^{-4}$, $\xi = 10^{-7}$ and $\beta = 0.8$.

The estimated margins and computation costs by these four methods are listed in table IV-1.

Note that the typical 4th order RK method is a 4-stage method, and the RKF45 method used here is a 6-stage method [29, 30]. The computation cost in table IV-1 is calculated as:

$$(VS + RST + RSK) \times Stage\ \ of\ \ method$$

For example, the computation cost of 4) is calculated as:

$$(2670 + 437 + 14) \times 6 = 3121 \times 6$$

Table IV-1 Comparison of computation cost with similar estimated margin

Methods	Estimated Margin	Valid Steps (*VS*)	Rejected Steps of Δt (*RST*)	Rejected Steps of k (*RSK*)	Computation Cost
1)	0.9379	444990	0	0	444990×4 (100%)
2)	0.9369	93132	0	14	93146×4 (20.932%)
3)	0.9394	10254	1697	0	10951×6 (3.691%)
4)	0.9385	2670	437	14	3121×6 (1.052%)

Table IV-1 indicates that all these four methods give almost the same estimation of the dynamic stability margin. However, computation costs among these methods are very different. Comparing solutions of 1) and 2), which have constant time steps, we can see that the computation can be accelerated by automatically adjusting k; while by comparing solutions of 3) and 4), we can see the synergy of our new scheme that automatically adjusts Δt and k altogether. It is clear that our new method is the most efficient one. The estimated reduction of computation cost confirms with our actual computing time reduction running on PCs. Moreover, comparing to eigenvalue analysis, the speedup will be more drastic. In this case, the computing time with eigenvalue analysis is about 700 times more as with our new method.

4.3 Comparison of primitive and optimal load adjustment approach

4.3.1 The optimal approach can guarantee the accuracy of estimate more strictly

Here we compare four cases to demonstrate the advantage of our new load adjustment technique:

1) RKF method, primitive approach, with $k_{\min} = 10^{-3}\ p.u./s$, primitive

2) RKF method, primitive approach, with $k_{\min} = 10^{-4}\ p.u./s$

3) RKF method, primitive approach ,with $k_{\min} = 10^{-5}\ p.u./s$

4) RKF method, optimal approach, with adjustment of k by (4.44).

For case 1) ~ 3), $\beta = 0.8$. And for all these four cases, the initial value of Δt is selected as 0.5, $\Delta t_{\min} = 10^{-4}$ and $\xi = 10^{-7}$.

Numerical solutions are demonstrated in Figure IV-10. From the enlarged part of this figure, we observe that bigger deviation of numerical solutions from the equilibrium manifold for bigger $k_{\min}$. When $k_{\min} = 10^{-3}$, the solution deviate from its equilibrium manifold far early before the bifurcation point is approached. Note that when $k_{\min}$ is too big, the load perturbation is no longer small and a transient will occur. Thus, the obtained PV curve is questionable and invalid for small disturbance voltage stability analysis. On the other hand, when $k_{\min} \le 10^{-4}$ or with k adjusted by our new approach, the numerical solution stays around the equilibrium manifold.

Table IV-2 listed the estimated loadability margin for each case. Comparing with eigenvalue analysis result, we can see that the result for case 1) is a wrong estimate. On the contrary, the results for the last three cases are pretty accurate, especially for the last two cases.

Table IV-2 Comparison of accuracy

Method	Estimated Margin	Relative Error
1)	0.8780	6.04%
2)	0.9287	0.61%
3)	0.9381	0.40%
4)	0.9382	0.41%

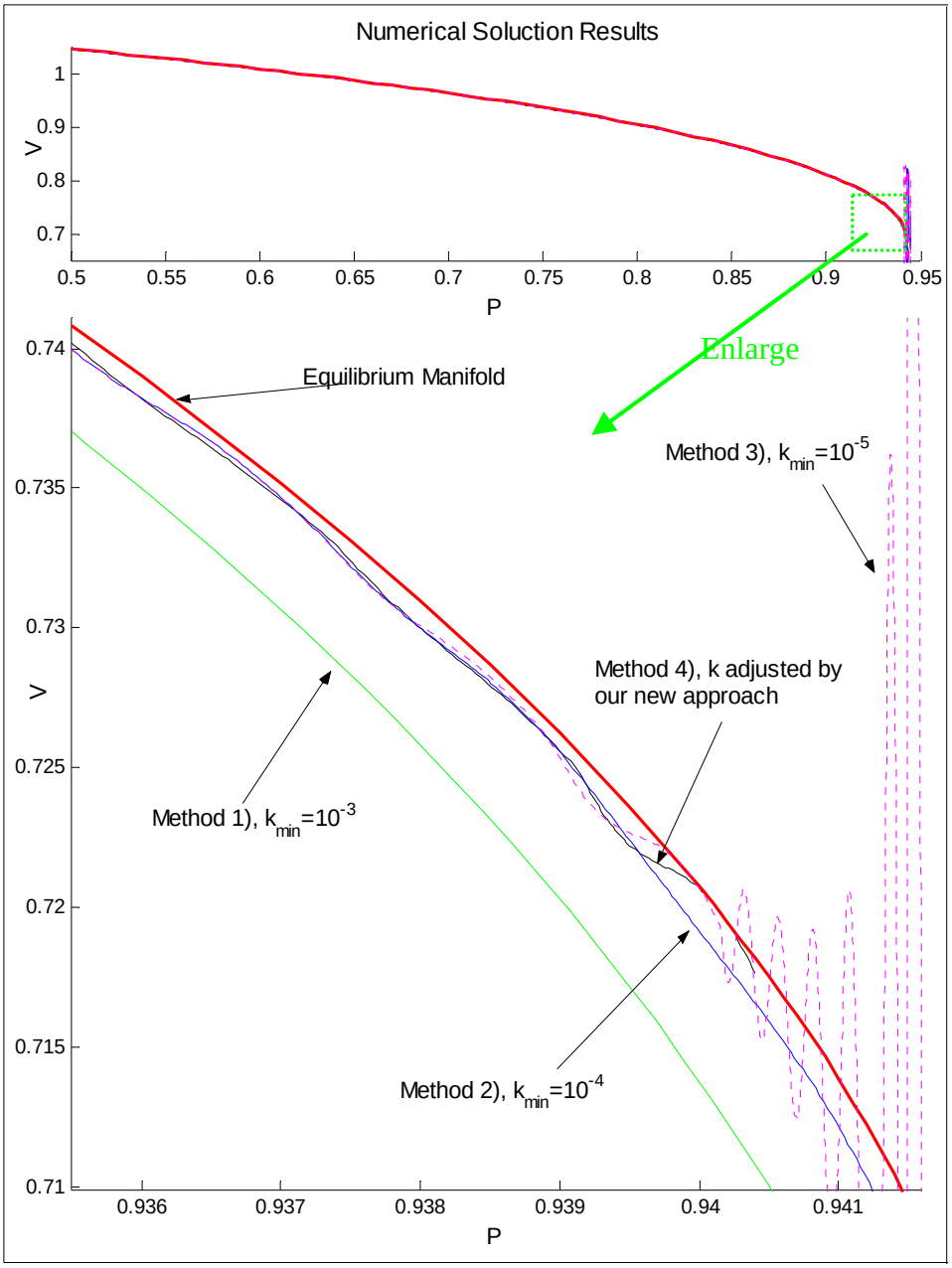

Figure IV-10 Comparison of numerical solutions

However, suppose that we have no eigenvalue analysis result, which is the general case for large systems due to the computation complexity of eigenvalue analysis, we have a question on how to judge the accuracy of our estimate. As shown before, we can mathematically guarantee it with our new approach. But if we detect loadability margin by a pre-selected selected $k_{\min}$, we may need extra work to verify our results. It is mathematically difficult to decide the reasonable value of $k_{\min}$. Thus, we may need to try a few smaller $k_{\min}$ and estimate the margin till we found that our estimates converge to a fixed-point value. For example, in case 2), we got an estimate as $P = 0.9287$, but we cannot tell it is accurate or not, so we decrease $k_{\min}$ as $k_{\min} = 10^{-5}$, then by comparing the results of case 2) and 3), we can claim we found the margin because the results for these two cases are very close.

4.3.2 The optimal approach can further enhance the computation efficiency

Here we compare 2 cases to demonstrate the computation efficiency of our new load adjustment technique:

1) RKF method, primitive approach, with $k_{\min} = 10^{-5}\ p.u./s$
2) RKF method, optimal approach, with adjustment of k by (4.44)

For these two cases, we selected the initial value of k as $0.1 p.u./s$, and other parameters the same as former test. The computation cost for these two cases are listed in table IV-3. Please note that, from 4.3.1, the estimations of stability margin are very close for these two cases. At the same accuracy level, now we will compare the computation costs of these two approaches.

From table IV-3, we can see that, with our new approach, we significantly improve the computation efficiency while maintaining the accuracy. We know that when system goes near to its bifurcation point, smaller *k* is needed to control *Err*, and the computation speed will slow down with smaller *k*. From Figure IV-11, we can see that as *p* increase to bifurcation point, method 1) tends to over adjust *k*, on the contrary, our new approach will select allowed biggest *k* at each adjustment. We know that the computation cost is roughly

determined by $1/(k\Delta t)$, so bigger k implies faster computation. As shown in Figure IV-4, k should be small in heavily loaded area to control *Err*, so the computation cost mainly comes from the calculation in this area. Figure IV-11 shows the adjustment of k in heavily loaded area. We can see that the optimal method needs slightly more adjustment, but have bigger k. Since the impact of k on computation cost is dominant, the optimal method has an advantage in computation efficiency.

Table IV-3 The advantage in computation efficiency of the optimal approach

Methods	Estimated Margin	Valid Steps (*VS*)	Rejected Steps of Δt (*RST*)	Rejected Steps of k (*RSK*)	Computation Cost
1)	0.9391	996	101	42	6139×6 (100%)
2)	0.9386	404	1096	3	3503×6 (57.06%)

We also found that, with this big initial value of k, method 1) take nine adjustments to control *Err* at the first step, which means that eight adjustments are rejected at first iteration. On the other hand, with our new approach, only one adjustment is necessary. Further investigation showed that, except when encountered by the bifurcation point, our adjustments by method 2) were all accepted. Accordingly, this advantage will further save the computation cost.

With these two numerical tests, we have demonstrated the advantage of the optimal approach. Numerical tests with other systems also verified it.

4.4 Our approach can be applied to big systems

Here the IEEE 162-bus 17-generator system will be used to demonstrate that our new approach is applicable to large systems.

Here we assume that all the loads in this system are constant power type load with a fixed power factor ($P = 2Q$). All numerical solutions begin with an equilibrium point determined by the initial value. At t=0s, all the loads in this system will change with the same ratio. When a bifurcation behavior is detected, the numerical solution will be stopped. In this example, two methods will be applied and compared:

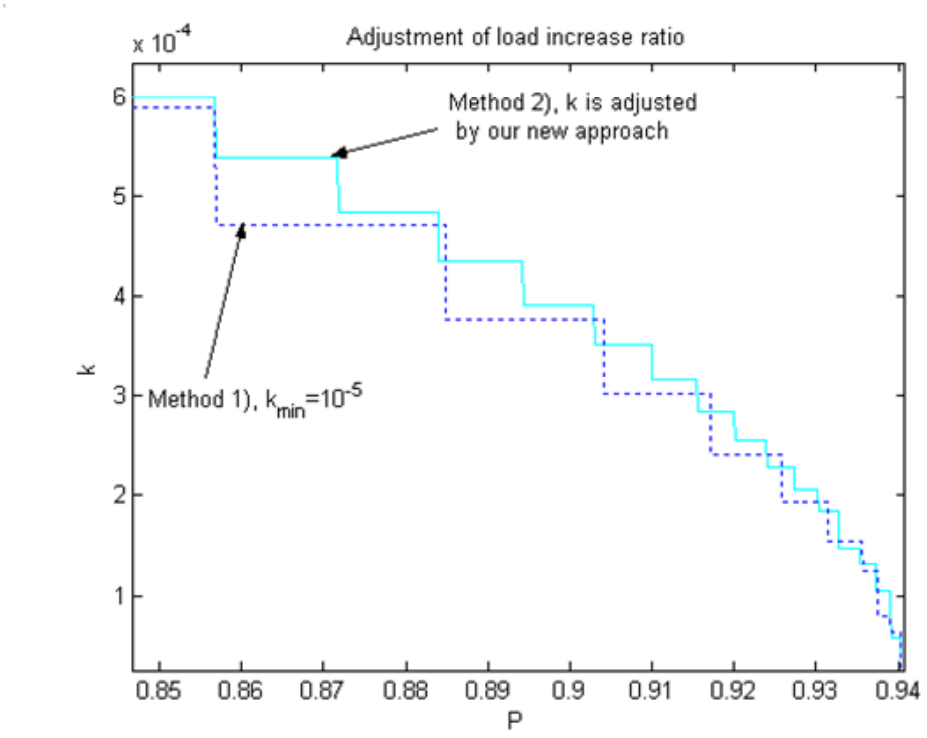

Figure IV-11 Comparison of adjustments of k

1) Typical RKF method—only Δt will be adjusted:

   $k = 10^{-4}\ p.u./s$, initial value of $\Delta t = 0.5$, $\Delta t_{\min} = 10^{-4}$ and $\xi = 10^{-7}$

2) Our new approach using RKF method with optimal adjustment of k by (4.44) —k and Δt are both adjusted:

   Initial value of $k = 0.001$, and $\varepsilon = 10^{-3}$; initial value of $\Delta t = 0.5$, $\Delta t_{\min} = 10^{-4}$ and $\xi = 10^{-7}$.

The estimated margins and computation costs by these two methods are listed in table IV-4. For methods 1), we found that when the load at bus 3 is increased to 174.21% of the original load at bus 3, a bifurcation behavior can be detected. So in table 4, we use 174.21% to denote the dynamic stability margin. While for method 2), the estimated margin is denoted by 173.88%.

Table IV-4 Comparison of computation cost

Methods	Estimated Margin	Valid Steps (*VS*)	Rejected Steps of Δt (*RST*)	Rejected Steps of k (*RSK*)	Computation Cost
1)	174.21%	.7782	2971	0	20753×6 (100%)
2)	173.88%	l809	922	3	5734×6 (27.63%)

Table IV-2 indicates both methods get almost the same estimate of the dynamic stability margin. However, our new scheme greatly enhances the computation efficiency. Similar results are expected and confirmed for many other big systems such as the IEEE 118 bus system since the computation cost is roughly determined by $1/(k\Delta t)$; and enhancement of computation efficiency comes from the adjustment of k. In each step of our new method, we use the allowed biggest k to enhance computation speed without loss of accuracy. Accordingly, our new method always enhances the computation speed despite the size of the system.

Compared to the RKF method without intelligent load adjustments, the speedup ratio of our method remains great for our two-bus system and 162 bus systems; and based on our experience with many other cases, similar speedup are expected for larger systems. Compared to the eigenvalue based approach, our approach has even better speedups. Our method avoids solving for equilibrium point and calculating the corresponding reduced Jacobean matrix (J_r) for each step, which is a time-consuming task for big systems. In

addition, our method replaces the complex and time consuming eigenvalue computation of J_r by a simple *Err* checking. Even for ideal cases, where *Jr* is very sparse and symmetric, computation cost of eigenvalue calculation will still increase as a polynomial function of system size. For example, when we apply QR [23, 24] method, a rather fast method for ideal cases, the computation cost is still at the level of $o(n^2)$, here *n* denotes the dimension of J_r. By contrast, the computation cost of our method is roughly a linear function of system size. Thus the bigger the system, the higher the speedup our method will be when compared to the eigenvalue based bifurcation analysis.

5. Conclusion

In this chapter, based on explicit Runge-Kutta methods, we prove rigorously that our new technique introduces synergy of simultaneously adjustment of time steps and load increasing ratios intelligently. The numerical tests show that our novel method not only has a great advantage in computation efficiency, but also has accuracy close to eigenvalue based bifurcation analysis for dynamic stability margin estimation. Moreover, unlike eigenvalue based bifurcation analysis, the computation cost of our method is only in linear relation with system size. Thus, the proposed technique has great potential for dynamic stability margin estimation for large systems.

CHAPTER V

FAST DYNAMIC VOLTAGE STABILITY MARGIN ESTIMATION USING IMPLICIT RK METHODS

1. Introduction

Our scheme investgated in Chapter IV is based on explicit RK methods. However, we know that when power system is in extreme loading conditions, it may approach its structurally unstable point, say, saddle node bifurcation, thus stiffness problem may appear. It is well known that explicit methods applied to stiff problems are generally not efficient [34]. Instead, when encountering stiffness, implicit methods should be applied for efficiency.

In this chapter, we further develop our new numerical scheme to deal with the stiffness problem and its associated ill-condtion issues for power system applications. When system is ill-conditioned, implicit method would be applied to achieve numerical stability. We further demonstrate the validity of our approach that combines the intelligent load adjustment technique with implicit method to save the computation cost without loss of accuracy.

Please note that in this chapter, ‘numerical stability’ will be one of the concerns, which is a totally different concept from ‘structure stability’. Essentially the ‘structure stability’ only depends on the physical network structure, load types and the generation systems of the power grids, and it has nothing to do with the chosen numerical simulation schemes to detect the structurally unstable point. On the other hand, ‘numerical stability’ depends heavily on of the chosen numerical methods. Basically, it is kind of accumulation of computation error and depends on the computing device and numerical method itself. For example, if we apply Euler and implicit Euler method to a stiff system respectively, different system structurally unstable point will be detected. But we should keep in mind that the system structurally unstable point is determined and should not vary with the

chosen numerical methods. The differences of the estimates only demonstrate different capability and suitable domains of these numerical methods.

As emphasized before, a key task of this dissertation is to detect the structurally unstable point of power system accurately and efficiently. It will be demonstrated that the EMD criterion proposed in Chapter IV is still valid to gauge the accuracy with stiff systems. And for ill-conditioned systems, a big challenge is to enhance the computation efficiency and keep solution numerically stable. Different implicit methods will be discussed in this Topic, and we will show that not all the implicit methods are capable to enhance the computation efficiency. Only those methods have A-stable [34] and L-stable [34] characters will be considered in this dissertation. And we will also attempt to integrate our intelligent load adjustment technique with proper implicit methods to further save computation costs without sacrificing accuracy.

2. Integrate load adjustment technique to implicit methods

In this section, we will first use a simple example to demonstrate the suitability of implicit methods for ill-conditioned system. Then several implicit methods will be introduced here. At last, the EMD criterion and the new load adjustment technique will be extended to implicit RK methods.

2.1 Implicit RK method is efficient for ill-conditioned system

A simple system, firstly introduced in [34], will be used here to demonstrate advantage of implicit methods in dealing with stiff problems.

$$\dot{x} = -50(x - \cos t) \qquad (5.1)$$

Equation (5.1) is a simple one-dimensional system. Apparently, the equilibrium manifold of this system is $x = \cos t$. Suppose that at $t = 0$, the system is in state (0, 0) due to a disturbance, we investigate the time response of this system after the disturbance. Here, two numerical methods are compared as follows:

- Explicit Euler method

❖ Implicit Euler method

The numerical simulation results are shown in Figure V-1 and V-2. Figure V-1 shows numerical simulation results with explicit Euler method. In this figure, we found that with step size $h < 2/50$, the simulation results are numerically stable, which is shown in case a) in Figure V-1. However, with $h \geq 2/50$, we found that the simulation results are numerically unstable, which is shown in case b). It is demonstrated that, with bigger h, there will be bigger oscillation. If $h < 2/50$, the oscillation is damped out, and the integration trajectory finally converges to equilibrium manifold. With $h = 2/50$, the oscillation can never be damped out and remains there with same amplitude. With $h > 2/50$, we have found that things could be even worse—the amplitude of the oscillation can increase and the integration trajectory can deviate further from equilibrium manifold.

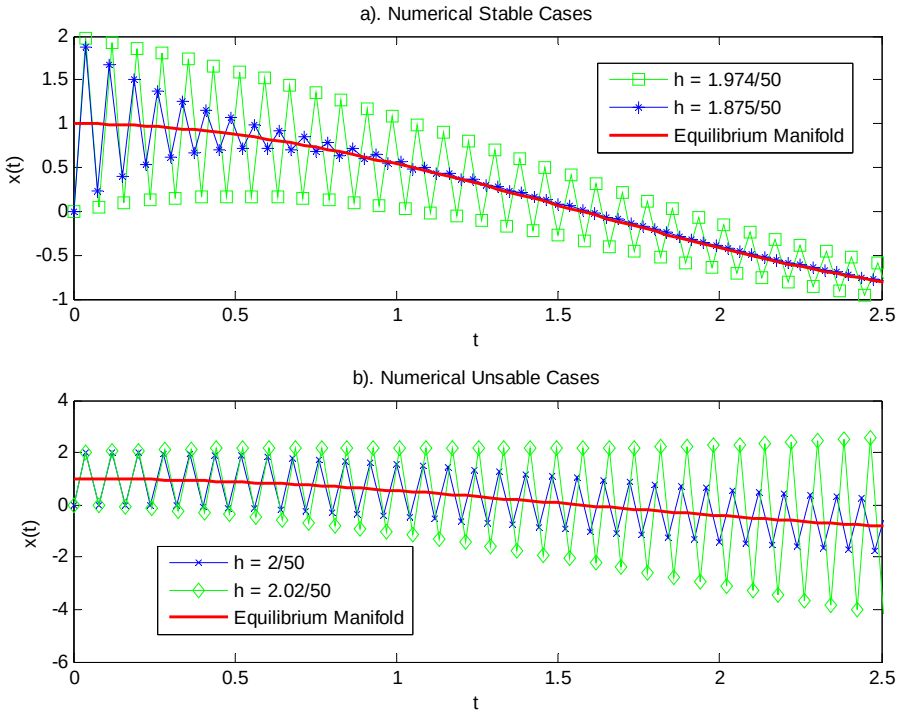

.

Figure V-1 Numerical simulation results with explicit Euler method

On the other hand, if we apply implicit Euler (IEuler) method, things are totally different. In Figure V-2, we have found that, even with a big step size $h = 0.5$, the simulation result exhibits numerical stability. In this figure, the integration trajectory converges to equilibrium manifold in just a few steps. However, for case a) in Figure V-1, a lot of integration steps are needed before the integration trajectories finally converge to equilibrium manifold, which means that a lot of computation efforts are wasted to damp out the transients caused by stiffness.

Moreover, in case b) of Figure V-1, the simulation results exhibit un-damped oscillations, which may lead to wrong conclusion that the system cannot survive from a disturbance $\Delta x = -1$, thus a numerically unstable case may be mistaken as a structurally unstable case.

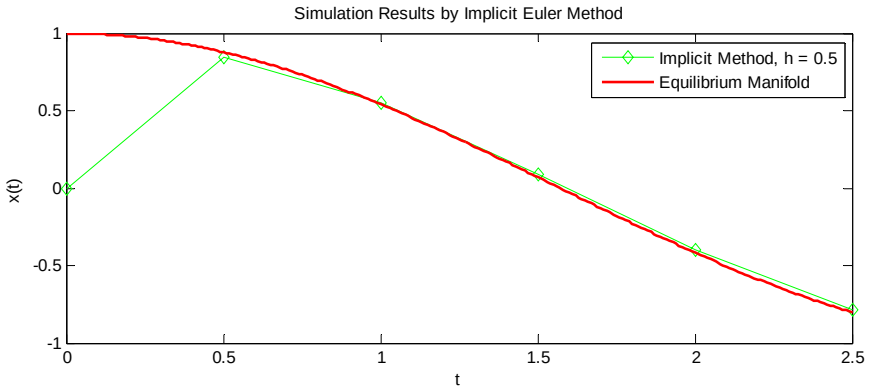

Figure V-2 Numerical simulation results with IEuler method

Now by numerical stability function [29], we will explain the difference between Figure V-1 and V-2. If we apply explicit Euler method $x_{n+1} = x_n + hf(t_n, x_n)$ to Dahluit's equation $\dot{x} = \lambda x$, we can get [34]:

$$x_{n+1} = R(z)x_n = (1 + h\lambda)x_n$$

Here $z = h\lambda$. $R(z)$ is the so called numerical stability function, and we should have $|R(z)| \le 1$ to get numerically stable solution [34]. Thus, the stable domain for explicit Euler method is $S = \{z \in C; |z-(-1) \le 1|\}$. For system (5.1), where $\lambda = -50$, we should have $0 \le h \le 2/50$ to satisfy $|R(z)| \le 1$. This explains that, in case a) of Figure V-1, when $h < 2/50$, the simulation results finally converge, and when $h \ge 2/50$, the integration trajectories exhibit numerically unstable behavior.

For implicit Euler method $x_{n+1} = x_n + hf(t_{n+1}, x_{n+1})$, its numerical stability function is $R(z) = \dfrac{1}{1-z}$, and the numerical stability domain covers the entire negative half-plane and a large part of the positive half-plane as well [34], which means that implicit Euler method is very stable. It mathematically explains that, even with a rather big step $h = 0.5$, the integration trajectory can easily converge to equilibrium manifold as demonstrated in Figure V-2.

2.2 Introduction of implicit methods

Generally, to solve equation $\dot{x} = f(t, x)$, the *s*-stage RK methods can be expressed as [30, 34]:

$$\begin{cases} K_i = x_0 + h\sum_{j=1}^{s} a_{ij} f(t_0 + c_j h, K_j) & i = 1,...,s \\ x_1 = x_0 + h\sum_{j=1}^{s} b_j f(t_0 + c_j h, K_j) \end{cases} \tag{5.2}$$

And for autonomous system $\dot{x} = f(x)$, equation (5.2) can be simplified as:

$$\begin{cases} K_i = x_0 + h\sum_{j=1}^{s} a_{ij} f(K_j) & i = 1,...,s \\ x_1 = x_0 + h\sum_{j=1}^{s} b_j f(K_j) \end{cases} \tag{5.3}$$

In (5.2), when $a_{ij} = 0$ for $i \geq j$, (5.2) will be an explicit Runge Kutta (ERK) method. If $a_{ij} = 0$ for $i > j$ and at least one $a_{ij} \neq 0$, we have a diagonal implicit RK (DIRK) method. If in addition all diagonal elements are identical $a_{ij} = \gamma$ for $i = 1,...,s$, (5.2) will be called as a singly diagonal implicit (SDIRK) method. In all other cases, we call (5.2) as implicit RK (IRK) method [30, 34].

With the paper of Butcher (1964) it became customary to symbolize method (5.2) by the tableau (5.4) [34]. From now on, we will use (5.4) to express all the RK methods discussed in this dissertation.

$$\begin{array}{c|ccccc} 0 & a_{11} & a_{12} & \dots & a_{1,s-1} & a_{1,s} \\ c_2 & a_{21} & a_{22} & \dots & a_{2,s-1} & a_{2,s} \\ c_3 & a_{31} & a_{32} & \dots & a_{3,s-1} & a_{3,s} \\ \vdots & \vdots & \vdots & \vdots & \vdots & \vdots \\ c_s & a_{s1} & a_{s2} & \dots & a_{s,s-1} & a_{s,s} \\ \hline & b_1 & b_2 & \dots & b_{s-1} & b_s \end{array} \qquad (5.4)$$

The numerical stability function of (5.2) is given as [34]:

$$R(z) = 1 + zb^T (I - zA)^{-1} E \qquad (5.5)$$

Here

$$b^T = (b_1,...,b_s), \quad A = \left(a_{ij}\right)_{i,j=1}^{s}, \quad E = (1,...,1)^T$$

Method (5.2) is called A-stable if its stability domain satisfies [34]

$$S \supset C^- = \{z; \ \operatorname{Re} z \leq 0\}$$

A-stable means that, as long as the Jacobian matrix of $\dot{x} = f(t,x)$ has no eigenvalue located in imaginary axis or in right half-plane, integration trajectory got with (5.2) will finally converge. Please note that not all implicit methods are A-stable [34]. However, an implicit method is A-stable may not guarantee efficiency in some cases. For example, the implicit midpoint method and trapezoidal rule method are A-stable implicit methods, and

both have stable function as $z=\frac{1+z/2}{1-z/2}$, thus, the stable domain of these two methods coincides exactly with the negative half-plane, and these two methods have a property as

$$\lim_{z\to-\infty}|R(z)|=\lim_{z\to\infty}|R(z)|=\lim_{z=iy,y\to\infty}|R(z)|=1$$

This means that, for z close to the real axis with a very large negative real part, $|R(a)|$ is, although <1, very close to 1. As a result, the transients are damped out only very slowly [34]. For example, if we change the parameter of system (5.1) as $\dot{x}=-5000(x-\cos t)$ and do the same simulation with implicit midpoint and trapezoidal rule method [34], we found that it will take a long time for oscillations to be damped out with increased stiffness of the system. It means that, A-stable cannot guarantee computation efficiency for severe stiff problems. Thus, in this chapter, we will focus on L-stable IRK methods.

Method (5.2) is called L-stable if it is A-stable and if in addition $\lim_{z\to-\infty}|R(z)|=0$. Apparently, implicit Euler method is L-stable [34]. Beside implicit Euler method, several other L-stable methods, such as the three order SDIRK method with $\gamma=(2\pm\sqrt{2})/2$ (SDIRK3), 5 order Radau IIA method (RADAU5), etc., will also be discussed in this chapter [34].

Detail forms of SDIRK3 and RADAU5 could be found in [30, 34]. And their numerical stability function are given as equation (5.6) and (5.7) respectively [34].

$$R(z)=\frac{1+z(1-2\gamma)+z^2(1/2-2\gamma+\gamma^2)}{(1-\gamma z)^2},\quad \gamma=(2\pm\sqrt{2})/2 \qquad (5.6)$$

$$R(z)=\frac{1+2z/5+z^2/20}{1-3z/5+3z^2/20-z^3/60} \qquad (5.7)$$

With (5.6) and (5.7), we can draw the numerically stable domain of these two methods, and it is easy to verify that these two methods are L-stable.

Among these three L-stable IRK methods mentioned above, RADAU5 has highest order and is the most complex one, and IEuler method is the simplest but with lowest order.

So later, we will mainly compare these two methods in numerical tests. Actually later we will show that, though more complex compared with IEuler, RADAU5 is more efficient with same requirement of accuracy.

With IRK methods, we need to solve nonlinear equation iteratively at each step. Here, as the results in n^{th} step could be used as initial values for the $n+1^{th}$ step, simplified Newton method is recommended to solve nonlinear equation efficiently [34].

2.3 Extend EMD criterion and load adjustment technique to L-stable IRK methods

EMD criterion is introduced in Chapter IV. The basic idea behind the EMD criterion is that, before a system approaches its bifurcation point, by definition the system should remain around equilibrium manifold after a small disturbance. Based on the definition of small disturbance voltage stability analysis, EMD criterion, which is used to guarantee the accuracy of estimate of structurally unstable point, has nothing to do with chosen numerical method to solve differential equations. Thus, it can be extended to all small disturbance analysis by its essential definition.

Similarly, we can still define a global EMD error and a local truncation EMD error as we did in Chapter IV. Now with IRK methods are considered, there are several questions need to be answered before we can integrate the automatic load adjustment technique with IRK methods.

In section 2.2 of Chapter IV, we have a rigorous impact analysis of k and Δt on Err. With ERK methods, we proved that, Err will be controlled if local EMD error per unit time $\frac{\overline{err}}{\Delta t_n}$ is controlled. And as proved, $\frac{\overline{err}}{\Delta t_n}$ is mainly determined by k, thus that Err is also mainly determined by k. The automatic load adjustment technique is proposed based on these conclusions. Therefore, a key question is that, will these conclusions still hold for IRK methods?

By review of Chapter IV, we know that if the *Theorem 1* proposed in Chapter IV still hold for IRK methods, then all these conclusions could be extended to IRK methods. As

demonstrated, the proof of *Theorem 1* is based on the proof of *Lemma 1* and *Lemma 2*. Thus, if *Lemma 1* and *2* could be proved with IRK methods, then *Theorem 1* can be easily extended to IRK methods. Now let us check the validity of these two Lemmas with IRK methods.

First, with IEuler method, we will show that *Lemma 1* can be extended to IRK methods, and a similar Lemma, denoted by *Lemma 1'*, is introduced and can be proved with IRK methods.

Lemma 1':

Applying single-step IRK methods to solve the system equation described as (4.2), we have the local EMD error $\overline{err}$ as shown in (5.8) with positive scalars k and Δt_n pulled out.

$$\overline{err} = \left\| \left(o(\Delta t_n) + C(x_n, y_n, p_n) \right) \right\| k \Delta t_n \tag{5.8}$$

Proof:

From (4.11), we know that

$$\begin{cases} \hat{e}_i \approx h_{i,x} \Delta x_n + h_{i,y} \Delta y_n + h_{i,p} \Delta p_n \\ \overline{err} = \left\| \hat{e} \right\| \end{cases} \tag{5.9}$$

Here $\Delta p_n = k \Delta t_n$, and Δy_n is obtained by power flow calculation, so we still have $\Delta y_n = \Phi(x_n, y_n, p_n) k \Delta t_n$ as given in equation (4.12).

Without loss of generality, suppose that IEuler method is applied to solve swing equation, we have

$$\begin{aligned} \Delta x_n &= x_{n+1} - x_n \\ &= \Delta t_n f(x_{n+1}, y_{n+1}, p_{n+1}) \\ &= \Delta t_n f(x_n + \Delta x_n, y_n + \Delta y_n, p_n + \Delta p_n) \end{aligned} \tag{5.10}$$

By Taylor's expansion, (5.10) can be written as

$$\Delta x_n = \Delta t_n \left[f(x_n, y_n, p_n) + f_x \Delta x_n + f_y \Delta y_n + f_p \Delta p_n \right]$$
$$\Delta x_n = \frac{\Delta t_n \left[f_y \Delta y_n + f_p \Delta p_n \right]}{1 - \Delta t_n f_x} \qquad (5.11)$$

Substituting $\Delta p_n = k\Delta t_n$ and $\Delta y_n = \Phi(x_n, y_n, p_n) k\Delta t_n$ into (5.11), we have

$$\Delta x_n = \frac{k\Delta t_n (\Phi f_y \Delta t_n + f_p \Delta t_n)}{1 - \Delta t_n f_x} \qquad (5.12)$$

Substituting Δp_n, Δy_n and (5.12) into (5.9), we have

$$\begin{aligned} \hat{e}_i &\approx h_{i,x}\Delta x_n + h_{i,y}\Delta y_n + h_{i,p}\Delta p_n \\ &= k\Delta t_n \left(\frac{h_{i,x}(\Phi f_y + f_p)\Delta t_n}{1 - \Delta t_n f_x} + h_{i,y}\Phi(x_n, y_n, p_n) + h_{i,p} \right) \\ &= \left(o(\Delta t_n) + C_i \right) k\Delta t_n \end{aligned} \qquad (5.13)$$

Where

$C_i = h_{i,y}\Phi + h_{i,p}$.

So we have:

$$\overline{err} = \left\| \left(o(\Delta t_n) + C(x_n, y_n, p_n) \right) k\Delta t_n \right\| \qquad (5.14)$$

Where

$C(x_n, y_n, p_n) = \sqrt{\sum_{i=1}^{n+m} C_i^2}$.

Thus, *Lemma 1'* is proved.

Second, we will show that *Lemma 2* can be extended to IRK methods, and a similar Lemma, denoted by *Lemma 2'*, is introduced and can be proved with IRK methods.

Lemma 2':

Suppose a system described as (4.2) satisfies the condition i), ii) and iii) of Theorem 1, then we have:

$$\left|x_{eq}(t)-\tilde{x}_h(t)\right| \le \frac{k\lambda}{L}\left(e^{L(t-t_0)}-1\right) \tag{5.15}$$

$$\left|y_{eq}(t)-\tilde{y}_h(t)\right| \le \frac{k\lambda}{L}\left(e^{L(t-t_0)}-1\right) \tag{5.16}$$

Here $\left[\tilde{x}_h(t),\tilde{y}_h(t)\right]$ denotes the numerical solution of the system starts from an equilibrium point (x_0, y_0, p_0, t_0), and $[x_{eq}(t), y_{eq}(t)]$ denotes the equilibrium manifold of the system, and L-stable IRK methods are applied here.

To prove *Lemma 2'*, one choice we have is to follow similar logic as shown in the proof of *Lemma 2*. Here, we will demonstrate another simpler way to prove it.

When we apply IRK methods to solve swing equations, there should be an internal iteration to solve nonlinear equations. For example, when IEuler method is applied, at each step, we should solve a nonlinear equation as

$$x_{n+1} - x_n = \Delta t_n f(x_{n+1}, y_{n+1}, p_{n+1}) \tag{5.17}$$

Here Newton-Raphson or simplified Newton method [34] will be applied to solve (5.17) iteratively till x_{n+1} converges.

On the other hand, when ERK is applied, as shown in Figure IV-1, we only take one step to solve swing equations. Thus, with same *k* and Δt_n, single step calculation by ERK methods should have worse convergence compared with multi-step iteration by IRK methods. This implies that, after calculation of swing equations at each iteration, the simulation trajectory calculated by IRK method will stay closer to Equilibrium Manifold than the one got with ERK method. As shown in Chapter IV, the trajectory calculated by ERK is denoted as $\left[x_h(t), y_h(t)\right]$, then we have

$$\begin{aligned}\left|x_{eq}(t)-\tilde{x}_h(t)\right| &\le \left|x_{eq}(t)-x_h(t)\right| \\ \left|y_{eq}(t)-\tilde{y}_h(t)\right| &\le \left|y_{eq}(t)-y_h(t)\right|\end{aligned} \tag{5.18}$$

And by Lemma 2, we already have

$$\left|x_{eq}(t)-x_h(t)\right| \le \frac{k\lambda}{L}\left(e^{L(t-t_0)}-1\right)$$
$$\left|y_{eq}(t)-y_h(t)\right| \le \frac{k\lambda}{L}\left(e^{L(t-t_0)}-1\right) \qquad (5.19)$$

By (5.18) and (5.19), *Lemma 2'* is proved.

Similarly, we know that *Theorem 1* is still valid with IRK methods. Thus, based on former discussion, we know that the automatic load adjustment technique, no matter the primitive one or the optimal one discussed in Chapter IV, could be integrated with IRK methods.

As shown in Figure V-3, when load adjustment technique is integrated with L-stable IRK methods, adjustment of Δt is no longer considered. The reason is that, as L-stable IRK methods are applied, numerical stability can be guaranteed, thus we can choose big Δt and no longer need to worry about the adjustment of Δt. However, within the internal iteration to solve swing equation, step-size control technique could be still helpful. Further research on this could be one part of future work.

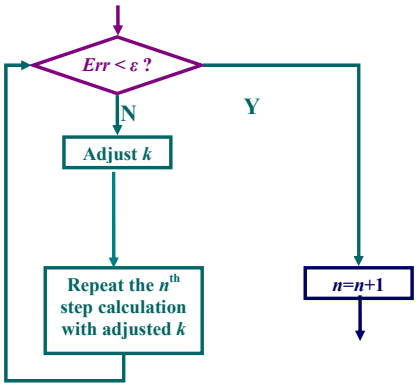

Figure V-3 Integration load adjustment with IRK methods

2.4 The new comprehensive numerical approach for long term dynamic small disturbance analysis

Before further discussion, we will demonstrate that, with load increase, the system may become stiff while approaching its bifurcation point. For example, with the same simple system used in Chapter IV, we found that, when $P > 0.85$, the condition number of the Jacobian matrix will begin to increase drastically, which is shown in Figure V-4. Correspondingly, if we apply RKF45 method to do simulation, just as case 3) in section 4.2 of Chapter IV, we can see that Δt will be adjusted frequently to remain integration trajectory numerically stable when system becomes stiff, which is shown in Figure V-5.

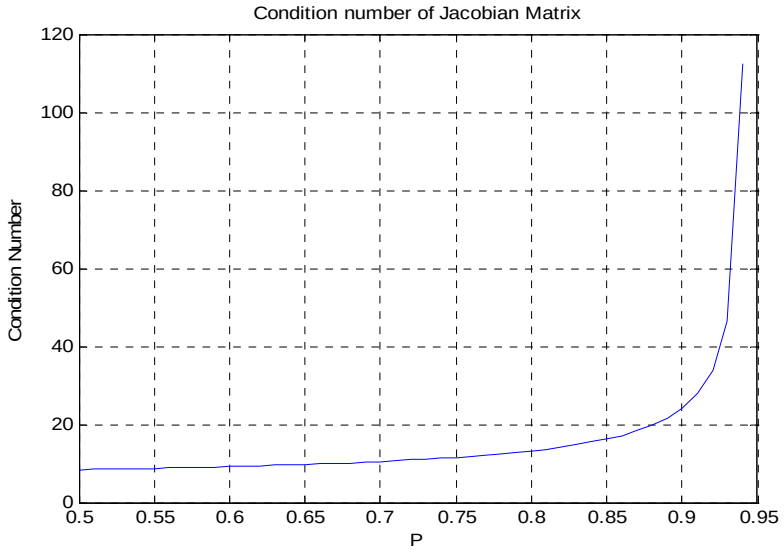

Figure V-4 Change of condition number with increased load

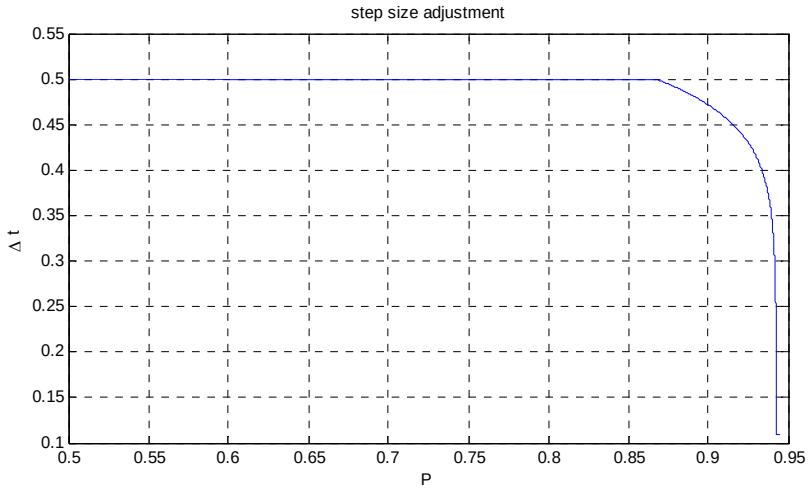

Figure V-5 Adjustment of Δt

2.4.1 Automatic stiffness detection

It is well known that implicit methods generally have better numerical stability than explicit methods [34]. However, for a general implicit approach, it needs to solve the nonlinear equations iteratively at each step and will incur extra computation burden. Thus, when system is lightly loaded or in normal operating conditions, explicit methods are naturally more attractive than implicit approach. On the other hand, when dealing with stiff problems, implicit method will be more efficient than explicit methods. So a burning question is that, during numerical simulations, how to detect stiffness automatically with cheap computation costs. With such a detection scheme, we can switch to a more suitable method to enhance the computation efficiency.

In 1977, Shampine & Hiebert proposed some ideas to deal with this problem [34], and there are other approaches in the literature [30], such as detecting stiffness by directly estimating the dominant eigenvalue of the Jacobian matrix of the problem [30]. This dissertation will apply the ideas of Shampine & hiebert to voltage stability analysis. Now we will give a brief introduction of this idea based on Dormand & Prince method of order 5 (DOPRI54).

DOPRI54 is a 7 stage and 5th order explicit embedded Runga-Kutta method [34]. Similarly as we can use (5.4) to express (5.2), DOPRI54 method can be described as in Table V-1.

Table V-1 Tableau of DOPRI54 method

0							
$\frac{1}{5}$	$\frac{1}{5}$						
$\frac{3}{10}$	$\frac{3}{40}$	$\frac{9}{40}$					
$\frac{4}{5}$	$\frac{44}{55}$	$-\frac{56}{15}$	$\frac{32}{9}$				
$\frac{8}{9}$	$\frac{19372}{6561}$	$-\frac{25360}{2187}$	$\frac{64448}{6561}$	$-\frac{212}{729}$			
1	$\frac{9017}{3168}$	$-\frac{355}{33}$	$\frac{46732}{5247}$	$\frac{49}{176}$	$-\frac{5130}{18656}$		
1	$\frac{35}{384}$	0	$\frac{500}{1113}$	$\frac{125}{192}$	$-\frac{2187}{6784}$	$\frac{11}{84}$	
y_1	$\frac{35}{384}$	0	$\frac{500}{1113}$	$\frac{125}{192}$	$-\frac{2187}{6784}$	$\frac{11}{84}$	0
$\hat{y}_1$	$\frac{5197}{57600}$	0	$\frac{7571}{16695}$	$\frac{393}{640}$	$-\frac{92097}{339200}$	$\frac{187}{2100}$	$\frac{1}{40}$

Similarly as embedded explicit RKF4(5) method, DOPRI method automatically adjust step size by equation (5.20) and (5.21).

$$\begin{cases} \theta = 0.9\left|\dfrac{\xi}{d^*_{n+1}}\right|^{1/5} \\ d^*_{n+1} = \Delta t_n\left(\dfrac{71}{57600}K_1 - \dfrac{71}{16695}K_3 + \dfrac{71}{1920}K_4 - \dfrac{17253}{339200}K_5 + \dfrac{22}{525}K_6 - \dfrac{1}{40}K_7\right) \end{cases} \tag{5.20}$$

$$\begin{cases} \Delta t_{n+1} = \theta \Delta t_n & \text{If } \theta < 1 \\ \Delta t_{n+1} = \Delta t_n & \text{If } \theta \geq 1 \end{cases} \tag{5.21}$$

DOPRI54 is not a stiff solver, and may become unstable if the solution changes rapidly over one time step. However, adapting the idea of Shampine & Hiebert to DOPRI54, we can have a simple stiffness detection scheme.

As shown in [34], we can construct an another local numerical truncation error estimation as

$$\tilde{d}^*_{n+1} = \Delta t_n \left(-2.134K_1 + 2.2K_2 - 0.24K_3 + 0.13K_4 + 0.144K_5 - 0.1K_6 \right)$$

During simulation, if $\left|\tilde{d}^*_{n+1}\right| < \left|d^*_{n+1}\right|$ occurs several times in succession (say 15 times), then switching to a L-stable IRK method will be more efficient.

Comparing DOPRI54 with RKF45 that mainly used in Chapter IV, we know that DOPRI54 is a 7-stage method and RKF45 is a 6-stage method, and both are 5^{th} order methods. Though DOPRI54 has one more stage and thus incur more computation cost, it does have bigger stable domain than RKF45, which is demonstrated in Fig. 2.8 of [34]. Also, with DOPRI54, it will be easier for automatically stiffness detection. That could also explain why DOPRI54 has been adopted as one of the main solvers of function 'ODE45' in MATLAB.

Due to our experience with power systems, we found that, when system is lightly loaded, generally it may have less chance to be stiff, which is the case shown in Figure V-4. So in normal conditions, as we have less worry about numerical stability, we can use RKF45 method without trying to detect stiffness. And when system is getting stressed, say one of the bus voltage drops below 0.9 or 0.85pu, we can switch to DOPRI54 method and try automatically stiffness detection. And if stiffness is detected, we can further switch to L-stable IRK methods, such as IEuler method and RADAU5 method. And with L-stable IRK method, numerical stability can be guaranteed, so big step size could be selected to enhance computation efficiency.

No matter ERK or IRK method we choose, EMD criterion always works, and we can apply automatically load adjustment technique to further enhance computation efficiency. Thus, a new comprehensive numerical simulation scheme is proposed in next sub-section.

2.4.2 The new general numerical simulation scheme

Figure V-6 shows a new comprehensive numerical scheme for long term small disturbance analysis. In this scheme, EMD criterion is still used to detect bifurcation behavior, and automatically load adjustment technique is integrated with ERK and IRK methods. Also, this new numerical scheme contains a logic to automatically detect stiffness. Thus, applying this comprehensive scheme, we can deal with all kinds of long term small disturbance analysis. Actually, as all our proof and deduction in this dissertation are based on a general DAE system shown as (5.22), the scheme shown in Figure V-6 can serve as a universal approach to detect structurally unstable point for a general DAE system. And with this scheme, no matter the system is stiff or not, the computation efficiency will be greatly enhanced without sacrificing accuracy.

$$\begin{cases} \dot{x} = f(x, y, p), & f : \Re^{n+m+q} \to \Re^{n} \\ 0 = g(x, y, p), & g : \Re^{n+m+q} \to \Re^{m} \end{cases} \qquad (5.22)$$
$$x \in X \subset \Re^{n},\ y \in Y \subset \Re^{m},\ p \in P \subset \Re^{k}$$

One thing we should emphasize is that, when we switch to IRK methods, there should be an internal iteration to solve nonlinear equations by simplified Newton method in 2nd step shown in Figure V-6 [34]. On the other hand, when ERK is applied, there is no internal iteration in 2nd step of above approach [32, 33].

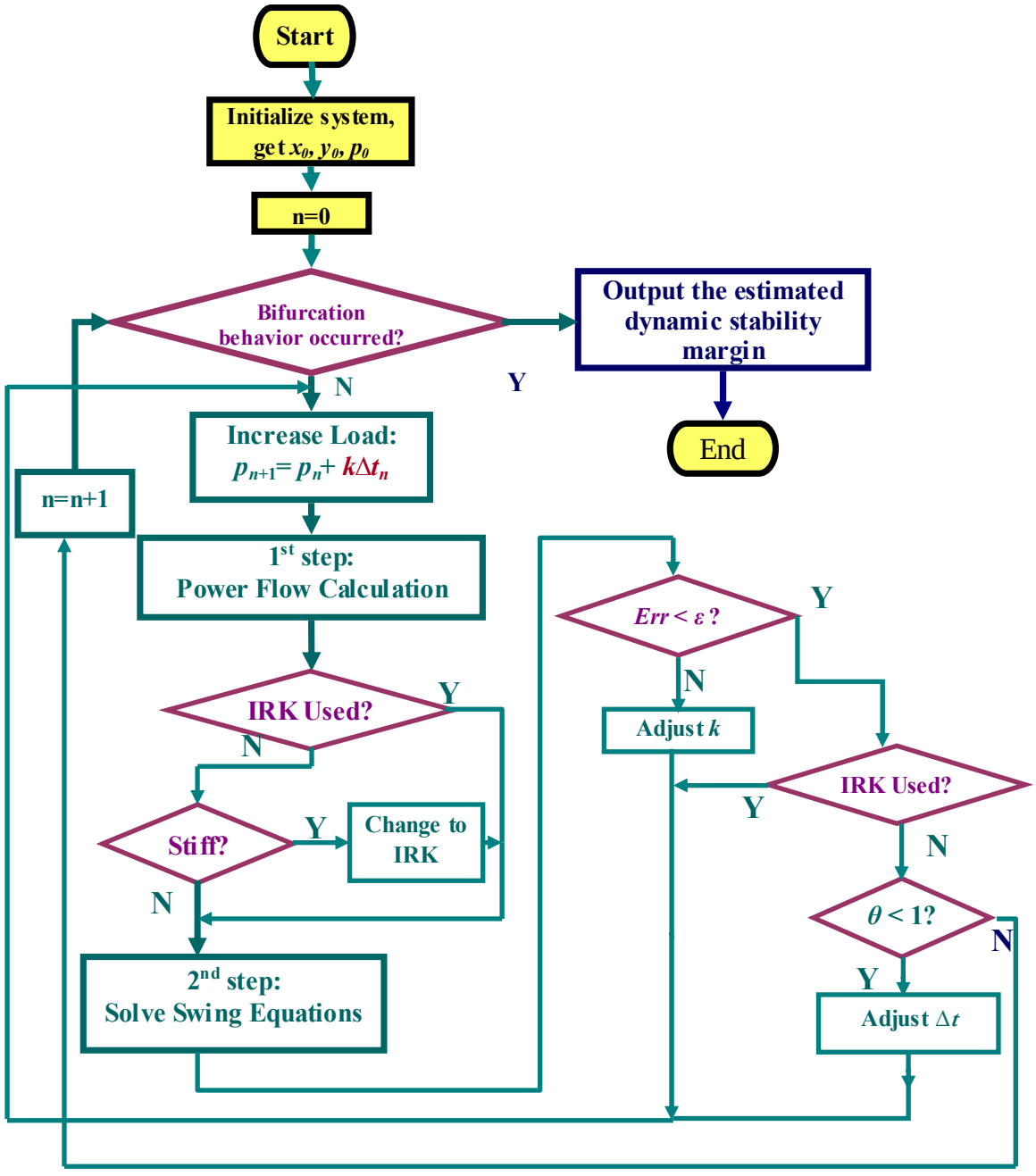

Figure V-6 The new comprehensive numerical scheme for long term small disturbance analysis

2.5 Numerical tests

2.5.1 Combining automatic load adjustment technique with L-stable IRK methods

With the same simple system used in Chapter IV, we demonstrate that our automatic load adjustment technique can be integrated with L-stable IRK methods to enhance computation efficiency. Here, four cases will be compared.

1) Implicit Euler method, with fixed $k = 10^{-4}\ p.u./s$, $\Delta t = 0.2$

2) Implicit Euler method, with *k* adjusted by equation (4.44), $\Delta t = 0.2$

3) SDIRK3 method, with *k* adjusted by equation (4.44), $\Delta t = 0.4$

4) RADAU5 method, with *k* adjusted by equation (4.44), $\Delta t = 0.5$

For all these four cases, Δt will not be adjusted. And for case 2), 3) and 4), the initial value of k is selected as $k = 10^{-2}\ p.u./s$. Now let us take a look at simulation results.

Table V-2 Estimated margin

Method	Estimated Margin	Relative Error
1)	0.9401	0.847%
2)	0.9382	0.643%
3)	0.9381	0.633%
4)	0.9312	0.1072%

Table V-2 shows that, the estimated margin for these four cases are very close to the real margin calculated by eigenvalue based bifurcation analysis. However, with the same level of accuracy, we found that there are big differences among computation costs of these cases, which is shown in Table V-3.

From Table V-3, we found that case 1) is the most time consuming one, and compare case 1) and 2), we can see that the computation cost is greatly enhanced with integration of automatic load adjustment.

With same level of accuracy, we also found that RADAU5 has higher computation efficiency than the other two L-stable methods. Though it has highest stages, but it need fewest internal iterations due to its high order of accuracy.

Table V-3 Computation costs

Method	Valid steps (*VS*)	Adjusted Steps of *k* (*ASK*)	Stage of Method	Average Internal iterations	Computation Cost
1)	22251	0	1	4.01172980989618	$(22251+0)\times 1\times 4.01172980989618$ (100%)
2)	8926	24	1	4.07003654080390	$(8926+24)\times 1\times 4.07003654080390$ (40.81%)
3)	3708	32	3	2.73751611516975	$(3708+32)\times 3\times 2.73751611516975$ (34.41%)
4)	2367	35	6	2.11915473755965	$(2367+35)\times 6\times 2.11915473755965$ (34.21%)

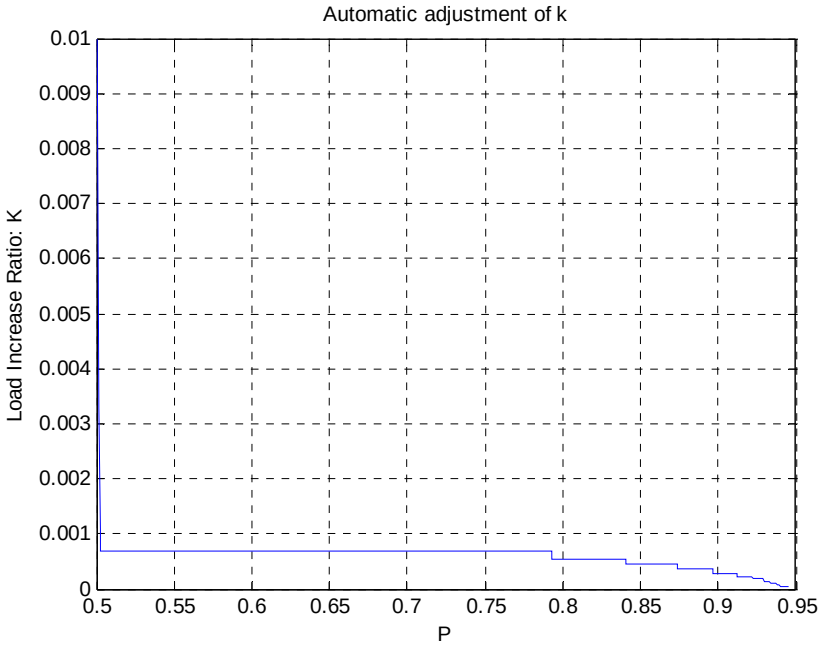

Figure V-7 Automatic adjustment of *k*

Figure V-7 shows that, in case 2), how load increase ratio is adjusted automatically. This explains that why the computation cost of case 1) is almost 2.5 times as the one of case 2).

2.5.2 The comprehensive scheme can further enhance computation efficiency

Now we will apply our new comprehensive scheme to the same system used with above examples. Here we will compare two cases.

1) RADAU5 method, with k adjusted by equation (4.44), $\Delta t = 0.5$

2) By our new comprehensive scheme, first explicit RKF45 method will be apply, then when bus voltage drops to 0.85p.u., it will automatically switches to DOPRI54 method with detection of stiffness. And if stiffness is detected, RADAU5 will be applied.

For these two cases, the initial value of k is selected as $k = 10^{-2}\ p.u./s$. And for case 2), the initial value of Δt is set as 0.5. Δt will be automatically adjusted by RKF45 and DOPRI54 respectively in different simulation time. When it switches from DOPRI54 to RADAU5, Δt will be set back to 0.5 and keep fixed.

Please note that here the case 1) is exactly the case 4) in 2.5.1, so its estimated margin and computation cost are already known. For case 2), its simulation results is given in figure V-8.

Table V-4 Computation cost of case 2

Different Simulation Period	Method	Valid Steps (*VS*)	Adjusted Steps of Δt (*AST*)	Adjusted Steps of k (*ASK*)	Stage of Method	Average Internal iterations	Computation Cost
P<=0.866	RKF45	2299	1	17	6	1	$(2299+1+17)\times 6\times 1$
0.866<P<0.89	DOPRI54	94	19	2	7	1	$(94+19+2)\times 7\times 1$
P>=0.89	RADAU5	252	0	7	6	2.23751611516975	$(252+0+7)\times 6\times 2.23751611516975$

By case 2), the estimated margin is 0.9331, and the relative error of estimation is 0.14%. Compared with case 1), it is also a very good estimate and has the same level of accuracy. For case 2), its computation cost is demonstrated in Table V-4. Compared with case 1), we found that the computation cost of case 2) is 59.54% of case 1).

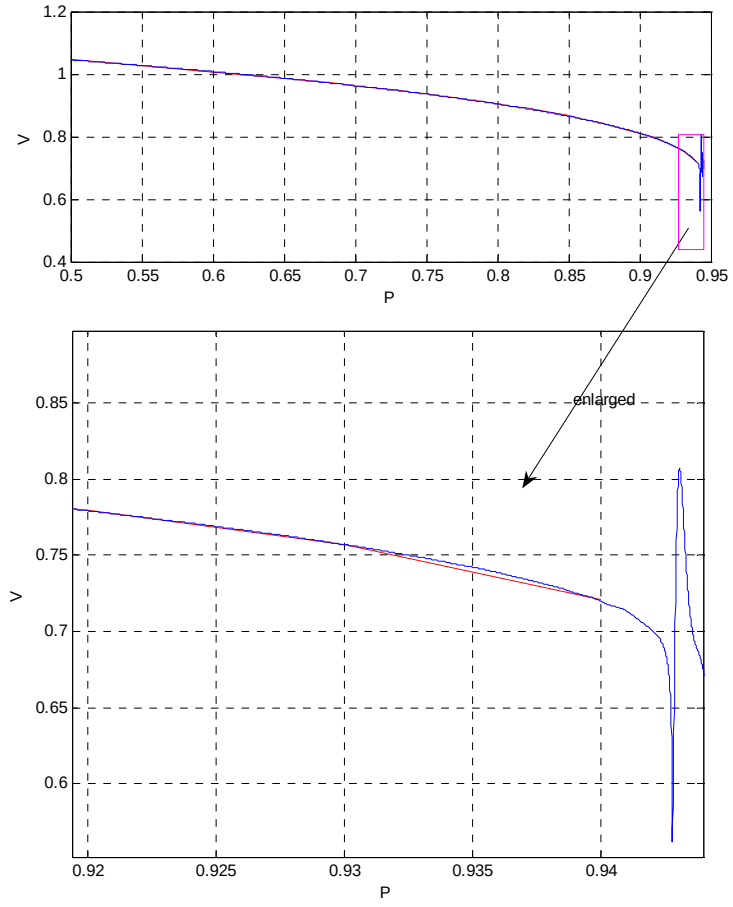

Figure V-8 Simulation results of case 2

2.5.3 The comprehensive scheme works with a large system

Here the IEEE 162-bus 17-generator system will be used to demonstrate that our new approach is applicable to large systems. It is the same system we used in section 4.4 of Chapter IV.

Here we still assume that all the loads in this system are constant power type load with a fixed power factor ($P = 2Q$). All numerical solutions begin with an equilibrium point determined by the initial value. At t=0s, all the loads in this system will change with the same ratio. When a bifurcation behavior is detected, the numerical solution will be stopped. In this example, two methods will be applied and compared:

1) Our new comprehensive scheme, as shown in Figure V-6:
   First explicit RKF45 method will be apply, then when any bus voltage drops to 0.85p.u., it will automatically switches to DOPRI54 method with detection of stiffness. And if stiffness is detected, RADAU5 will be applied.
2) RKF method with optimal adjustment of k —k and Δt are both adjusted:
   This is the same case as case 2) in section 4.4 of Chapter IV.

Table V-5 Computation cost of case 1

Different Simulation Period	Method	Valid Steps (*VS*)	Adjusted Steps of Δt (*AST*)	Adjusted Steps of k (*ASK*)	Stage of Method	Average Internal iterations	Computation Cost
|V|>=0.85	RKF45	3527	571	14	6	1	$(3527+571+14)\times 6\times 1$
|V|<0.85	DOPRI54	161	151	4	7	1	$(161+151+4)\times 7\times 1$
Stiffness detected	RADAU5	277	0	22	6	2.2137516116245	$(277+0+22)\times 6\times 2.2137516116245$

From Chapter IV, we already found that when the load at bus 3 is increased to 173.88% of the original load at bus 3, a bifurcation behavior can be detected for case 2). Similarly as in Chapter IV, here we use 173.88% to denote the dynamic stability margin. While for case

1), the estimated margin is denoted by 174.71%. The computation cost of case 2) is already given in section 4.4 of Chapter IV. Now let's take a look at the computation cost of case 1).

Table V-5 shows the computation cost of case 1) in different simulation stage. Compared with Case 2), its computation cost is nearly 89.96% of case 2). For these two cases, we get almost the same estimate of the dynamic stability margin. However, our new scheme could enhance the computation efficiency. Similar results are expected and confirmed for many other big systems.

3. Conclusion

In this chapter, we demonstrate the advantage of L-stable IRK methods in dealing with stiff problems. It is proved that, the EMD criterion and automatic load adjustment technique can be integrated with L-stable IRK to estimate stability margin for ill-conditioned systems. With this integration, computation efficiency is greatly enhanced, and the numerical stability and the accuracy of estimate can still be guaranteed.

This chapter also discussed automatic stiffness detection based on DOPRI54 method and the idea of Shampine & Hiebert. Moreover, with our experience on power systems, a simple but practical approach is proposed here to further enhance computation efficiency.

At last, a comprehensive numerical scheme is proposed in this Topic, which integrates the automatic stiffness detection, the intelligent load adjustment skill, the EMD criterion to detect bifurcation behavior, ERK and L-stable IRK methods. Essentially, this comprehensive scheme can be taken as a universal approach to detect structurally unstable point for a general DAE system.

CHAPTER VI

CONCLUSIONS

1. A summary of the research contributions

With growing concerns on voltage stability, this dissertation focuses on long term small disturbance analysis of power system in an increasingly competitive environment.

First of all, to enhance competition and efficiency of energy market, eigenvalue based bifurcation analysis is applied to give some insights about how to allocate contribution of voltage stability. We investigate how parameters of the system influence the bifurcation points. Three bifurcations (the singularity induced bifurcation, saddle-node and Hopf bifurcation, and their relationship to several commonly used controllers are analyzed. Based on these analyses, we found a way to allocate the contribution by analyzing the relative positions of the bifurcations. Analyzing the influence of the system parameters on voltage stability also benefits us in designing and optimizing the system.

Second, based on some basic scenario summarized in eigenvalue based analysis, an algorithm to choose proper exciter size is developed in, which aims to maximize the loadability of system to fully utilize the generator.

Third, due to complexity of eigenvalue calculation, numerical approach was applied to estimate dynamic stability margin for large systems. As we know, accurately estimating voltage stability margin for big systems online is a big challenge for engineers. To gauge the accuracy of numerical estimate, a reasonable and easy-for-calculation criterion, called EMD criterion, is proposed in this dissertation. Then based on EMD criterion, an automatic load adjustment technique is proposed. We integrated this technique with step size control technique, and based on single step ERK methods, we proposed a new numerical scheme to detect dynamic stability margin. We prove rigorously that our new approach introduces synergy of simultaneously adjustment of time steps and load increasing ratios intelligently. The numerical tests show that our novel method not only has a great advantage in computation efficiency, but also has accuracy close to eigenvalue based bifurcation analysis

for dynamic stability margin estimation. Moreover, unlike eigenvalue based bifurcation analysis, the computation cost of our method is only in linear relation with system size. Thus, the proposed technique has great potential for dynamic stability margin estimation for large systems.

Fourth, we have successfully extended our new numerical scheme to stiffness problem of power systems. It is proved that, the EMD criterion and automatic load adjustment technique can be integrated with L-stable IRK to estimate stability margin for ill-conditioned systems. With this integration, computation efficiency is greatly enhanced, and the numerical stability and the accuracy of estimates can still be guaranteed. Moreover, a comprehensive numerical scheme is proposed in this dissertation, which integrates the automatic stiffness detection, the intelligent load adjustment skill, EMD criterion to detect bifurcation behavior, ERK and L-stable IRK methods. Essentially, this comprehensive scheme can be taken as a universal approach to detect structurally unstable point for a general DAE system.

2. Suggestions for future research

We think the work reported in this dissertation can be an important basis for future research activities related to voltage stability analysis. In general, future research directions based on this dissertation are summarized below.

2.1 Contribution/responsibility allocation for voltage stability of large systems

In chapter II, eigenvalue based bifurcation analysis is applied to give some hints on how to allocate contribution/responsibility for voltage stability. Though it is very enlighten, it is hard to be extended to large system due the complexity of eigenvalue analysis.

In Chapter V, a new comprehensive numerical approach is proposed, which is very efficient and promising for large system analysis. Thus, it is naturally to probe the possibility to adapt some idea into numerical scheme. For example, try to find some typical

scenario of numerical simulation results in corresponding to the basic scenario we summarized in Chapter II.

2.2 Multi-step Runge Kutta Methods

Till now, only single step Runge Kutta methods are discussed in this dissertation. Different with multi-step RK methods, the single step RK methods do not utilize previous numerical results of integration, thus, its computation efficiency may be impaired [34].

The idea of integrating our optimal load adjustment technique with Multi-step RK methods sounds pretty attempting. Also, to further enhance the computation efficiency, parallel computation technique could also be integrated to our numerical scheme to make it more efficient and comprehensive.

2.3 With implicit method, step size control for internal iteration

When load adjustment technique is integrated with L-stable IRK methods, adjustment of Δt is no longer considered. The reason is that, as L-stable IRK methods are applied, numerical stability can be guaranteed, thus we can choose big Δt and no longer need to worry about the adjustment of Δt. However, within the internal iteration to solve swing equation, step-size control technique could be still helpful. We also found that, adjustment of k may have some impacts of the convergence of internal iteration. Therefore, further research on this could be one part of future work.

REFERENCES

[1] T. V. Cutsem, "Voltage instability: Phenomena, countermeasures, and analysis methods," in *Proc. IEEE*, vol. 88, no. 2, pp. 208-227, Feb. 2000.

[2] T. V. Cutsem , C. Vournas, *Voltage Stability of Electric Power Systems*, Boston, MA: Springer, 1998.

[3] C. W. Taylor, *Power System Voltage Stability*, New York: McGraw-Hill, Inc. 1994.

[4] G. Huang, H. Zhang, "Dynamic voltage stability reserve studies for deregulated environment", in *Proc. IEEE/PES Summer Meeting*, Vancouver, Canada, July 2001, pp. 301-306.

[5] G. Huang, K. Men, "Contribution allocation for voltage stability in deregulated power systems", in *Proc. IEEE/PES Summer Meeting*, vol. 3, Chicago, July 2002, pp. 1290 -1295.

[6] G. Huang, L. Zhao, X. Song, "A new bifurcation analysis for power system dynamic voltage stability studies", in *Proc. IEEE/PES Winter meeting*, New York, 2002, pp. 882-887.

[7] V. Venkatasubramanian, H. Schaettler and J. Zaborazky, "Local bifurcations feasibility regions in differential-algebraic systems", *IEEE Transactions on Automatic Control*, vol. 40, no. 12, pp.1992-2013, Dec. 1995.

[8] Y. Tamura, H. Mori and S. Iwamoto, "Relationship between voltage instability and multiple load flow solutions in electric power systems," *IEEE Trans. on Power Apparatus and Systems*, vol. PAS-102, no. 5, pp. 1115-1125, May 1983.

[9] V. Ajjarapu, C. Christy, "The continuation power flow: A tool for steady state voltage stability analysis," *IEEE Trans. on Power Systems*, vol. 7, no. 1, pp. 416-423, Feb. 1992.

[10] G. Huang, T. Zhu, "TCSC as a transient voltage stabilizing controller," in *Proc. IEEE/PES Winter Meeting*, vol. 2, Columbus, OH, Jan. 2001, pp. 628-633.

[11] G. Huang, T. Zhu, "Voltage security assessments using the Arnoldi algorithm," in

Proc. IEEE/PES Summer Meeting, vol. 2, Edmonton, Alta., Canada, Jul. 1999, pp. 635-640.

[12] G. Huang, T. Zhu, "A new method to find the voltage collapse point," in *Proc. IEEE/PES Summer Meeting*, vol. 2, Vancouver, Canada, Jul. 2001, pp. 1324-1329.

[13] F. D. Galinana, M. Phelan, "Allocation of transmission losses to bilateral contracts in a competitive environment," *IEEE Trans. on Power Systems*, vol. 15, no. 1, pp. 143-150, Feb. 2000.

[14] M. A. Pai, K. R. Padiyar, *Small Signal Analysis of Power Systems*, New York: Alpha Science Int'l Ltd., 2004.

[15] P. W. Sauer and M. A. Pai, *Power System Dynamics and Stability*, Upper Saddle River, NJ: Prentice-Hall, 1998.

[16] H. Saadat, *Power System Analysis*. Boston: McGraw-Hill, 1999.

[17] G. K. Morison, B. Gao, P. Kundar, "Voltage stability analysis using static and dynamic approaches," *IEEE Trans. on Power Systems*, vol. 8, no.3, Aug. 1993, pp. 1159-1171.

[18] V. Venkatasubramanian, H. Schaettler and J. Zaborazky, "Voltage dynamics: Study of a generator with voltage control, transmission, and matched MW load", *IEEE Transaction on Automatic Control*, vol 37, no.11, pp. 1717-1733, November 1992.

[19] IEEE Committee Report, "Excitation system model for power system stability studies", *IEEE Trans. Power Apparatus Syst*., vol. PAS-100, no.2, pp. 494-509, Feb.1981.

[20] R. C. Schaefer and K. Kim, "Excitation control of the synchronous generator", *IEEE Industry Applications Magazine*, pp. 37-43, March/April 2001.

[21] R. Safaric, K. Jezernik and D. Borojevic, "PI-controller for avoiding integrator wind-up in system with input saturation", in *Proc. IEEE/PES Electrotechnical Conference*, vol.2, Chicago, 1991, pp. 803-806.

[22] Y. Ni, *Dynamic Power System Theorem and Analysis*, Beijing, China:Tsinghua University Publisher, 1998.

[23] J. Cullum and R. A. Willoughby, “Large scale eigenvalue problems”, in *Proc. of the IBM Europe Institute Workshop on Large Scale Eigenvalue Problems*, Oberlech, Austria, July 8-12, 1985, pp. 405-412.

[24] B. N. Parlett, *The Symmetric Eigenvalue Problem*, Englewood Cliff, NJ: Prentice-Hall, Inc., 1980.

[25] P. M. Anderson, A. A. Fouad, *Power System Control and Stability*. Piscataway, NJ: IEEE Press, 1993.

[26] P. Kundur, *Power System Stability and Control*. New York: McGraw-Hill, 1994

[27] P. M. Anderson and A. A. Fouad, *Power System Control and Stability*, Ames, IA: The Iowa State University Press, 1977.

[28] B. Gao, G. K. Morison, P. Kundar, “Voltage stability evaluation using modal analysis,” *IEEE Trans. on Power Systems*, vol. 7, no. 4, pp. 1529-1542, Nov. 1992.

[29] R. L. Burden, and J. D. Faires, *Numerical Analysis*, 3rd edtion, Boston, MA: Weber & Schmidt, 1985.

[30] E. Isaacson, and H. B. Keller, *Analysis of Numerical Methods*, New York: John Wiley & Sons, 1966.

[31] T. Kailath, *Linear System*. Englewood Ciffs, NJ: Prentice-Hall, 1980.

[32] G. Huang, K. Men, "A new fast simulation scheme for long-term small disturbance voltage stability analysis", in *Proc. IEEE/PES Power System Conference and Exposition*, Atlanta, 2006, pp. 1728-1734.

[33] G. Huang, K. Men, "Fast dynamic voltage stability margin estimation by integration with intelligent load adjustments", in *Proc. IEEE Power Engineering Society General Meeting*, San Francisco, 2005, pp.1985-1992.

[34] E. Hairer, S. P. Norsett, G. Wanner, *Solving Ordinary Differential Equations II, Stiff and Differential-Algebraic Problems*, 2nd Edition. Berlin, Spring-Verlag, 1993.

[35] C. A. Canizares, F. L. Alvarado, “Point of collapse and continuation method for large AC/DC systems,” *IEEE Trans. on Power Systems*, vol. 8, no.1, pp. 1-8, Feb.

1993.

[36] H. K. Khalil, *Nonlinear Systems,* 3rd edition, Upper Saddle River, NJ: Prentice-Hall Inc., 1996.

[37] G. Huang, K. Men, "Impact analysis of exciter sizes on voltage stability". in *Proc. the 4th International Conference on Power Transmission & Distribution Technology*, Changsha, China, October, 2003, pp. 461-468.

[38] E. Hairer, S. P. Norsett, G. Wanner, *Solving Ordinary Differential Equations I, Nonstiff Problems*, 2nd Edition. Berlin: Spring-Verlag, 1993.

VITA

Kun Men received his BS degree in Electrical Engineering from Xi'an Jiaotong University, Xi'an, China and MS degree in Electrical Engineering from Tsinghua University, Beijing, China, in 1996 and 2001 respectively. He joined Texas A&M University in September 2001 as a Ph.D. student under the guidance of Dr. Garng M. Huang and received his Ph.D. in December 2007. He worked at the US Corporate Research Center, ABB Inc., as a summer intern in 2005. His current research interests include power system stability analysis and network applications in power market.

Mr. Men may be reached at the Siemens PT&D, 10900 Wayzata Blvd., Suite 400, Minnetonka, MN, 55305. His email address is kun.men@siemens.com.